THE INVESTIGATION OF BLAST RESPONSE OF SANDWICH PANELS WITH BIO-INSPIRED CORES

A Thesis Submitted to
The Graduate School of Engineering and Sciences of
İzmir Institute of Technology
in Partial Fulfillment of the Requirements for the Degree of

MASTER OF SCIENCE

in Mechanical Engineering

by
Fırat TÜZGEL

July 2017
İZMİR

We approve the thesis of **Fırat TÜZGEL**

Examining Committee Members:

_____

Prof. Dr. Alper TAŞDEMİRCİ

Department of Mechanical Engineering, İzmir Institute of Technology

_____

Prof. Dr. Bülent YARDIMOĞLU

Department of Mechanical Engineering, İzmir Institute of Technology

_____

Assist. Prof. Dr. Levent AYDIN

Department of Mechanical Engineering, İzmir Katip Çelebi University

20 July 2017

_____

Prof. Dr. Alper TAŞDEMİRCİ
Supervisor, Department of
Mechanical Engineering
İzmir Institute of Technology

_____

Prof. Dr. Mustafa GÜDEN
Co-Supervisor, Department of
Mechanical Engineering
İzmir Institute of Technology

_____

Prof. Dr. Metin TANOĞLU
Head of the Department of
Mechanical Engineering

_____

Prof. Dr. Aysun SOFUOĞLU
Dean of the Graduate School of
Engineering and Sciences

ACKNOWLEDGEMENTS

First of all, I would like to thank to my supervisor Prof. Dr. Alper TAŞDEMİRCİ for accepting me Dynamic Testing and Modelling Laboratory, giving me opportunity to research on the blast phenomenon, and for patience, guidance, precious and instructive comments during the entire thesis study. Secondly, I would like to express thanks to my co-advisor Prof. Dr. Mustafa GÜDEN for him support and gaining me different point of view on the study even in short conversation.

I am also grateful for grant #214M339 project provided by The Scientific and Technological Research Council of Turkey (TÜBİTAK). My thesis study which is a just part of this project was made possible thanks to this grant.

I owe all my colleagues a debt of gratitude, especially my team-mates who worked together on the project; Fulya AKBULUT and Erkan GÜZEL, other my esteemed colleagues in DTM lab; Kıvanç TURAN, Alper ÇANKAYA, Çetin UYSAL, Semih SEVEN, and Mustafa Kemal SARIKAYA for both their collaboration and friendship that I would not forget throughout my life.

I would also thank to Dr. Ali KARA who works in CMS Jant Sanayii A.Ş. for him technical support and contributions on my thesis study.

Last but not least, I would like to express my deepest and sincere gratitude to my family, my father Ahmet TÜZGEL, my mother Hürriyet TÜZGEL, my elder brother Murat TÜZGEL, and my venerable grandmother Gülendam YEŞİLAY, for being supportive and promotive in every nerve-racking situations. Their presence makes it easier to overcome all challenges.

ABSTRACT

THE INVESTIGATION OF BLAST RESPONSE OF SANDWICH PANELS WITH BIO-INSPIRED CORES

In this thesis, blast response of sandwich structures with bio-inspired cores having applicable potential for protection against blast loading, balanus, were investigated in detail. The proposed geometry consists of outer shell and inner core which separately manufactured using deep-drawing method. Commonly used blast simulation methods which are pure Lagrangian, Arbitrary Lagrangian Eulerian (ALE), and hybrid (coupled other two approaches) approaches were comparatively investigated as finding their main outstanding features and drawbacks after investigation of blast phenomenon. Calibration study with facesheet of sandwich structure was conducted to demonstrate practically performance of blast simulation methods and tune essential parameters. Well proximity between results was obtained in calibration study. Converge analysis which is especially mandatory in ALE approach was also implemented employing Grid Converge Index (GCI) for selection of mesh density of air and plate in calibration study. Pure Lagrangian approach is conservative approach among the studied blast simulation methods was shown. Direct Pressure Pulse (DPP) experiments were separately conducted for facesheets of sandwich and complete sandwich structures to reveal dynamic performance of them. Equivalent blast loading conditions corresponding to each DPP experiment were found as considering deformation levels of the structures. Therefore, DPP experiment as lab-scale experiment effectively mimicked blast-type loading was revealed. Effect of heat treatment and placement of proposed geometries subjected to blast loading were also examined creating large scaled sandwich structures. Finally, it was demonstrated sandwich structure with balanus cores revealed good blast mitigation performance even at low-scaled distance and would be able to satisfied requirement of defence industry.

ÖZET

DOĞADAN İLHAM ALINAN BİR ÇEKİRDEK MALZEME İHTİVA EDEN SANDVİÇ PANELLERİN PATLAMA KARŞISINDAKİ DAVRANIŞININ İNCELENMESİ

Bu tezde, patlama yüküne karşı koruma potansiyeline sahip biyo-benzetim çekirdekli sandviç yapıların patlama karşısındaki davranışı ayrıntılı olarak incelenmiştir. Önerilen geometri, balanus, derin çekme yöntemi kullanılarak ayrı olarak imal edilen bir dış kabuk ve iç çekirdekten oluşmaktadır. Patlama olgusunun detaylı olarak araştırılmasından sonra, yaygın olarak kullanılan patlama modelleme yöntemleri, salt Lagrangian metodu, Arbitrary Lagrangian Eulerian (ALE) metodu ve birleşik (diğer iki yaklaşımı birleştiren) yaklaşım, ayırt edici özellikleri ve dezavantajları ortaya koyarak karşılaştırmalı olarak incelendi. Sandviç yapının yüzey tabakası kullanılarak patlama simülasyon yöntemlerinin performansını pratikte göstermek ve modellerle ilgili gerekli parametreleri ayarlamak için kalibrasyon çalışması gerçekleştirildi. Bu çalışmada, sonuçlar arasında oldukça iyi bir yakınlık elde edildi. Kalibrasyon çalışmasındaki hava ve plakanın çözüm ağı yoğunluğunun belirlenmesi için özellikle ALE yaklaşımında zorunlu olan yakınsama analizi, Grid Convergence Index (GCI), uygulandı. Üzerinde çalışılan patlama simülasyon metotları arasında salt Lagrangian yaklaşımının konservatif yaklaşım olduğu bulundu. Ardından, tam sandviç ve sandviç yapıların yüzey levhalarının dinamik performanslarını ortaya çıkarmak için ayrı olarak Doğrudan Basınç Dalgası (DBD) deneyleri yürütüldü. Yapıların deformasyon seviyeleri göz önüne alınarak her DBD deneyine karşılık gelen eşdeğer patlama koşulu bulundu. Böylece, laboratuvar ölçekli deney olarak DBD, patlama tipi yüklemeye etkili bir şekilde benzediği ortaya çıkarıldı. Büyük ölçekli sandviç yapılar oluşturularak, patlama yüküne tabi tutulan geometrilerin ısıl işlem ve sandviç yapı içinde ki yerleşimlerinin etkileri de incelendi. Son olarak, balan çekirdekli sandviç yapının, düşük ölçekli mesafelerde dahi iyi bir patlama yükü hafifletme performansı gösterdiği ve savunma sanayinin ihtiyacını karşılayabileceği açığa çıkarıldı.

TABLE OF CONTENTS

LIST OF FIGURES

Figure **Page**

LIST OF TABLES

CHAPTER 1

INTRODUCTION

1.1. Motivation, Problem Statement and Limitations

There has always been a state of war due to economic and politic reasons since the early days of states being established. State of war was named with different names, i.e. World War I-II, Cold War, even though hot battlefield was not explicitly come into existence between the parties as such in Cold War. Especially, there has been numerous terrorist activities and assaults around the world in the period that called post-Cold War came up with ending Cold War in the 1991. Even if terrorism was not begun in the 1990s, it took place common global problem for countries which shows rising incrementally tendency for quarter-century. Turkey has been also faced with several terrorist organizations due to political uncertainties and conflicts of its neighbors. These organizations had to tend their activities to bombing attack which be used improvised explosive device (IED) in consequence of continual empowering and developing Turkish security forces, and besides, ease of access and having low cost of this explosive type.

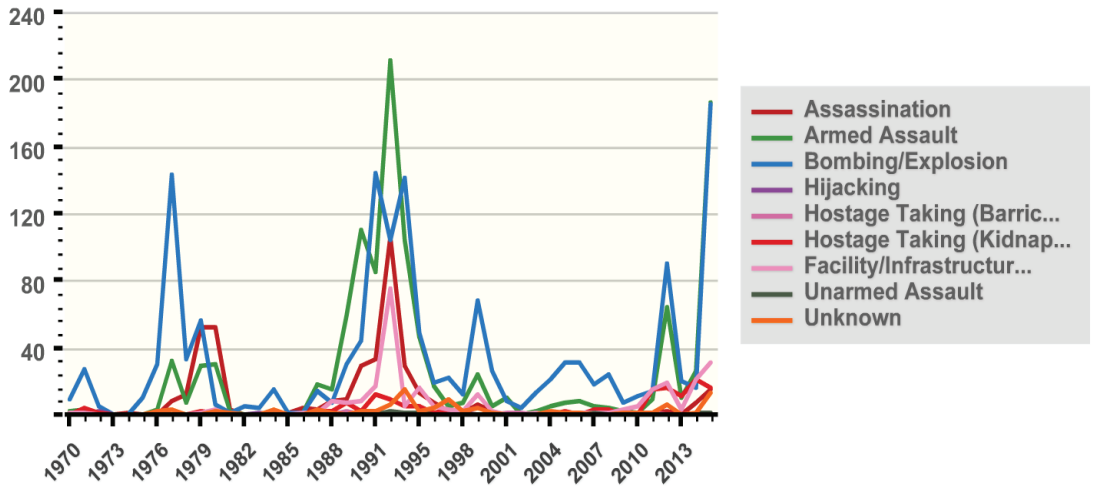

Figure 1.1. Number of Incident – Year Graph for Turkey
(Source: National Consortium for the Study of Terrorism and Responses to Terrorism, 2016).

Number of incident versus years (1970-2015) in terms of attack types of terrorist organizations against Turkey can be seen in Figure 1.1. Making provision against bombing/explosion attack types is imperative in order to provide survivability of occupants as a direct objective and to reduce damage of vehicles as an indirect objective. Moreover, development of defense industry must be kept in parallel with development of attack systems around the world by keeping in sight not only existed threats such as terrorism but also possible threats in the future. However, there are some constraints in construction of any armored vehicles. One of the constraints is that the armored vehicle must be comprised light weighted sub-structures in order to deploy resources and provide mobility in the situation of hot battlefield. Second one is that the armored vehicle must be national as fully as possible because of reducing foreign dependency and providing added value in national economy as exporting. Third one is that sub-structure of armored vehicle must be reproducible and composed of available materials having lower cost. Taking into account all of requirements and constraints, both investigation of dynamic response of the structures with various testing methods and development of innovative blast resistant structures are of particular importance.

1.2. Blast Testing Methodologies

Many researchers exerted effort to examine of dynamic response of structures with different testing methodologies in the last half century. These methodologies can be classified as full and small scale blast testing, non-explosive used blast-like testing, and numerical investigations. Even though full-scale blast testing is the one of the most realistic case among testing methodologies, it may not be suitable for pre-testing of prototypes or preliminary design of sub-structures of armored vehicles due to reasons that are need to strict safety instructions prescribed by governments, not enabling to track deformation progression and hard to protect measurement equipment due to gas products of explosive, requiring wide open field and high amount of explosives. Whereas full-scale blast testing is expensive, time-consuming, hard-to-access, and hard-to-repeatable due to aforementioned reasons, it is obvious having unique capabilities which are huge impact effective area and achieving severe amount of overpressures in a very short time that cannot be acquired by other methodologies. Small scale testing is another testing methodology based on scaled distance theory which is a relation between equivalent mass

of TNT and stand-off distance that is known as Hopkinson-Cranz (or cube root) scaling law (Baker, Cox, Westine, Kulesz, & Strehlow, 1985). Equivalent blast waves can be obtained at same scaled distances so that requirement of high amount of explosive is eliminated, but rest of the restrictions relevant to explosive products remains over to be employed explosive. In non-explosive blast test, there are several blast-like test method that could be conducted in laboratory conditions producing overpressure in a short time which is similar to explosive blast event with various implementation of pressure such as direct pressure pulse experiment set-up (Amini, Simon, & Nemat-Nasser, 2010), pendulum impact (W. Chen & Hao, 2014), shock tube (Wang & Shukla, 2012), blast simulator (Whisler & Kim, 2014), and metal foam projectile (Jing, Wang, & Zhao, 2016). Blast-like test methods provide advantages to conduct in repeatable, controllable and safe manner as enabling specimen visibility, even though overpressure value and size of effective area are limited. In addition of the whole techniques, numerical investigation which is one of vulnerable tools to evaluate blast response of structure may be used. Numerical investigation provides insight about interested issue, besides it is the cheapest and less time consuming method. CONWEP algorithm, Arbitrary Lagrangian Eulerian (ALE) method, coupling method, Smooth Particle Hydrodynamics (SPH) method are fundamental methods to investigate blast response numerically. Subsequent sections are going to be contained detailed view of some of these methods.

1.3. Sandwich Structures

Sandwich structures which have been more quite popular recently in engineering structures which are exposed to high severe impulsive loads such as blast loading are more convenient, once not only offered light weighted structures but also features articulated in the below were born in mind (Vinson, 1999):

- Superior flexural strength-to-weight ratio (increasing moment of inertia by increasing distance between face sheet plates as analogous I-beam)
- Great stiffness-to-weight ratio (reducing deflection correspondingly improvement of rigidity and remaining stable of face sheet plates during deflection)

- Excellent energy absorption capacity (providing local plastic deformation of core material and global plastic deformation of face sheet plate materials)
- Enhancement blast wave resistance (reducing arrival time of blast wave to protected zone by reflecting waves, if cellular core type is used.)
- High thermal resistance (contribution to thermal isolation with voids in core material, if cellular core type is used.)
- Ease to integration and maintenance

Sandwich structures generally comprises of two identical thin face sheet plates and a thick core having whichever material and geometry depending on the restrictions and requirements; for instance, polymeric foams (Wang & Shukla, 2012), metallic foams (Guden, Yuksel, Tasdemirci, & Tanoglu, 2007; Jing et al., 2016), square honeycomb (Alberdi, Przywara, & Khandelwal, 2013; Dharmasena, Wadley, Xue, & Hutchinson, 2008; Vaziri, Xue, & Hutchinson, 2006; Xue & Hutchinson, 2004), hexagonal honeycomb (Alberdi et al., 2013; Crupi, Epasto, & Guglielmino, 2012; Hu & Yu, 2013), corrugated (folded) structures (Alberdi et al., 2013; Dharmasena, Wadley, Williams, Xue, & Hutchinson, 2011; Li, Wang, Zhu, Wu, & Zhao, 2014; Vaziri et al., 2006; Xue & Hutchinson, 2004; Zhang, Cheng, Liu, Li, & Zhang, 2016), trusses (Xue & Hutchinson, 2004), repetitive metallic structures (Tasdemirci, Kara, Turan, Sahin, & Guden, 2016) and their foam filling variations. Moreover, fairly recent developments from a different viewpoint about sandwich structures corresponding to various requirements are available including bio-based materials such as biofiber and PLA (Poly lactic acid) (Du, Yan, & Kortschot, 2014), bio-inspired geometries such as biomimetic fully integrated honeycomb plates (J. Chen et al., 2016), composite structure inspired from nacre (Tran, Ngo, & Mendis, 2014), and Kagome truss core structure inspired from cancellous bone (Ullah, Elambasseril, Brandt, & Feih, 2014) and applications of nanotechnology such as nanocomposite honeycomb sandwich structure to absorb microwave (Khurram et al., 2015).

The basic function of face sheet subordinated to blast loading is to distribute incident pressure to the core as contributing energy absorption. However, the majority of incident pressure is mitigated by core member deforming plastically by means of increment of strain energy and dissipating heat energy. Therefore, sandwich structures as

sacrificial cladding which are lesser weighted than those of monocoque plates as enabling to better performance are appropriated for protection against blast loading.

1.4. Biomimicry

Development and designing in engineering structure are somewhat more complicated due to their conditions and requirements such as light weight, fracture resistance, high loading carrying capability. When faced such a complicated problem, nature having vastly large and deeply varieties can be contained solution methods. Since evolutions against extreme conditions which created in itself have been taking time for billions of years. Such a continual facility may not be existed in hand of mankind to alter their design and adapt against extreme conditions. In addition, nature thanks to wide variety can led about convenience of structures in terms of comparability, durability and feasibility. There are many process, material and structure which were imitated by nature observation ranging from nano and micro to macro and mega to provide benefits in human life (Bar-Cohen, 2006).

Even though the term biomimetics was brought forward by Otto H Schmitt (Schmitt, 1969), the idea of imitation of nature dates back to as early as 1500s. Leonardo Da Vinci's "Flying machine" (Highfield, 2016), inspired from bat structure is one of the early examples of biomimicry. The Shinkansen Bullet Train (Figure 1.2(a)) inspired from kingfishers is a high speed train which reduces noise level and consumption of energy by 15% whereas speeds can be increased by 10% due to the their shape that reduces efficiently air drag (AskNature Team, 2015). The lotus flowers (Figure 1.2(b)) have the water-repellent and relatively clean surface considering environmental conditions, water-repellent feature which gives self-cleaning mechanism that means carrying dust and dirt particles with raindrops due to high contact angle between water droplet and surface (Karthick & Maheshwari, 2008). Lotus-inspired nanotechnology can be applied paint material in order to reduce cleaning expense and time. The pattern inspired from tubercles on the humpback whales (Figure 1.2(c)) can be applied to all wing-like structures edges to reduce drag and increase lifting forces by reducing spanwise flow and strength of the tip vortex (Fish, Weber, Murray, & Howle, 2011).

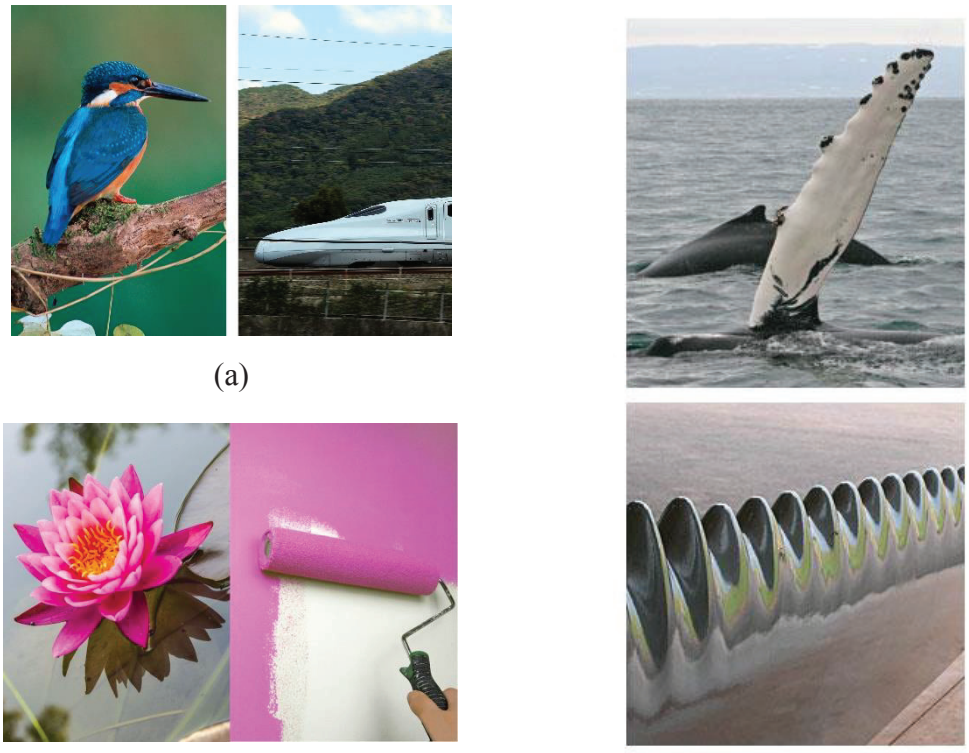

(a)

(b)

(c)

Figure 1.2. (a) The Shinkansen Bullet Train and Kingfishers (Source: www.bloomberg.com) (b) The Lotus flower and painting (Source: www.mnn.com), and (c) Humpback whales and turbine blades (Source: www.umt.edu).

Biomimicry has also been served to improve defense systems. The first example of bio-inspired construct for protection of the full body is plate armors mimicked from crustaceans that live both on earth and underwater such as snails, turtles, mussels, etc. that are capable of protection against any sharp-edged object. In the modern research, honeycomb structure inspired from honeycomb is the most common sandwich structure because of providing robust and light weighted structure.

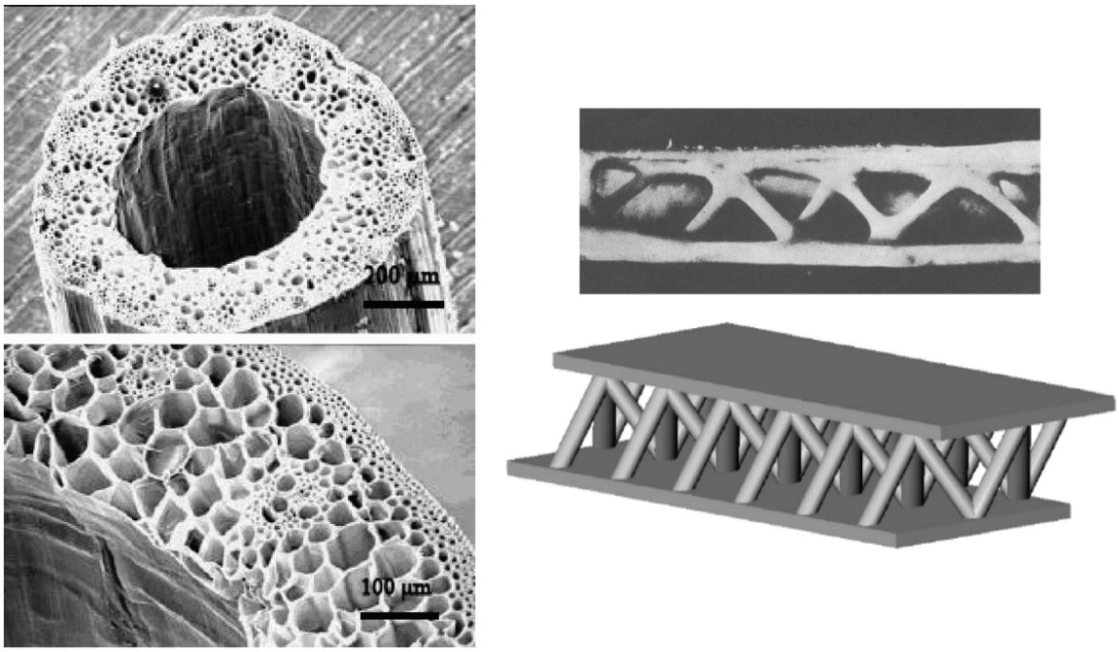

(a) (b)

Figure 1.3. (a) Grass stem, and (b) Vulture wing bone and similar to truss core structure (Source: Myers, Chen, Albert, & Seki, 2008).

Interestingly, structures such as foam and truss core sandwiches that ensure stiffness as remaining light weight, which developed by researchers can be found equivalency in the biological system. Grass stem that resembles foam core and wing bone of vulture (Figure 1.3) that resembles truss core sandwiches exhibit very good mechanical performance in the nature for many years (Myers et al., 2008).

In the current investigation, it has been inspired from a marine crustaceans resembled mollusks in appearance that called as "Balanus" in order to utilize their geometry in core member of a sandwich structure. They are crustaceans in Arthropoda phylum included creatures such as crabs and lobsters as well. Balanus is a member of genus Barnacles in the family Balanidae of phylum Arthropoda according to biological taxonomy. There are more than 50 species within genus balanus that vary depending on the dimensions and the environmental conditions they live in (Chan & Southward, 2011). They anchor on the solid objects such as surface of the submerged of the ships, rocky shores, and outer shell of the other marine crustaceans thanks to their cement glands. An adult balanus mainly consists of outer exoskeleton made of several calcareous plates and two pairs of calcareous plates located its inside (Keith Davey, 2000).

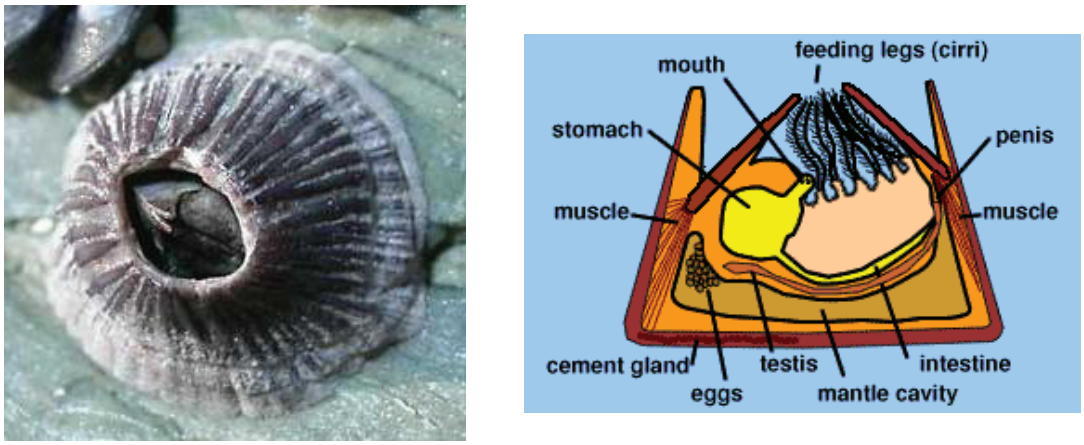

(a) (b)

Figure 1.4. (a) Balanus (Source: www.giovannipinto.it), and (b) Illustration of anatomy of balanus (Source: Keith Davey, 2000).

When the balanus is exposed to the overloading such as wave motions due to tide and flows generated by ship movement, the outer exoskeleton is closed up to interior plates resulted in structural consolidation to protect its structural integrity (Harris, 1990). This protection mechanism is one characteristic feature that makes the balanus unique. Indeed, balanus are considered as biological fouling for shipping, which resist movement of ships resulted in increasing fuel consumption because of their stiff and efficacious structure as emphasized previously (Institute U.S. Naval Annapolis, 1952). As shown Figure 1.5, adult balanus are sessile and mostly live in colonies in their habitat for mating, having stable environment and protection of themselves (Combes, 2001).

Figure 1.5. Colonized balanus habitat (Source: www.inaturalist.org).

1.5. Aim and Scope of the Study

The focus of the current study is to investigate blast response of sandwich structures comprised of bio-inspired cores which is lightweight, national, applicable duplicate production, made of easily attainable material as finding out energy absorbing capabilities at various blast treats. To do this, blast loading on the structure is created in different manner by making use of numerical tools, while structural behavior of sandwich structures at high strain rates is extensively examined in terms of strain rate effect and deformation mechanism through direct pressure pulse (DPP) experiment set-up. Comprehension of dynamic deformation behavior is crucial because of enhancement of energy absorption capacity and improving fracture resistance of structures. It is also aimed that equivalent blast loading conditions corresponding to DPP experiment are found considering deformation amount and mode of sandwich structure.

This thesis consists of six chapters. Chapter 1 is introduction included motivation, limitations, problem statement and aim of the thesis, besides, brief identification about sandwich structures, blast test methodologies and biomimicry. In subsequent chapter, Chapter 2, literature background dealing with blast testing methodologies, plates and especially sandwich structures involved different core topologies, blast response and performance of them is given to form a basis relevant to blast response of structures. In Chapter 3, basic material and manufacturing method of core member are introduced. Material characterization and model is briefly explained. In addition, DPP experiment set-up containing two different test conditions is clarified in detail. In Chapter 4, brief introduction about fundamentals of explosion, scaled distance theory, TNT equivalency, test standard within scope of blast phenomenon section prior to numerical investigation of blast are elaborated in order to understand logic behind a blast circumstance. Then, strengths and weaknesses of some numerical blast models are examined thoroughly in the consideration of blast phenomenon and literature review. Applications of numerical blast method are demonstrated in a calibration study. In Chapter 5, both direct pressure pulse experiment and blast simulation results of sandwich structure with bio-inspired cores are provided as analyzing deformation behavior and energy absorbing capabilities of them. Finally in Chapter 6, conclusion is drawn from different aspects as deducing from detailed experimental and numerical investigations.

CHAPTER 2

LITERATURE SURVEY

Requirement of blast resistant structure has been gradually increasing because of increasing terrorist activities and turning their actions into bombing attack type so that investigation of blast response has particular importance recently as emphasized in introduction. Many researches have made effort for half century to be adapted defensive systems against developing treats. They have dedicated many energy absorbing structure and material having potential of application as sacrificial cladding; besides, they have tried to develop effective blast testing methodologies to facilitate intricate tests. In this chapter, response of related structures subjected to blast and blast-like loading was investigated and results were discussed in detail based on cause and effect relation.

2.1. Blast-Like Loading on the Structures

Amini et al. investigated performance of polyurea layer under blast-like loading using direct pressure-pulse experiment set-up. To create pressure pulse, they used both confined soft polyurethane and water layer in front of specimen as a loading medium with two different confinements (Figure 2.1) and found that utilization of polyurethane layer instead of water layer created identical impact on the specimen in terms of the wave properties. They separately examined DH-36 monolithic circular steel plates and the steel-polyurea bilayer plates with various impulsive loads to put forward effect of plate thickness, location of polyurea layer and loading on the failure mechanism of the plates. Once the initial kinetic energy per unit thickness (J/cm) exceeded a threshold that depends on the test condition, sample failed severely. For almost same initial kinetic energy per unit thickness (~16700 J/cm), the steel plate coated the polyurea on its back face revealed no failure, whereas the monolithic steel plate and the steel plate coated polyurea on the impact side revealed severe and moderate failure respectively. It was clearly stated that when the impact side of the plate is coated with polyurea layer, shock effect was transmitted to steel plate with little reduction of initial pressure because of increasing the

stiffness of polyurea layer; on the contrary, when the opposite side of impact side was coated with polyurea layer, shock effect was imitated because of viscoelasticity of polyurea layer (Amini et al., 2010).

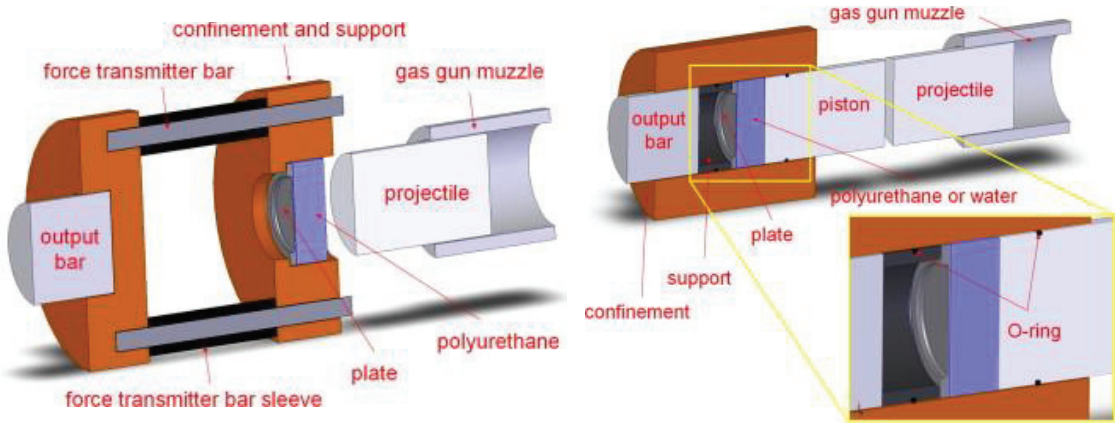

(a) (b)

Figure 2.1. Testing set-ups with (a) allowance to monitor deformation, and (b) unfeasible to monitor deformation (Source: Amini et al., 2010).

Wang and Shukla conducted experimental study to investigate dynamic response of sandwich composites subjected to coupling in-plane pre-compression loads and transverse impulsive loading corresponding to air blast using, a laboratory scale non-explosive test method, shock tube apparatus (Figure 2.2). The sandwich composite consisted of E-Glass Vinyl Ester composite as facesheets material and Corecell^{TM} P600 styrene foam as a core material. They referred three main buckling modes of sandwich composites: (i) elastic buckling, (ii) plastic micro-buckling of faces, and (iii) face wrinkling. The in-plane compressive loads (0, 15, and 25 kN) were chosen considering buckling failure modes to prevent pre-deformation of panels. The results showed that imposition of in-plane compressive loads were adversely affected to blast performance of panels reducing overall strength of them, even though shear crack formation in the core was delayed at 15 and 25 kN compression loads (Figure 2.3.). Reduction of strength was due to formation of displacement transition area on the front facesheet developing out of localized influence of incident impulsive load (Wang & Shukla, 2012).

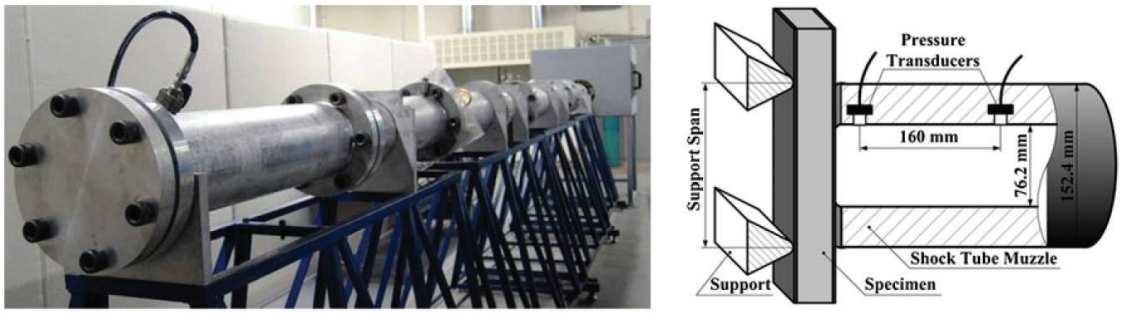

Figure 2.2. Shock tube apparatus and illustration
(Source: Wang & Shukla, 2012).

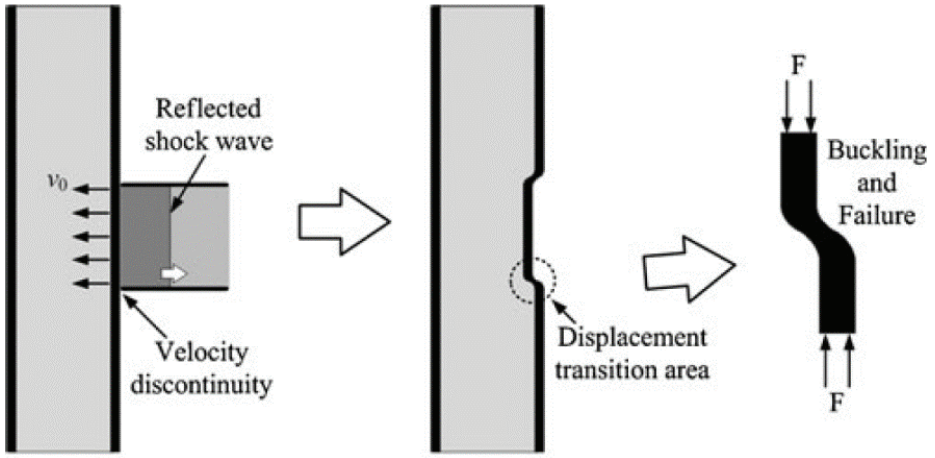

Figure 2.3. Illustration of displacement transition area
(Source: Wang & Shukla, 2012).

Chen and Hao performed experimental and numerical studies to assess dynamic response of the multi-arc double-layered panel that exposed to impulsive blast-like loading generated by using pendulum impact test apparatus (Figure 2.4). An airbag that was placed in front of the panel was utilized in order to create distributed pressure pulse onto structure. They evaluated performance of panels with a range of experimental study as varying arc properties and numbers, and back layer thickness. They demonstrated that increase in arc height, thickness, and number in general improved blast resistance of panels with regard to back plate deflection. Numerical model of the test system was also prepared to acquire results that could not be acquired from experimental study such as reaction forces, Von Mises stress distribution over panel, etc. After numerical validation was done in terms of back plate deflections and deformation modes, it was found that the best panel configuration among the tested panels having 6 arc layers, 0.9 mm arc layer thickness, 50 mm arc height, and 0.55 mm back plate thickness was reduced support

reaction forces in the x, y and z directions by 74%, 81% and 3% respectively when compared to flat panel having 1.2 mm thickness. In addition, it was concluded thanks to numerical study that directly proportional relation between back plate deflection and support reaction force was existed (W. Chen & Hao, 2014).

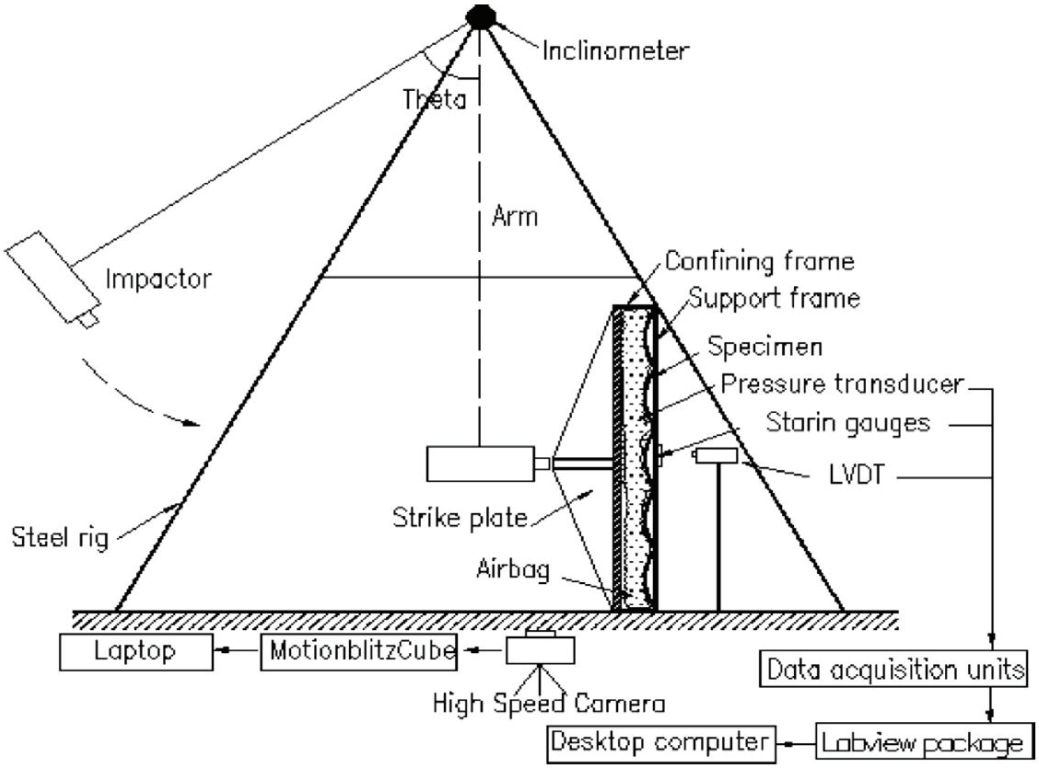

Figure 2.4. Schematic of pendulum impact apparatus
(Source: W. Chen & Hao, 2014).

Whisler and Kim proposed novel laboratory scale test methodology simulated blast event that called as “Blast Simulator”. The main distinctive feature from other lab-scale testing was that it had wider impact area (Figure 2.5(a)). In order to create blast-like loading, they created bulk projectile comprised of 25 small distinct projectile that would be generated spherical blast effect on the structure as arranging mass of each projectile in accordance with desired impulse (Figure 2.5(b)). Equivalent explosive blast parameters were determined according to impulse that acquired from Blast Simulator and full-field testing was realized with those parameters for comparison purposes. They tested nine different sandwich composition and one rolled homogeneous armor (*RHA*) steel via both explosive and non-explosive blast tests. It was found that good matching between explosive and non-explosive blast test results in terms of transmitted impulse, permanent deflection, and damage and failure mechanisms, except burning of surface in explosive

used test due to generated heat. All sandwich panel configurations outperformed RHA plate as reducing initial-average and maximum accelerations up to 36.6% and 75.9%, respectively. The sandwich panel consisted of composite face sheets and double stainless steel honeycomb core exhibited the maximum mitigation of blast load (Whisler & Kim, 2014).

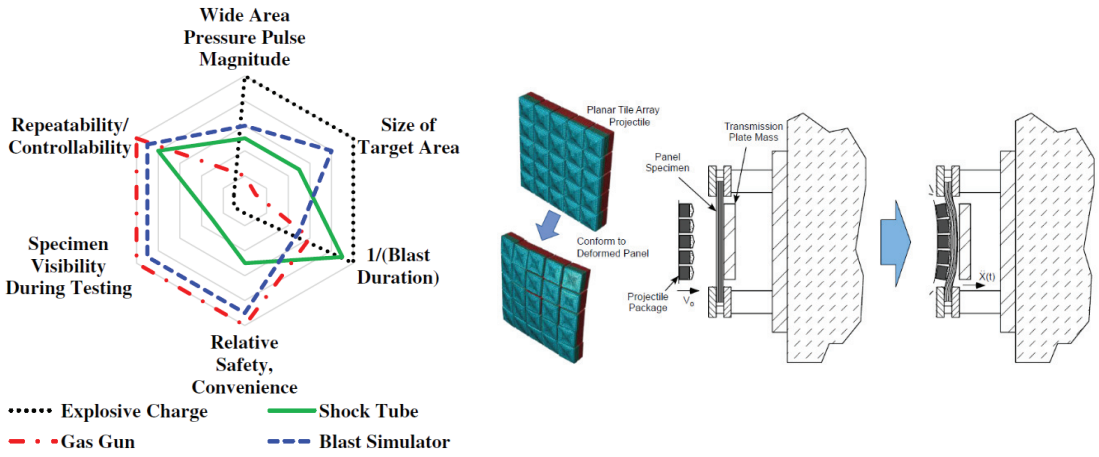

(a) (b)

Figure 2.5. (a) A hexagonal plot to compare explosive and non-explosive test methods, and (b) projectile and loading on the panel specimen (Source: Whisler & Kim, 2014).

Jing et al. compared dynamic performance of three different sandwich panels consisting of closed-cell and open-cell metallic foam core, aluminum honeycomb core and monolithic plate subjected to experimentally generated localized impulsive loading using metal foam projectile (Figure 2.6). Sandwich panels and monolithic plate were kept with same weight to evaluate objectively. The findings showed that honeycomb core sandwich panel had minimum back face deflection and then closed-cell foam core, monolithic and open-cell foam core panel followed respectively. All sandwich panels suffered local failure at the center due to be imparted localized impulse loading and core delamination and shearing gradually reduced overall blast resistance of panels having closed-cell foam core (Figure 2.7). Moreover, it was found that decrease in cell size and increase in core height enhanced blast resistance of structures as contributing stiffness of structures and enabling core deformation longer period, respectively (Jing et al., 2016).

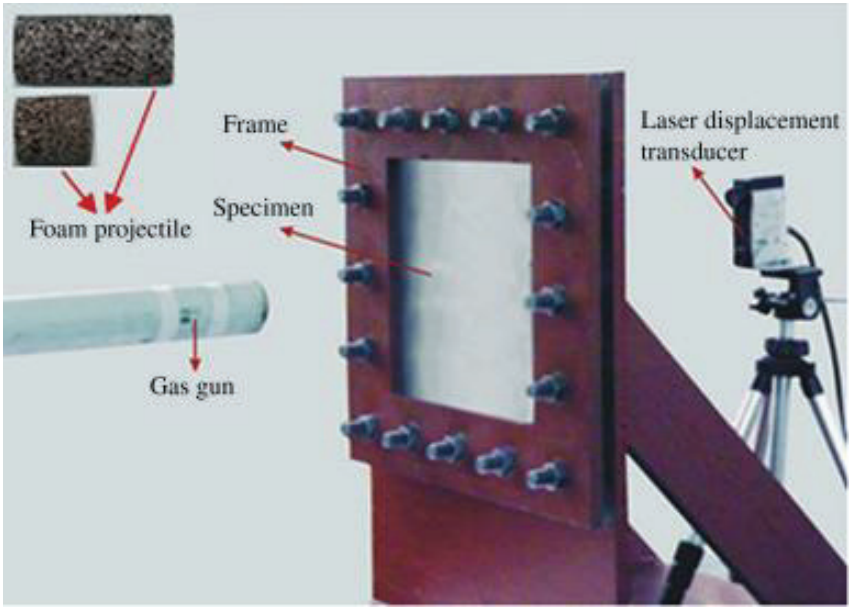

Figure 2.6. Experimental set-up including picture of undeformed and deformed projectiles (Source: Jing et al., 2016).

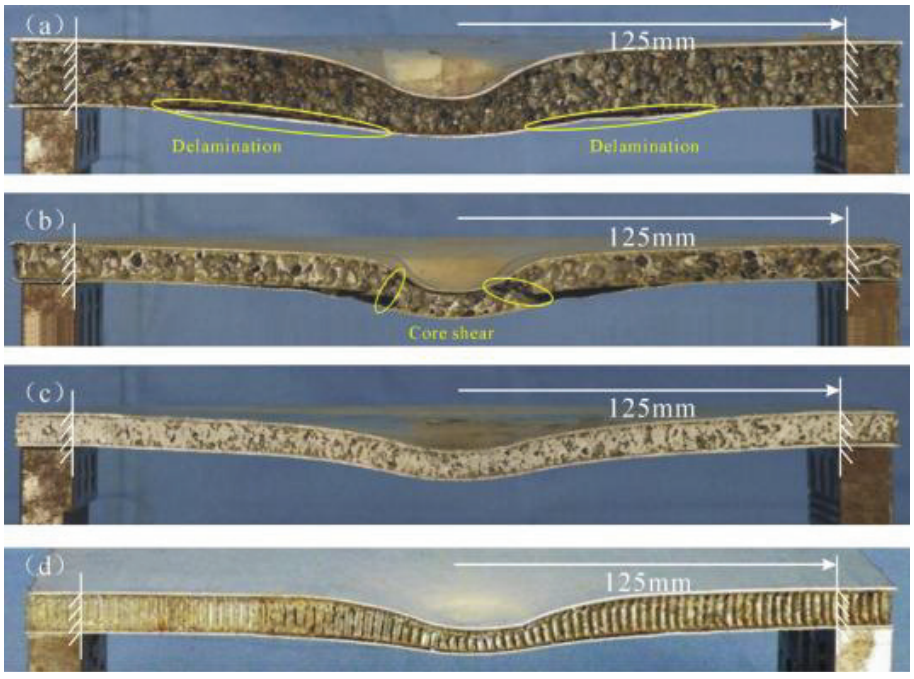

Figure 2.7. Deformed panels (a) and (b) closed-cell foam core having different core height and plate thickness (c) open-cell foam core and (d) honeycomb core (Source: Jing et al., 2016).

2.2. Blast Loading on the Structures

Fleck and Deshpande (2004) proposed analytical methodology to evaluate dynamic response of clamped sandwich beams on the assumptions that one-dimensional interaction, neglecting support reactions and uniform impulse acting on plate. They defined three stages that correspond to sequential dynamic response of a structure subjected to the blast loading: the first stage expresses fluid-structure interaction that could be explained acceleration of upper plate from stationary situation to a dynamic condition with a uniform velocity, the second stage is core crushing stage that proceeds until it is balanced velocities of upper plate and core member, third stage is overall beam bending and facesheet stretching where back face sheet had an initial velocity. These three sequential steps also were illustrated (Figure 2.8) by Dharmesane et al. (2008). Moreover, they investigated various core topologies and theoretically ideal core. It was found that diamond-celled core was resulted in lower back face deflection that was close to that of the ideal core because of having high strength at two directions which were thickness and longitudinal.

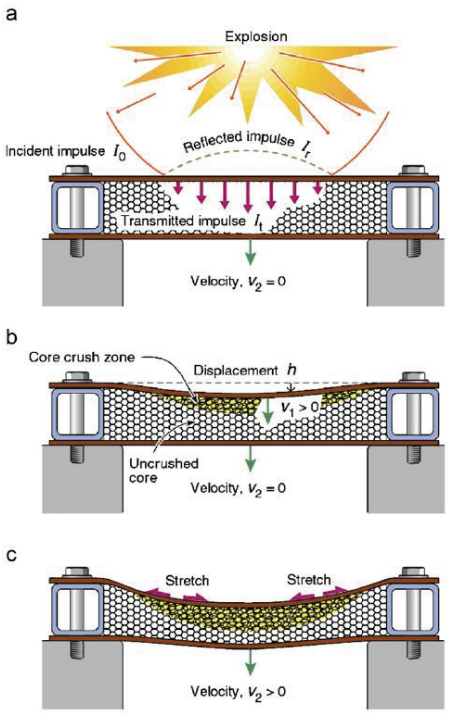

Figure 2.8. Sequential response of sandwich panels under impulsive loading (a) fluid-structure interaction (stage I) (b) core crushing (stage II) and (c) overall bending and stretching (stage III) (Source: Dharmasena et al., 2008).

Xue and Hutchinson carried out a comparative study to able to bring out effect of fluid structure interaction (*FSI*) and deformation of the diverse metallic sandwich structures (pyramidal truss, folded plate and square honeycomb) and those of mass and material equivalent monolithic plate subjected to impulsive loading that generated numerically using ABAQUS Explicit software. They analyzed just one repeated part of the each major structure with implementation of proper boundary conditions. Stainless steel (#304) was used as a material, but it was not counted rate sensitivity and fracture in material model to observe maximum deflection of the structures. It was clearly stated that aforementioned three types of sandwich structures outperformed those of mass and material equivalent solid plate. Moreover, the folded plate and square honeycomb cores offered higher in-plane stretching resistance exhibited further performance compared to pyramidal truss sandwich (Figure 2.9(b)). They also pointed out beneficial fluid-structure interaction by making use of Taylor's relations which are:

$$\frac{I}{I_0} = 2q^{q/(1-q)} \tag{2.1}$$

$$q = \frac{t_0}{t_*} \tag{2.2}$$

$$t_* = \frac{\rho h}{\rho_f c_f} \tag{2.3}$$

where I and I_0 are the uniform impulse per area affected on the plate and the free-field momentum per area, respectively. t_0 is the pulse decay period. t_* is reference time scale. ρ and ρ_f are the density of plate and fluid, respectively. h is the plate thickness and c_f is the speed of sound at that medium. It was found that transferred momentum to the plate increased twice for air medium because the plate acted as rigid resulted in impedance mismatch due to the less density of air, whereas the transferred momentum to the plate could be proportionally reduced for water medium with reduction of the thickness of the front face sheet of the sandwich structure (Figure 2.9(a)). It could be concluded that blast imitation performance of sandwich structures incrementally increased for denser medium compared to monolithic thicker solid plate (Xue & Hutchinson, 2004).

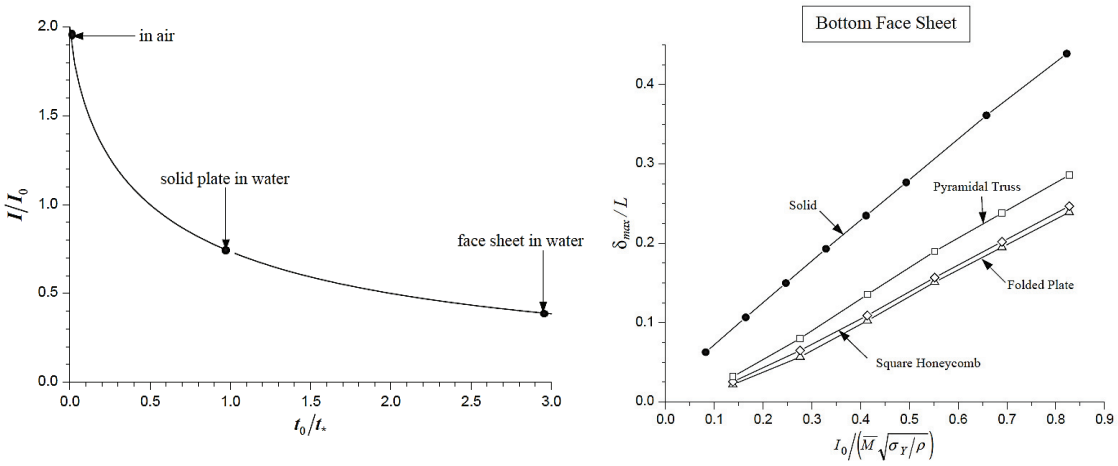

(a) (b)

Figure 2.9. (a) Effect of FSI, and (b) Normalized maximum deflection versus normalized impulse results (Source: Xue & Hutchinson, 2004).

Vaziri et al. studied on the foam filled square honeycomb and folded plate (or corrugated) metallic sandwich panels to emerge dynamic effectiveness of structural foams numerically. 304 stainless steel as core and facesheet materials and a closed-cell foam PVC foam as foam material were used. Sandwich panels separately filled foam having two different densities for each core topology and those of mass equivalent empty sandwich panels were compared. Foam filler reduced core deformation for all cases, but overall deflection of sandwich panel was not changed. This was because foam filler improved buckling resistance of core members as supplying lateral support, which was resulted in lower core deformation. In actual fact, energy absorption was shared with foam and core member as reducing core deformation, therefore resultant center deflection of sandwiches did not alter (Figure 2.10). It was suggested that the structural foam would be used to supply acoustic and thermal isolations (Vaziri et al., 2006).

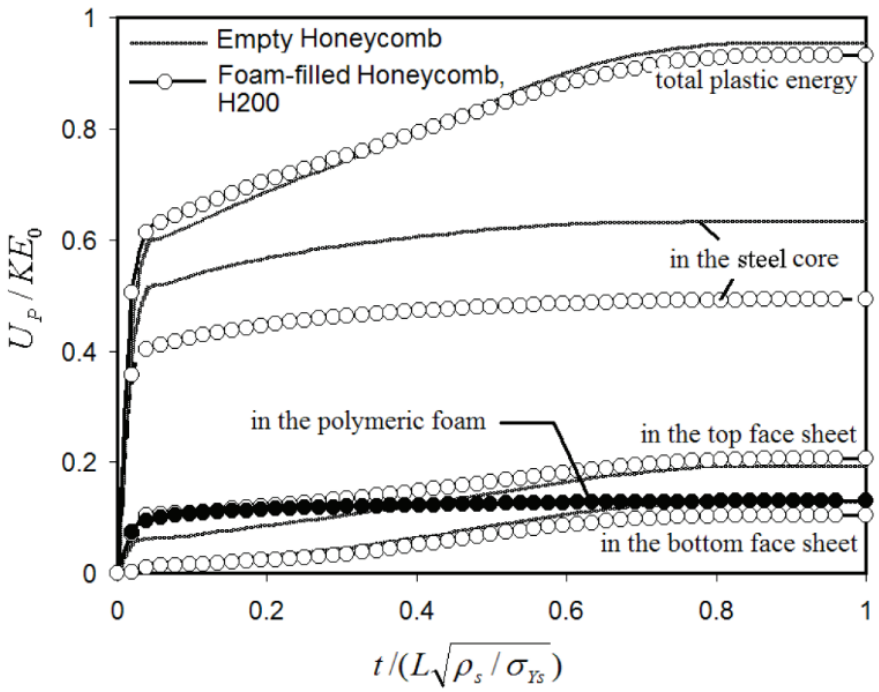

Figure 2.10. Normalized plastic dissipation-time histories for foam-filled and empty honeycomb (Source: Vaziri et al., 2006).

Spuskanyuk et al. investigated metallic core deformation behavior under water blast loading as taking into account three sequential deformation stages of sandwich structure. It was proposed a relation (Π) which was a ratio between the durations corresponding to stage II and stage III:

$$\Pi \equiv \frac{t_{\mathrm{II}}}{t_{\mathrm{III}}} \approx \frac{2I_T}{L\sigma_{YD}^c}\sqrt{\frac{\sigma_Y}{\rho}} \tag{2.4}$$

where I_T was transmitted impulse through stage I, L was half-width of the sandwich beam, σ_{YD}^c and σ_Y were dynamic yield stress of the core and yield stress of base material respectively, ρ was density of base material. According to a critical value, Π_{th}, was estimated as considering all results, if $\Pi < \Pi_{th}$, core member was represented as strong in the way that stage II and stage III were clearly distinguishable, if $\Pi > \Pi_{th}$, core member was represented as soft in the way that stage II and stage III were combined into one stage without common velocity. They found that soft cores exhibited less back face sheet deflection, front and back face strain, and so less transmitted force to the support when compared strong one. This was because face sheets and soft core did not have a common velocity and core compression was maintained. It was known that more energy

was absorbed in the stage II so that less energy was absorbed by panels having strong core because those panels passed the stage III in a shorter time. The energy at the end of stage II was dissipated via overall bending, stretching, etc. in the stage III, then remaining energy was directly transmitted to support. This was why the transmitted force was high for the panels having strong core (Spuskanyuk et al., 2007).

Dharmasena et al. performed experimental and numerical study to investigate dynamic response of clamped square honeycomb sandwich panel and their equivalent solid plate in terms of areal density that subjected to free air blast. The impulse intensity was regulated changing mass of explosive (1, 2, and 3 kg TNT) at constant standoff distance (10 cm). Numerical study was performed using ConWep formulation in ABAQUS/Explicit finite element solver. The sandwich panels exhibited lower back face deflections, 40% and 90% of deflection of monolithic plate for lowest and highest impulsive load respectively, compared to mass equivalent monolithic plate. They indicated that numerical solutions executed with ConWep formulation brought to reasonable results in terms of center deflections, core collapsing mechanism except densest impulsive load (Figure 2.11). This was because debonding condition was not incorporated in numerical simulations, but separation between core member and face sheets resulted at higher impulses that created weakness on the overall strength of the structure (Dharmasena et al., 2008).

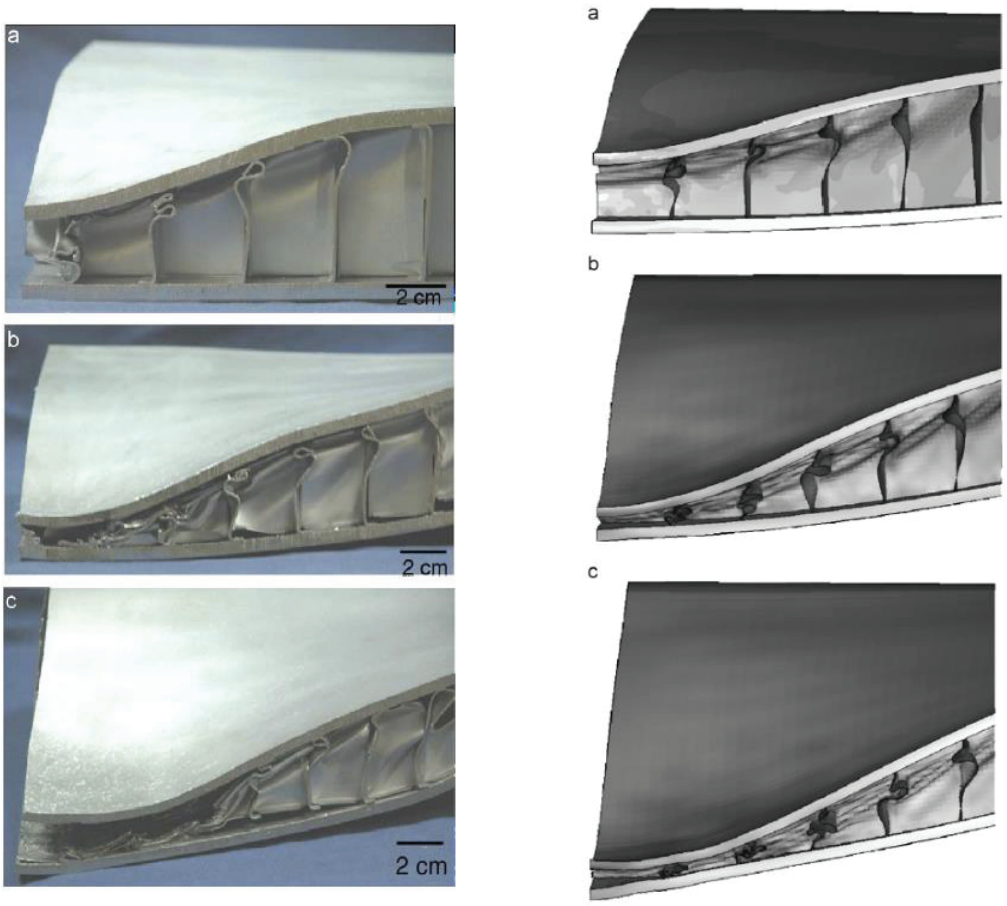

(a) (b)

Figure 2.11. The result of sandwich panels subjected to blast loads 21.5 kPa s, 28.4 kPa s, and 33.7 kPa s, respectively; (a) experimental results, and (b) numerical results (Source: Dharmasena et al., 2008).

Dharmasena et al. analyzed the response of fully clamped metallic pyramidal lattice core sandwich panels and those of mass equivalent solid plate exposed to the various blast loadings both experimentally and numerically. Small scale explosive blast testing was performed for generation localized impulse with constant mass of explosive (150 g spherical C-4). The effect of both varying facesheet thickness (0.76, 1.52 and 1.90 mm) at constant impulse (2.3 kPa s) and varying impulse (1.5, 2.3 and 7.6 kPa s) with constant facesheet thickness (1.52 mm) were separately identified for sandwich panels. ConWep function in ABAQUS/Explicit finite element software was utilized to observe deformation sequence and to attain transferred force to the support from clamped edges. Predicted results were fairly consistent with experimental result in terms of center deflection of front and back facesheets and monolithic plate, even perforation of the front face. Tearing on the front facesheet was originated from increase of front facesheet velocity as a result of decreasing areal density of facesheet reducing its thickness and then

tensile and compressive loads occurred at the same time on the front facesheet since there was no time for deformation of core (Figure 2.12).

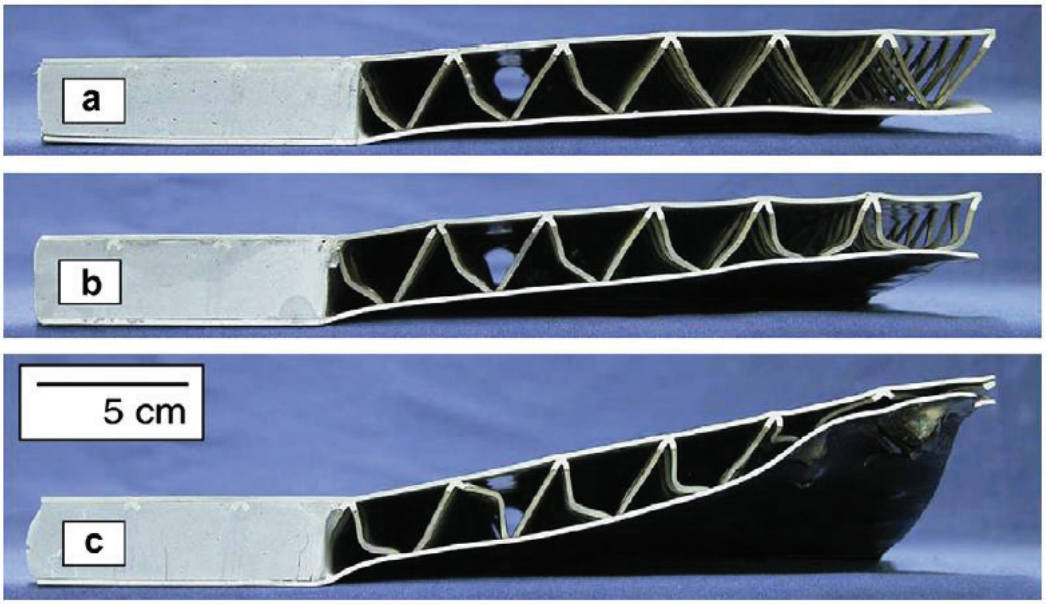

Figure 2.12. Deformed sandwich panels with constant face sheet thickness (1.52 mm) at various blast loads (a) 1.5 kPa s, (b) 2.3 kPa s, and (c) 7.6 kPa s (Source: Dharmasena et al., 2011).

The main function of front facesheet in any sandwich panel that was distribution of incident impulsive load was eliminated in that case and incident impulsive load was quite localized at center of panel so that the back facesheet deflection increased. Reduction of deformation of core members from center to clamped edges and rupture of front facesheet of sandwich panel were demonstrated (Figure 2.13). It was apparent that pyramidal lattice core significantly outperformed their equivalent solid plate in terms of maximum vertical component of transmitted force to the support for all cases, but the back face deflections and transmitted forces to the support horizontally in sandwich panels were slightly less than those of equivalent monolithic plates except a few specific conditions because of little in-plane stretch resistance characteristic of pyramidal lattice core and absence of beneficial FSI effect (Dharmasena et al., 2011).

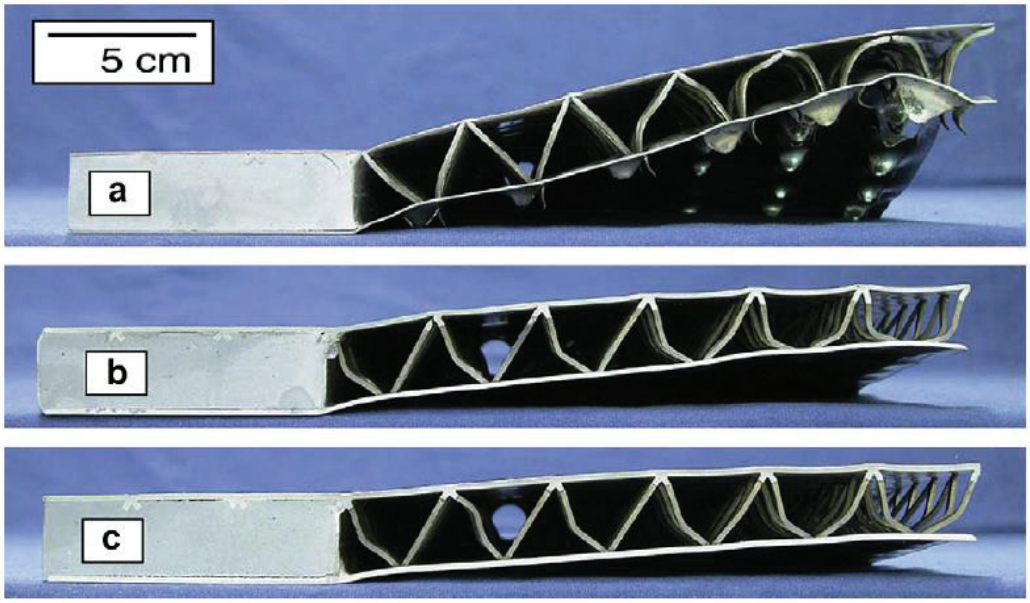

Figure 2.13. Deformed sandwich panels at constant blast load (2.3 kPa s) with various face sheet thicknesses: (a) 0.76 mm, (b) 1.52 mm, and (c) 1.90 mm (Source: Dharmasena et al., 2011).

Soutis et al. carried out comparative study to ascertain reliability of some blast modelling methods which were ConWep and multi-material Arbitrary Lagrangian Eulerian (*MMALE*) formulations using LS-DYNA finite element software. They used glass fiber reinforced laminate (*GLARE*) panels which is hybrid composite and compared their solutions with experimental result in terms of mid-point deflection. The simulations used MMALE formulation resulted in more accurate result, just as ConWep approach provided consistent result in reasonable manner with error less than 5%. They attracted notice that ConWep calculations took approximately 10 times lesser time than MMALE formulations. On the other hand, as MMALE approach resulted in more stable deflection of plates, relative springback effect was observed in the ConWep approach (Figure 2.14) (Soutis, Mohamed, & Hodzic, 2011).

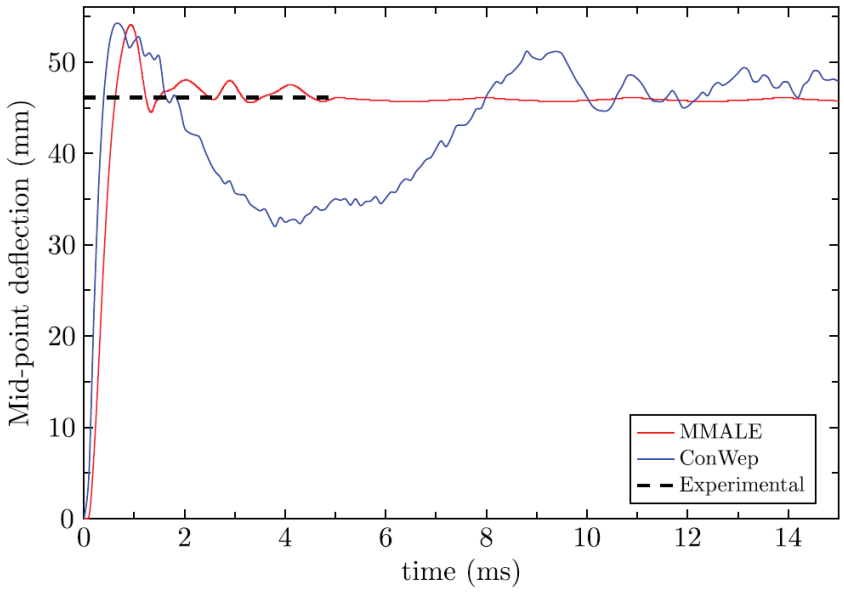

Figure 2.14. Comparison of mid-point deflection of the plates (Source: Soutis et al., 2011).

Alberdi et al. studied the dynamic performance of sandwich structures having conventional core topologies which were corrugated cores including triangular (TF), Y-frame (YF) and diamond (DF) folded core structures and honeycomb cores including hexagonal (HH), square (SH) and triangular (TH) honeycomb structures for different blast loadings and boundary conditions by numerically using LS-DYNA finite element software. CONWEP function embedded in LS-DYNA was used for modelling of blast with Lagrangian approach. It was obvious that energy dissipation decreases as increasing front face thickness for all topologies and increase of back face thickness did not remarkably impinge on total energy dissipation, front face deflection and transmitted force except back face deflection. The force transmitted to support decreased as increasing front face thickness of folded cores topologies, but it increased as increasing front face thickness of honeycomb cores topologies. Folded core topologies came up with result lower back face deflection and higher energy dissipation than honeycomb topologies because of enabling of plastic deformation of cores in the folded core topologies. Whereas the front plate was dominant in distribution of energy dissipation for clamped boundary conditions, it was shown that contribution of energy dissipation depended on core configuration for fixed boundary condition. For the specific equivalent mass of TNT and boundary condition; while diamond folded core topology revealed good performance in terms of back face deflection and force transmission at 0.5 kg equivalent mass of TNT and under clamped boundary conditions, the hexagonal and square

honeycomb topologies transmitted less force to the support at 4 kg equivalent mass of TNT and could withstand larger blast loads when the others failed (Figure 2.15). Strain rate effect was also identified. The diamond folded core having 0.3 mm plate thickness was examined using low (0.5 kg) and high (2 kg) amount of TNT equivalent. The models which were included strain rate dependency revealed good performance in terms of the less force transferred to support. Transmitted force was reduced included strain rate effect by 12% for high amount of TNT equivalent, 7% for low amount of TNT equivalent (Alberdi et al., 2013).

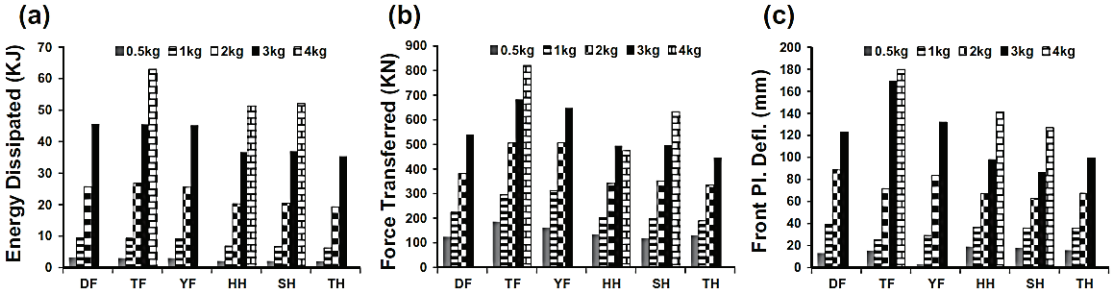

Figure 2.15. Structural performance of core topologies at different blast loads (a) energy dissipated (b) force transferred, and (c) front plate deflection (Source: Alberdi et al., 2013).

Li et al. performed experimental and numerical study in order to investigate air blast response of fully clamped aluminum corrugated sandwich panels with two different configurations of corrugated cores (Table 2.1). Experimental study was conducted employing small scale explosive by making use of a four-cable ballistic pendulum system, which includes a laser displacement sensor, to estimate impulse that experienced by the specimen. The result showed that first configuration exhibited lower back face deflection compared to second configuration. In addition, they stated when the deformation of center of core reached its densification level, global plastic deformation initiated; hence energy absorption contribution of core members decreased at higher impulses for two configuration due to the global plastic deformation of sandwich panel. In the numerical study, air blast was modelled using ALE (Arbitrary Lagrangian Euler) approach in AUTODYN finite element solver. They showed that the maximum back face residual deflection was gradually reduced as increasing thickness and yield stress of both facesheet and core member (Figure 2.16). Moreover, different core types with same mass were examined and as corrugation angle increased, the deflection of back facesheet decreased because of increasing contact area between core member and front facesheet

resulted in enhancement bending stiffness and strength of overall sandwich panel (Li et al., 2014).

Table 2.1. Geometrical specifications of two configuration of sandwich panels (Unit: millimeter) (Source: Li et al., 2014).

Configuration	H_f/Face sheet thickness	H_c/Core height	t/Core thickness	Length/ a	Length/ b	θ	Cell length/s
1	0.8	4	0.2	4	8	63.4	12
2	0.8	8	0.2	7	14	66.4	21

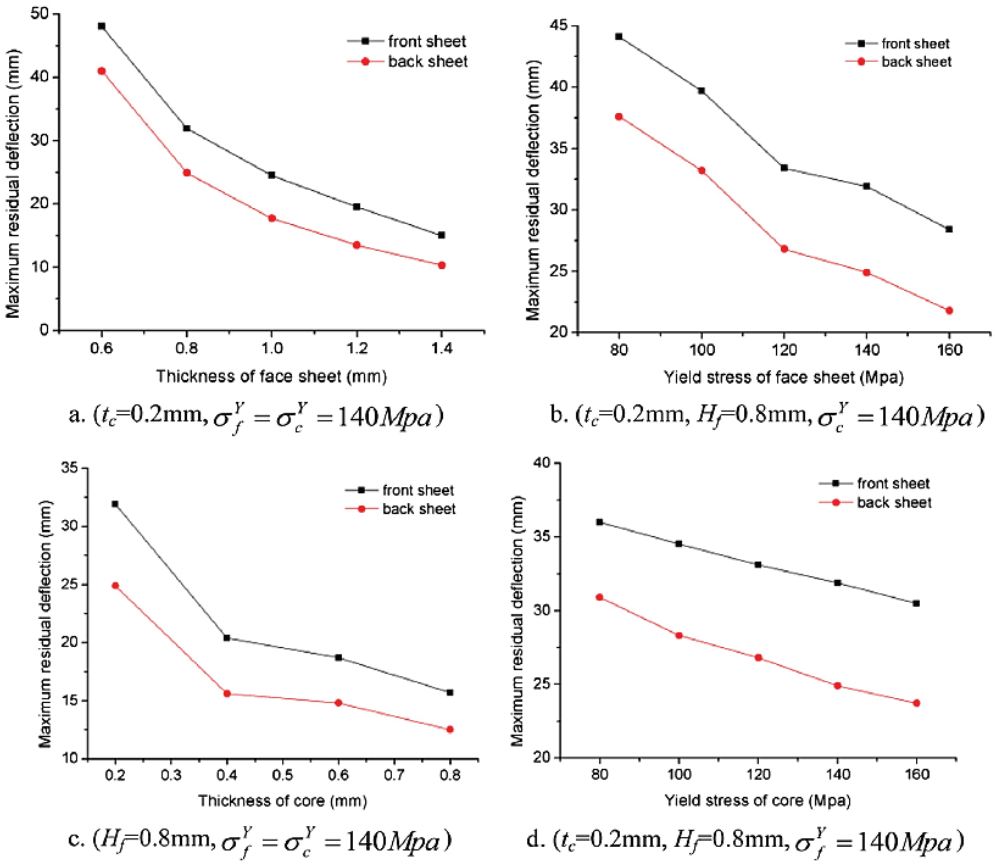

a. (t_c=0.2mm, $\sigma_f^Y = \sigma_c^Y = 140Mpa$)

b. (t_c=0.2mm, H_f=0.8mm, $\sigma_c^Y = 140Mpa$)

c. (H_f=0.8mm, $\sigma_f^Y = \sigma_c^Y = 140Mpa$)

d. (t_c=0.2mm, H_f=0.8mm, $\sigma_f^Y = 140Mpa$)

Figure 2.16. Effect of thickness and yield stress of both core and facesheet on the maximum residual deflection (Source: Li et al., 2014).

Tasdemirci et al. investigated dynamic response of the combined of hemi-spherical cap and cylindrical shells core sandwich subjected to air blast numerically. They analyzed effect of some facts on the dynamic performance of those geometries, which were heat treatment and core position (forward and reversed positioning against incident blast wave), whereafter numerical verification was done with experimental result of

quasi-static and low velocity impact responses. They figured out that transmitted force to the support was inversely proportional to compression level of core member. However, they stated that if compression level of core was attained its densification level, the transmitted force would have been increased dramatically. It was apparent that presence of plastic strain also directly was affected to compression level. While the level of core compression increased due to absence of plastic strain (heat-treated condition), it increased at the reverse positioning due to higher presence of plastic strain in the hemi-spherical portion than which in cylindrical portion of core member. Therefore, both reverse positioning and heat-treated condition of core was resulted in minimum transmitted force value as reverse positioning was the dominant effect for this type core structure when considered force transmission (Figure 2.17). Furthermore, reverse positioned cores had lesser arrival time than forward positioned one because contact area during the deformation in the cylinder portion was higher than spherical portion (Tasdemirci et al., 2016).

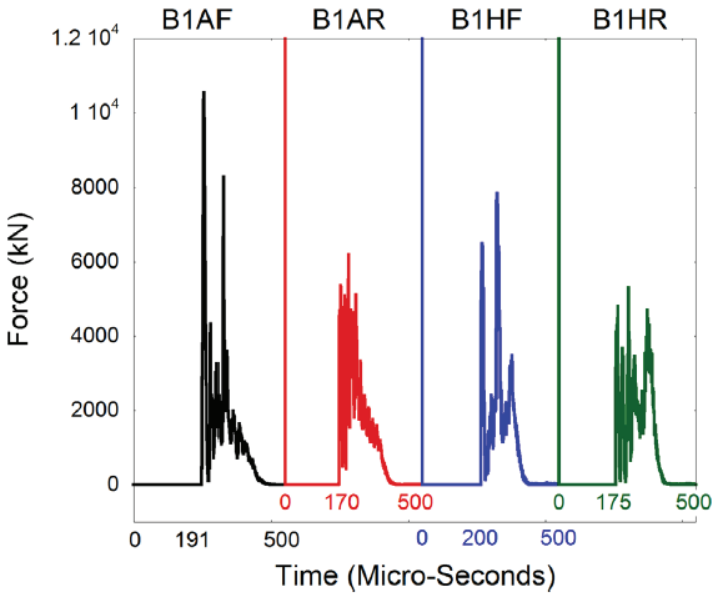

Figure 2.17. Transmitted force-time histories various configurations of core H: Heat-treated condition, R: Reverse positioning, A: As-received, F: Forward positioning (Source: Tasdemirci et al., 2016).

Zhang et al. (2016) investigated dynamic response of foam inserted into corrugated core sandwich panels using small scale explosive. They used 304 stainless steel as base material and PVC foam as filler material with various filling strategy (Figure 2.18). In contrast to Vaziri et al. (2006), they proved that foam filling approach improved

blast resistance of corrugated sandwich panels in terms of back face deflection and fracture formation as acting on deformation modes of panels. Empty sandwich panels, especially at lower stand-off distances, were catastrophically damaged, while the foam inserted sandwich panels' damage was remarkably diminished. The positive influence of foam filling was attributed general foam features which were origination of acoustic mismatch between foam and base materials and contribution to energy mitigation in that of crushing stage. In addition, they stated that the activation of these features was directly related to deformation modes of panels; therefore, selection of optimal filling strategy was become more significant (Figure 2.19).

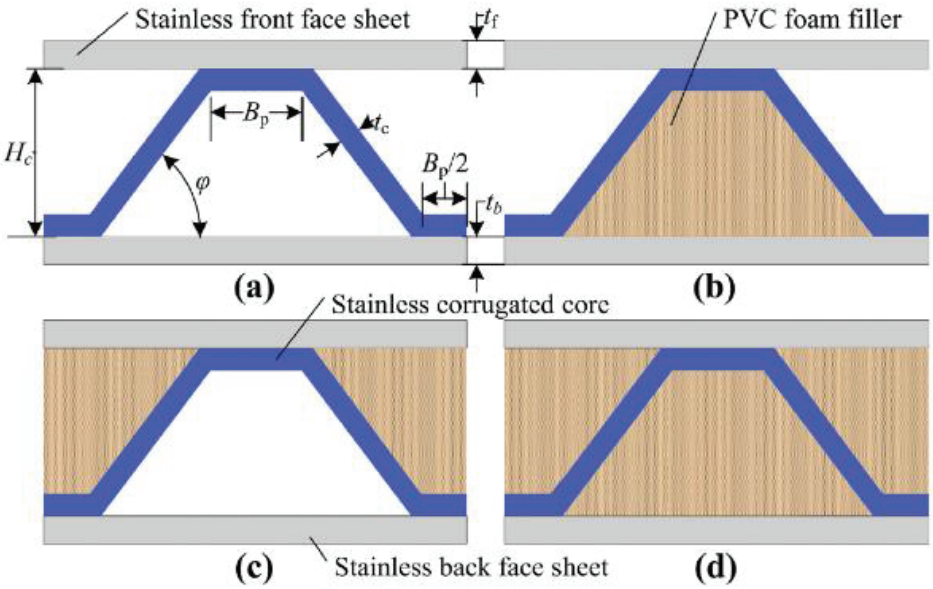

Figure 2.18. Filling strategies of corrugated core sandwich panels (a) empty (EP) (b) back side filled (BSFP) (c) front side fillet (FSFP), and (d) fully filled (FFP) (Source: Zhang et al., 2016).

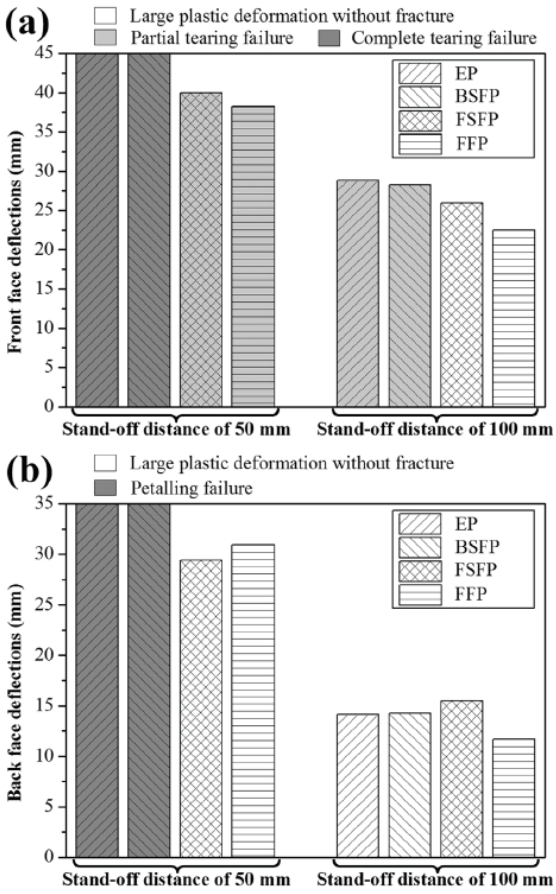

Figure 2.19. Deflection amount for 50 and 100 mm stand-off distances (a) front face, and (b) back face (Source: Zhang et al., 2016).

A study similar to Soutis et al.'s (2011) investigation was conducted by Kilic and Bedir (2016). They also found that residual deflections in their numerical model including MMALE approach were good in agreement with their full-field experimental results (Figure 2.20) except which in sensor locations 1 and 10 due to the fact that it might be arisen from structural imperfection. They indicated that the use of spherical air domain instead of Cartesian air domain in MMALE approach was resulted in more constituent with that of ConWep formulations in terms of reflected impulse and pressure since advection was fulfilled in easier way in spherical domain (Figure 2.21). Furthermore, they highlighted that mesh sensitivity was directly affected structural response in the numerical model. However, it was obvious that total CPU time dramatically increased as decreasing element size.

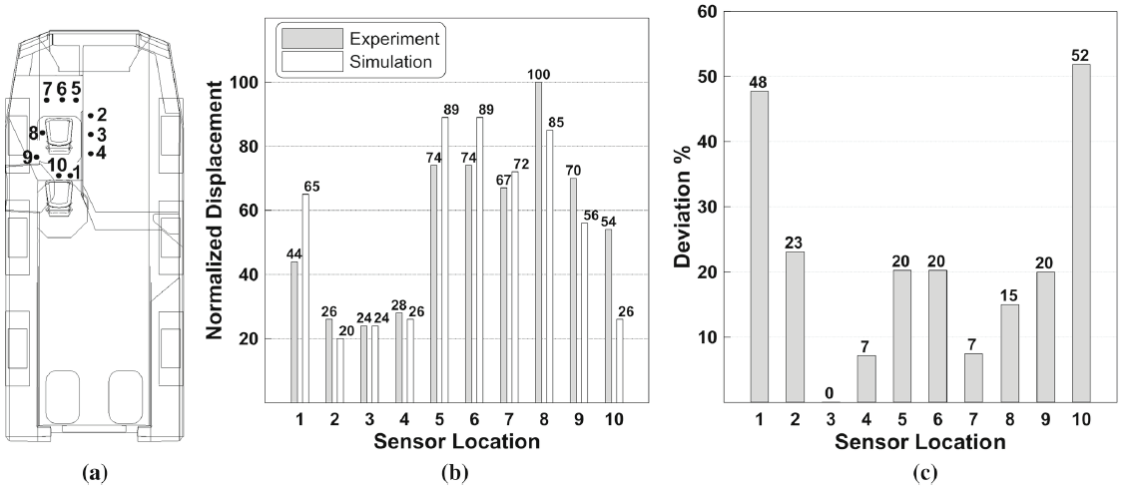

Figure 2.20. (a) Sensor locations (b) comparison between experiment and simulation results, and (c) representation of deviation (%) versus sensor location (Source: Kilic & Bedir, 2016).

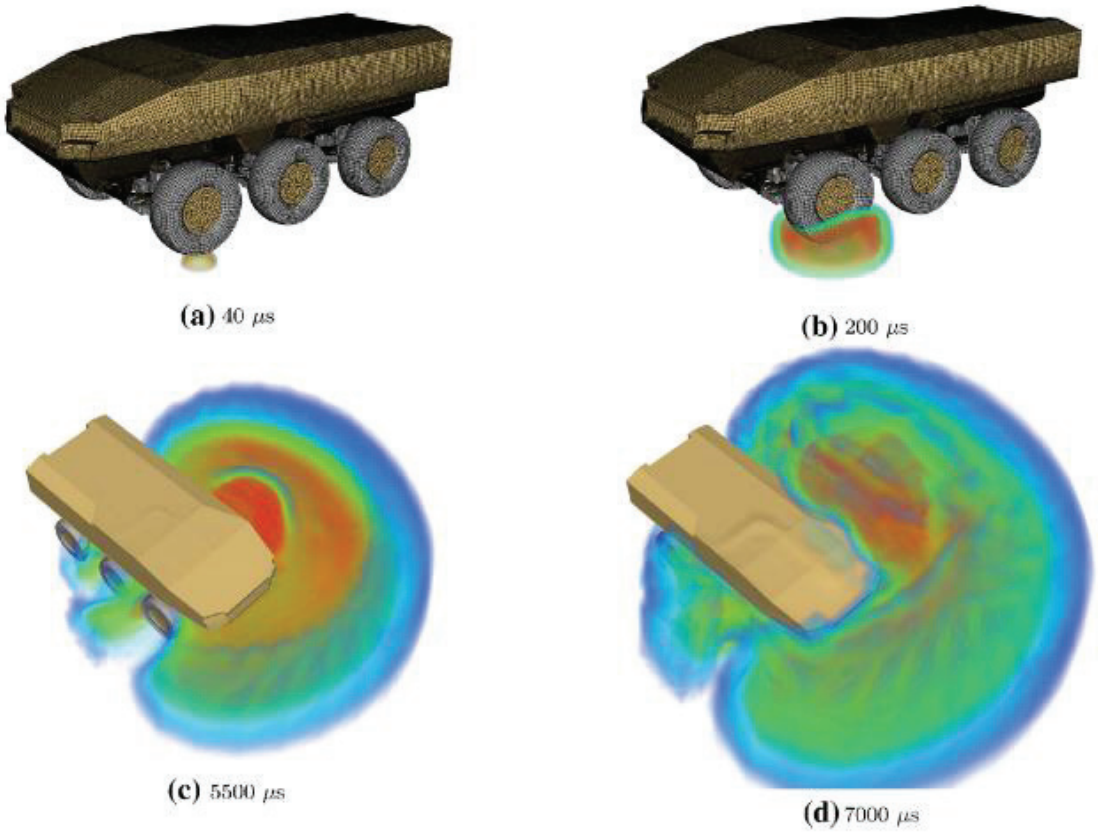

Figure 2.21. Illustration of advection in the hemispherical domain (Source: Kilic & Bedir, 2016).

As a result of literature review, blast response of structures differs greatly depending on specification of material and structures as well as boundary conditions. In sandwich structures, core member is designed to allow deformation thereby energy is absorbed taking into account possible threat level. Face sheet plates, especially the plate subjected to blast loading, should be designed as remain stable during the deformation to do their distribution of incident pressure duty, as contributing energy absorption capacity of sandwich structure even at low levels. In short, the blast performance of any blast resistant structure depends on not only structural and material properties but also the sort and magnitude of exposed load, face sheet plate parameters and boundary conditions. It is possible to design optimized blast resistant structure considering the whole limitations and conditions.

CHAPTER 3

MANUFACTURING AND EXPERIMENTAL DETAILS

This chapter mainly consists of two sub-sections which are material and manufacturing, and experimental details. In the first section, material properties and manufacturing method for induvial and sandwich specimens used in this study are explained. In the second section, material characterization and model, and experimental technique to evaluate dynamic response of the structures (Direct Pressure Pulse Experiment) are presented in detail.

3.1. Material and Manufacturing

3.1.1. Material

The balanus geometry introduced in this study comprises of two thin walled metallic structures. AISI 304L stainless steel was used as a production material for both constituent parts of balanus and face sheets of sandwich structure. The following facts make this material attractive to use in wide range of applications including structures that resist an explosion:

- Exhibition strain rate sensitive
- High ductility
- Excellent plastic formability
- Oxidization and corrosion resistance
- Having knowledge about how to machining in industry

AISI 304L stainless steel which comprises higher amount of chromium and lower amount of carbon is a stainless steel alloy. Grade 304L contains extra low carbon content than grade 304 which pertains for welding applications by diminishing carbide precipitation during the welding. Many examples of this material used in blast resistant

structures in the literature were emphasized in previous section. The chemical ingredients of AISI 304L stainless steel in terms of percentage by weight is presented in Table 3.1.

Table 3.1. Ingredients of AISI 304L stainless steel.

C (%wt)	Cr (%wt)	Ni (%wt)	Mn (%wt)
0.03	17.5-19.5	8.0-10.0	2.0

3.1.2. Manufacturing of Balanus and Sandwich Structures

The balanus geometry used in current study as core member of sandwich structure consists of two separate geometries, which are conical thin walled tube that is going to be termed as "Shell" and thin walled frusta with shallow spherical caps that is going to be termed as "Core" throughout subsequent sections. The balanus geometry is easily created by freely releasing of shell over core without requiring any manufacturing process. Shell encases to core structure thanks to its higher diameter in just the same way as bio-inspired Balanus creatures. The aim in this combination is that load carrying ability of core member of sandwich structure is to improve as creating an interface effect between shell and core. Core and shell geometries with dimension of its diameter and height and balanus geometry can be seen in Figure 3.1. Both of core and shell structures have same corrugation angle of 75°.

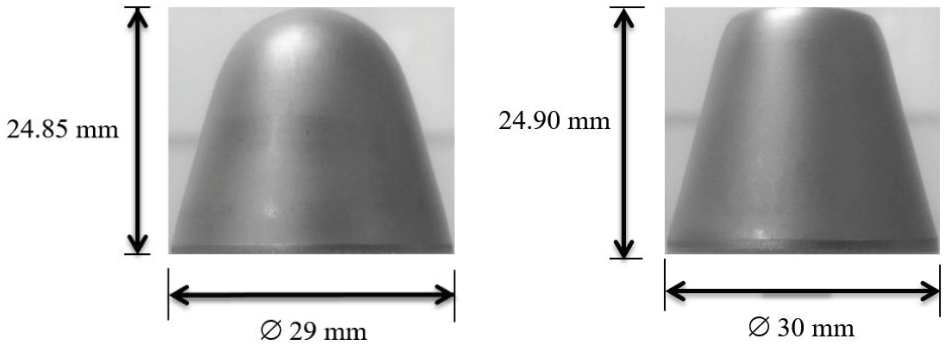

(a) (b)

Figure 3.1. Sample units of (a) core (b) shell, and (c) balanus.

(cont. on next page)

(c)

Figure 3.1. (cont.)

Core and shell were separately manufactured from circular sheet metal blank initially having thickness of 0.5 mm by using deep drawing process which is one of the cold forming methods. The process is also very convenient way for manufacturing of these type geometries besides enabling duplicate production and intentionally inducing work hardening. Work hardening on the structure resulted in plastic deformation occurs during the manufacturing process, which provides extra strength to the structure as improving its mechanical behavior. Shell and core geometries were manufactured into three steps including a drawn step, a redrawn step to intermediate shape, and trimming step to achieve the desired shape, as applying appropriate force and employing suitable punch and die apparatuses to prevent any manufacturing defects such as tearing and wrinkling. The manufacturing process is another significant quality as much as utilization of inspired geometry and material, which makes this study special. Detailed information about the manufacturing method can be found in related project report (Taşdemirci, Güden, Tüzgel, Akbulut, & Güzel, 2016).

In order to investigate dynamic response of sandwich structures, small scale sandwich structures which consist of two identical circular face sheets and core member were manufactured. Face sheets made of AISI 304L stainless steel were used to hold mechanical behavior stable. Core, shell and balanus geometries were separately sandwiched between face sheets having thickness of 3 mm and diameter of 75 mm. Face sheets were selected to be relatively thick, since it is desired core members are merely deformed in order to assert performance of core member. In the preparation of sandwich specimen, a template designed for this purpose was used to be positioned of core member in standardize and accurate manner. An adhesive based on epoxy is used to bond face

sheets and core members. Template and a prepared sandwich specimen can be seen in Figure 3.2.

(a) (b)

Figure 3.2. (a) Template for preparation sandwich specimens, and (b) A sample of balanus sandwich

3.2. Experimental Details

3.2.1. Material Characterization and Model of AISI 304L Stainless Steel

Material characterization is essential to acquire input parameters of material models that is going to be used in numerical study. Besides, determination of strain rate sensitivity of AISI 304L stainless steel is inevitable because proposed structure is going to be subjected to severe impulsive loads and the material exhibits strain rate sensitive behavior as emphasized previously. For this purpose, mechanical tension tests were conducted at low and high strain rates. While quasi static tension tests were carried out using tensile testing machine (Shimadzu AG-X 300 kN) pertinent to ASTM E8M-04 at quasi static strain rates (10^{-3}, 10^{-2}, 10^{-1} s^{-1}), dynamic tension tests were carried out using Split Hopkinson Tension Bar at high strain rates (1580 and 2235 s^{-1}). Testing equipment and related test specimens are presented in Figure 3.3.

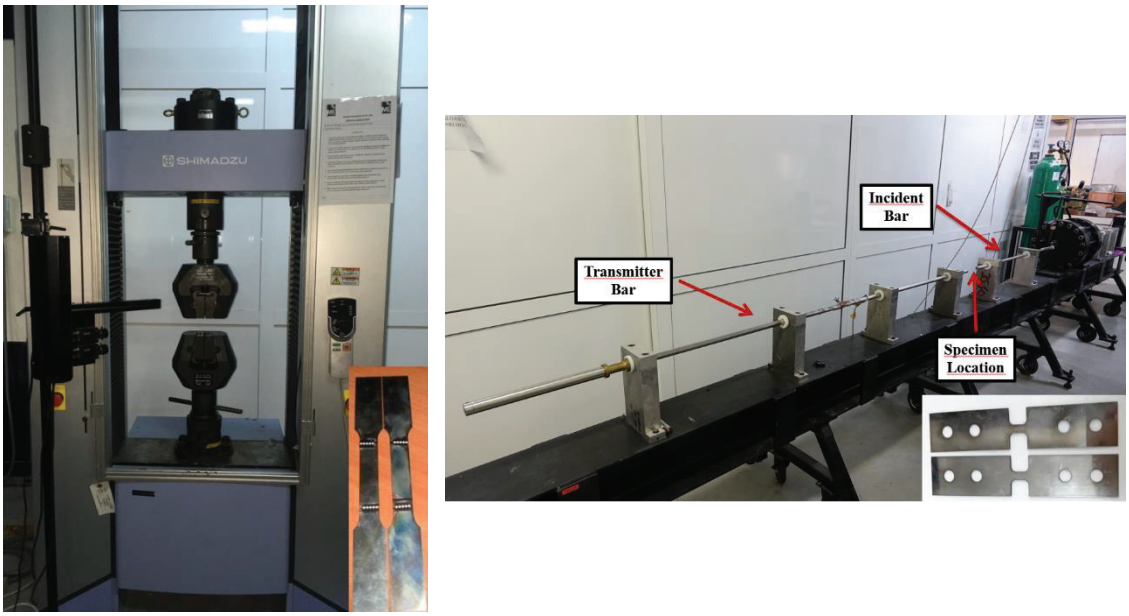

(a) (b)

Figure 3.3. Testing equipment with relevant test specimen, and (a) Tensile testing machine (b) Split Hopkinson Tension Bar

Split Hopkinson Tension Bar consists of striker tube, gas gun, transmitter and incident bars. Tension test specimen is fixed between incident and transmitter bar. A striker tube which is propelled by gas gun strikes to the incident bar, which creates a tension elastic wave on incident bar and propagates up to specimen. When this wave arrives to the specimen, some part of the wave is transmitted to transmitter bar and other part of the wave is reflected back to incident bar depending on acoustic impedance difference between bar and specimen materials. Stress waves were recorded employing strain gages located certain points on the transmitted and incident bars. Obtained voltage-time histories are then converted to dynamic stress-time and strain-time curves utilizing Hopkinson Pressure Bar stress wave theory. A typical voltage-time history acquired by strain gages can be seen in Figure 3.4.

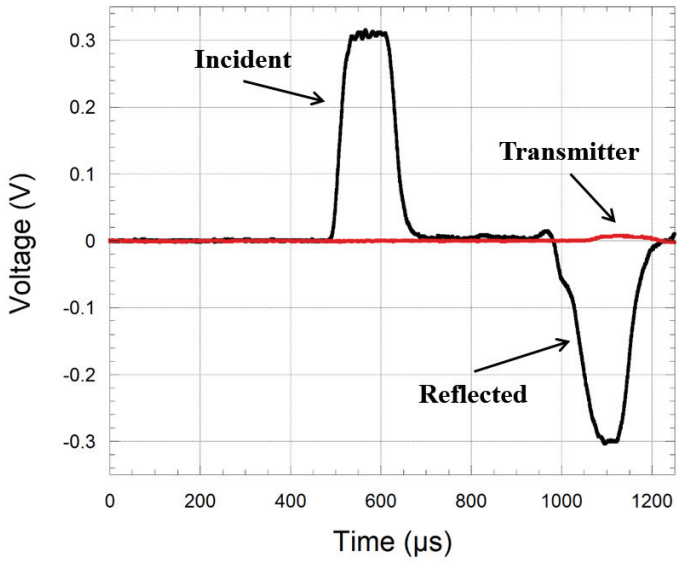

Figure 3.4. An example of voltage-time history for AISI 304L Stainless Steel

The true stress-plastic strain curves of used material at quasi static and high strain rates are presented in Figure 3.5. Strain rate effect can be clearly seen in this figure. Material model parameters are obtained by making use of at least square fit to these data points. Determined parameter are presented in Table 3.2 placed at the end of this section. Detailed information about the material characterization can be found in related project by Tasdemirci et al. (2016).

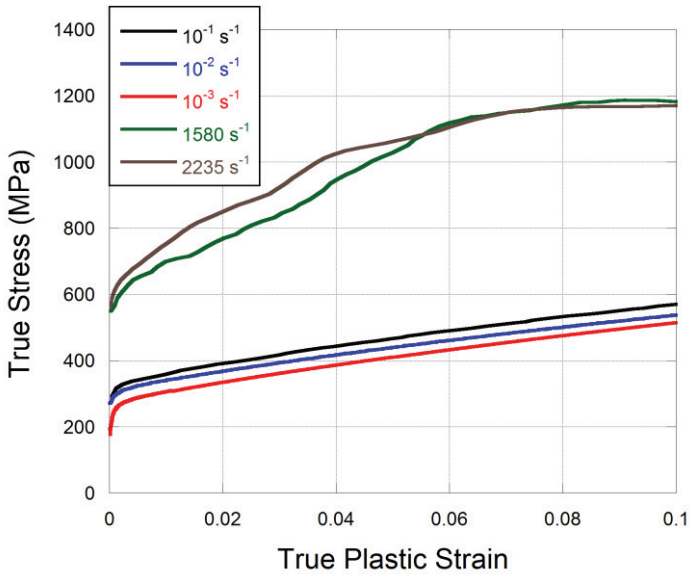

Figure 3.5. True stress-true plastic strain curves for high and quasi-static strain rates.

Material model selection is vital to represent mechanical behavior of materials in various conditions. In current study, Johnson Cook plasticity model was employed. Johnson Cook (JC) material model which has strain rate sensitivity, or viscoplasticity and temperature sensitivity material model is used to describe plastic behavior of materials (Johnson & Cook, 1983). When a structure which made of strain rate sensitive material is exposed to the blast loading, structure reveals different mechanical behavior at large plastic deformation due to the influence of inertia and strain rate. In addition, temperature rising without any heat transfer from outskirt (adiabatic condition) may cause material softening. The JC material model is more suitable as taking into account blast loading which terminated by large plastic deformation and temperature rising. AISI 304L stainless steel used in this study as base material is rate sensitive material as shown in literature survey in Chapter 2 so that JC material model is adopted to capture flow stress in plastic region. While flow stress can be calculated by Hooke's Law for the elastic region, flow stress in the plastic region can be properly represented by Johnson Cook constitutive material model as function of strain (ε), strain rate ($\dot{\varepsilon}$) and temperature (T), such that:

$$\sigma(\varepsilon,\dot{\varepsilon},T)=\begin{cases}\varepsilon E, & \varepsilon \le \frac{\sigma_0}{E}\left(1+C\ln\left(\frac{\dot{\varepsilon}}{\dot{\varepsilon}_0}\right)\right)\left(1-\left[\frac{T-T_r}{T_m-T_r}\right]^m\right)\\ (\sigma_0+B\varepsilon^n)\left(1+C\ln\left(\frac{\dot{\varepsilon}}{\dot{\varepsilon}_0}\right)\right)\left(1-\left[\frac{T-T_r}{T_m-T_r}\right]^m\right), & \varepsilon > \frac{\sigma_0}{E}\left(1+C\ln\left(\frac{\dot{\varepsilon}}{\dot{\varepsilon}_0}\right)\right)\left(1-\left[\frac{T-T_r}{T_m-T_r}\right]^m\right)\end{cases} \quad (3.1)$$

where T_r is the reference temperature which is generally room temperature, T_m is the melting temperature, σ_0 is yield stress at which the lowest strain rate and reference temperature, $\dot{\varepsilon}_0$ is the user defined reference strain rate which is generally the lowest strain rate, B is the strain-hardening coefficient and n and m is the strain-hardening and thermal softening exponents, respectively.

Johnson Cook damage model as a failure criterion was also taken into account through the study because of again presence of high plastic deformation in the blast phenomenon. When the damage parameter, D, is equal or larger than 1, fracture arises.

$$D=\sum\frac{\Delta\varepsilon_P}{\varepsilon_f} \quad (3.2)$$

where $\Delta\varepsilon_P$ is the increment in the plastic strain, ε_f is the fracture strain. Fracture strain is expressed as:

$$\varepsilon_f = \left[D_1 + D_2 e^{D_3 \sigma^*}\right]\left[1 + D_4\, ln\left(\frac{\dot{\varepsilon}}{\dot{\varepsilon}_0}\right)\right]\left(1 + D_5\left[\frac{T - T_r}{T_m - T_r}\right]\right) \tag{3.3}$$

in which D_1, D_2, D_3, D_4 and D_5 are damage constants, $\sigma^* = P/\sigma_{eff}$ is the ratio of pressure and effective stress. In the current investigation, D_2 and D_5 were set to zero so that the equation is reduced to following form:

$$\varepsilon_f = D_1\left[1 + D_4\, ln\left(\frac{\dot{\varepsilon}}{\dot{\varepsilon}_0}\right)\right] \tag{3.4}$$

Table 3.2. Determined JC material and damage model parameters
(Source: Taşdemirci et al., 2016)

ρ (kg/m^3)	**G (GPa)**	**E (GPa)**	**υ**	**A (GPa)**	**B (GPa)**	**n**	**C**
7830	80	193	0.305	0.218	1.905	0.879	0.11429
$D1$	**$D2$**	**$D3$**	**$D4$**	**$D5$**	**T_R (^{o}K)**	**T_m (^{o}K)**	**m**
0.85677	0	0	-0.01105	0	296	1698	1

3.2.2. Material Characterization of Polyurethane

A polyurethane material is used in direct pressure pulse experimental set-up, intended use of which is going to be explained in the following section. Polyurethane is a polymeric material which has 40 Shore A durometer hardness reveals nearly incompressibility. Material characterization of the polyurethane is also essential to construct numerical model of the experimental set-up. Therefore, material model parameters which acquired throughout material characterization of polyurethane were taken from related study performed by Tasdemirci et al. (2014).

3.2.3. Direct Pressure Pulse (DPP) Experiments

In order to assess dynamic response and deformation of sandwich structures with balan cores and their plates, a laboratory scale blast-like experiment, which creates pressure pulse in a relatively short time was used to simulate blast loading. The experimental setup consists of a gas gun, specimen holder (mold) corresponding to requirement, 2000 mm long transmitter bar, a 142 mm long striker bar and 46 mm long piston with a diameter of 75 mm, velocity measuring system, and data acquisition system including strain gauges, oscilloscope and a conditioner. A general view of experimental setup with unconfined mold is presented in Fig. 3.6.

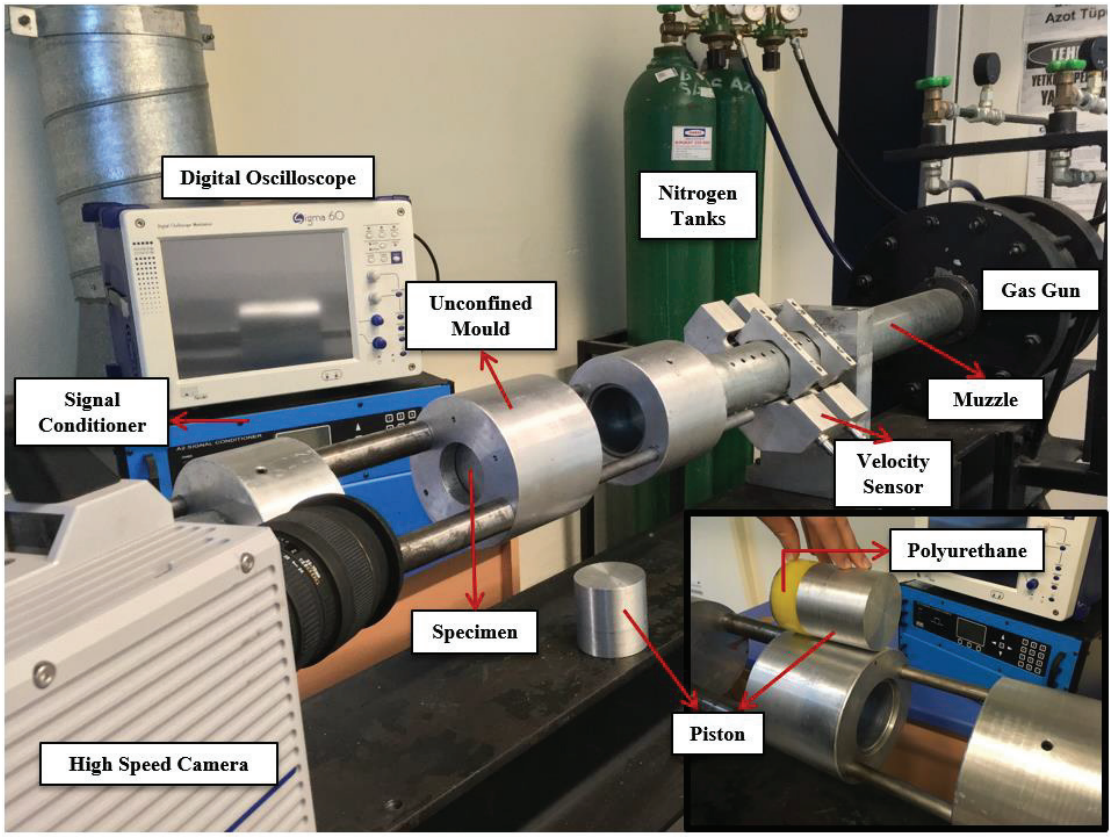

Figure 3.6. DPP experimental setup with unconfined mold and inside of the mold.

While confined mold (Figure 3.7) is used to ensure radial and back-face constraint of specimen as both translation and rotational constraints, unconfined mold is used to ensure radial and a part of back-face constraint as both translation and rotational constraints. The part of back-face constraint between specimen and specimen holder is provided with peripheral constraint having 1 cm width so that analogous of simply

supported boundary conditions have been acquired utilizing this mold. Unconfined mold provides not only defining specific boundary condition but also allowance to monitor deformation progression and failure formation of specimen using high speed camera. Opportunity of monitoring deformation is the one of the characteristic feature of this laboratory scale experiment because it is challenge to monitor deformation progression and to protect facilities due to blast wind including gas product, dust and rising temperature in explosive used experiments.

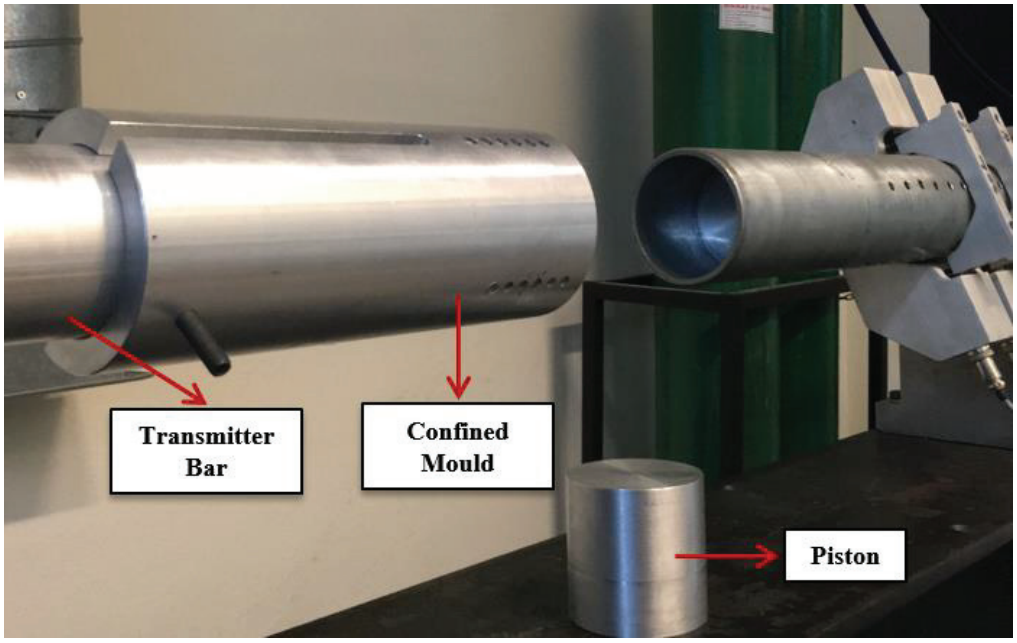

Figure 3.7. DPP experimental setup with confined mold

Experiments were separately conducted with two sets of experimental setup for sandwich structures and face sheet plates. The working mechanism of the typical experimental setup is that when the gas gun that is filled up with nitrogen is stimulated, the striker is accelerated through the gas gun muzzle and strikes to the piston with a high momentum. Piston was used to transfer to the pressure pulse and to avoid any collision or friction between specimen holder and striker. Because of having same diameter and same material, any impedance mismatch between piston and striker cannot be formed. Material properties of test setup is given in Table 3.3. Velocity is measured with laser velocity sensor which mounted on the end of the gas gun muzzle. Therefore, a test method which is non-explosive used blast-like controlled testing method had been employed.

Table 3.3. Some mechanical parameters of bar material.

Material	Density (kg/m^3)	Modulus of elasticity (GPa)	Poisson's ratio	Tensile yield strength (MPa)
7075-T6 Aluminum	2810	71.7	0.33	503

In order to implement one-dimensional elastic wave theory, whereas specimen is plastically deformed, the parts of experimental setup have to be just elastically deformed. Even though the bars were manufactured relatively large diameter, a critical impact velocity without any plastic deformation of striker has to be calculated corresponding to used material of the bars. The critical impact velocity (V_{cr}) was calculated using the following equations:

$$\sigma_y = \frac{1}{2}\rho C_0 V_{cr} \tag{3.5}$$

$$C_0 = \sqrt{\frac{E}{\rho}} \tag{3.6}$$

$$V_{cr} = \frac{2\sigma_y}{\sqrt{\rho E}} \tag{3.7}$$

where σ_y, C_0, E, and ρ are the yield stress, infinite wave velocity, elastic modulus and density of the bar material, respectively. The critical impact velocity (V_{cr}) was found as $V_{cr} = 71\ m/s$ using data given in Table 3.3 and the striker is able to provide kinetic energy up to 4443 J.

The transmitted pressure pulse from specimen to transmitter bar for each set of experimental setup was measured by two stain gauges attached the certain point on the transmitter bar. Strain history is recorded using an oscilloscope as voltage-time history ($\varepsilon_T(V)$) output and then converted to strain-time history (ε_T) by making use of full bridge strain gauge formulation. The bar stress (σ_T) was calculated considering elastically deformed of the bar. The transmitted force history (F_T) was acquired using stress history. Equations are sequentially presented as follows

$$\varepsilon_T = \frac{2\,\varepsilon_T(V)}{V_e\,G_g\,K_g\,(1+\upsilon)} \tag{3.8}$$

$$\sigma_T = \left(\frac{D_b}{D_s}\right)^2 E_b\,\varepsilon_T \tag{3.9}$$

$$F_T = \sigma_T\,A_b \tag{3.10}$$

where E_b, D_b and A_b are the modulus elasticity, diameter and area of the aluminum bar, respectively. D_s is the diameter of the specimen. V_e is the excitation voltage, G_g is the gain, and K_g is the gauge factor. In the experiments, 200 and 10 V were used as the gain and excitation voltage, respectively.

Experiments were conducted for face sheet plates using unconfined mold and polyurethane. Polyurethane is a material which has 40A durometer hardness reveals nearly incompressibility and was placed between piston and face sheet plate. Thanks to their incompressibility, a loading medium is produced in front of the plate. That is, the pressure pulse which created by hitting striker bar to the piston is transmitted to specimen through this medium.

CHAPTER 4

BLAST PHENOMENON AND FINITE ELEMENT MODELLING

In this chapter of the thesis, a general outlook on the explosion phenomena and blast modelling are presented. After exploration of the fundamentals of explosion, numerical details of the current study is explained. Material models for explosive, specimen and air are given with their equation of state in the finite element analysis section. Finite element analysis (FEA) is essential to achieve of some results that could not be acquired from experimental study such as Von Mises stress distribution through the deformation and experiments that cannot be conducted empirically such as crushing behavior of structures at constant and high velocities. In addition, FEA enables visualization, detailed analysis and insight of the simulated condition and/or structure in conjunction with being cost and time effective method.

4.1. Blast Phenomenon

Blast phenomenon is one of the most complicated phenomenon because of including non-linear physics and complexity of their empirical studies. The observation of responses of structures subjected blast loading is also more complicated. Therefore, investigation of blast nature is crucial prior to exploration their responses on the structure. Explosions result in systemic damage on the human body as distinct from collisions, which are respectively: 1) direct effect of overpressure on organs 2) striking shrapnel or projectiles on body which are mobilized by explosion 3) dispersing around and striking other objects of whole body due to blast wind 4) burning due to thermal effect of explosion (Bellamy & Mil, 1988; Hicks, Fertig, Desrocher, Koroshetz, & Pancrazio, 2010). Shock front of blast wave which is characterized by overpressure of explosion is the main destructive influence in the blast phenomenon. Duration of the blast wave is another significant parameter that enhances damage on the structure.

In details of blast wave, detonation wave at the center of explosive is created with ignition of explosive. Once the detonation wave owning detonation velocity (6800 m/s for TNT (Boschstrasse, 2015)) arrives to the boundary between explosive and air, it generates shock wave that thin overcompressed air layer forms and accelerates up to supersonic levels because of the low density and high compressibility of air. Then, blast wind which is high speed gas product of explosive follows shock wave by decaying their pressure because of movement of air and gas product. Therefore, blast wave can be explained by combination of shock wave and blast wind that generated by explosion (Cullis, 2001). The process is going to be repeated until explosive losses the whole energy because some detonation waves are going to be reflected boundary and another compressed shock wave is going to be generated (Neff & Fiume, 1999). In addition, reflected waves from ground will not be considered within scope of this thesis. Free air burst explosion, which shock wave propagates spherically from center of charge to outward in free air, is just taken account including only reflected wave from structure without amplification from ground (Figure 4.1). When the interaction between blast wave and structure is formed, some part of incident wave is transmitted, some part of it is absorbed and rest of it is reflected in compliance with acoustic impedance of materials. The main objective in the protection of personnel against blast wave is that transmitted wave to protected zone is to keep as possible as low levels and have a delay in the arrival time of the transmitted wave to the protected zone.

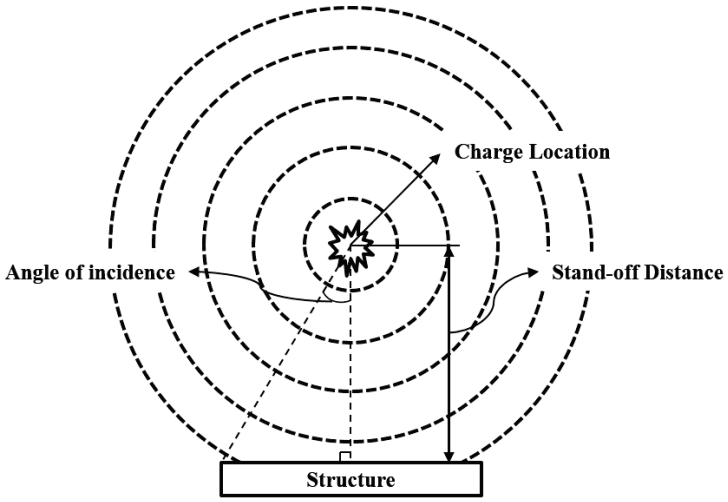

Figure 4.1. Free air burst explosion representation

A pressure profile that created free-field air blast includes three steps, which the sudden increase of pressure resulting from sudden energy release of explosives and exponential decay in millisecond within two phases which are positive and negative phases depending upon ambient pressure. This negative phase is mostly ignored due to relatively small influence compared to positive phase. In the reality, detonation properties and explosive types identify development and dissipation of blast wave so that the pressure profile which can be modelled by the Friedlander equation as a function of time may be used to idealize blast pressure profile (Figure 4.2(a)). A recorded typical free-field blast wave can be seen in Figure 4.2(b). Blast wave can be formed depending on their environment condition, as well as explosive type. A complex wave is characteristically formed by reflected wave caused diminishing and enhancement in some portion of the blast wave. Wave reflection is resulted from any medium alteration in parallel with acoustic mismatch between mediums. Shock wave in the form of overcompressed air layer was also illustrated with corresponding position in the pressure time history.

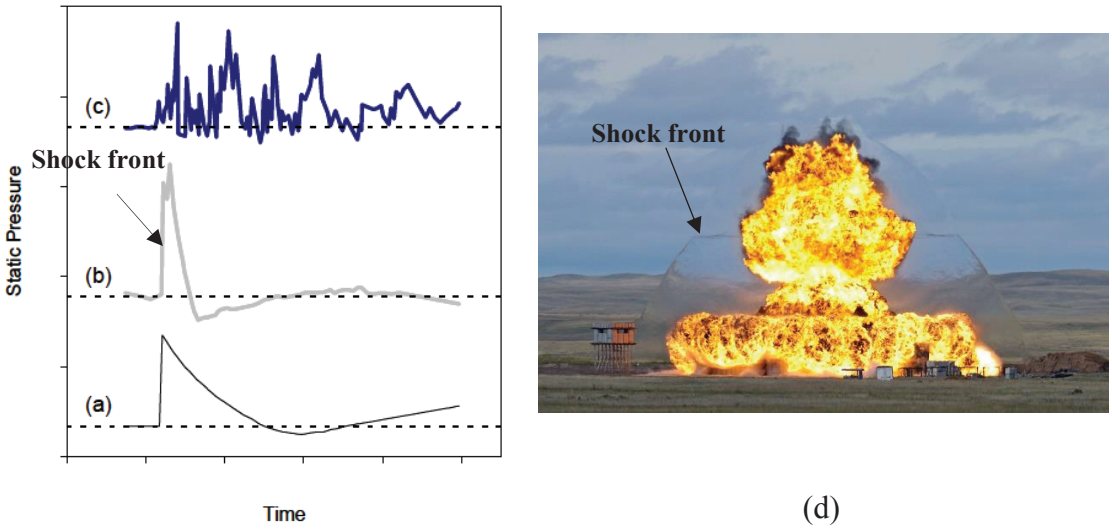

Figure 4.2. (a) Idealized Friedlander waveform (b) Typical free-field blast wave (c) Complex blast wave (Source: Committee on Gulf War and Health: Long-Term Effects of Blast Exposures, 2005), and (d) Shock wave propagation into the air (Source: www.drdc-rddc.gc.ca).

An ideal blast wave produced by free-field air burst without interaction other objects can be described Friedlander waveform (Figure 4.3) as aforementioned before. Incident pressure having shock front velocity arrives to a reference point at arrival time

along with its peak overpressure value. It afterward decreases exponentially because velocity of blast wind is less than that of shock front. After drop of pressure a level less than ambient pressure, ultimately pressure returns back ambient pressure.

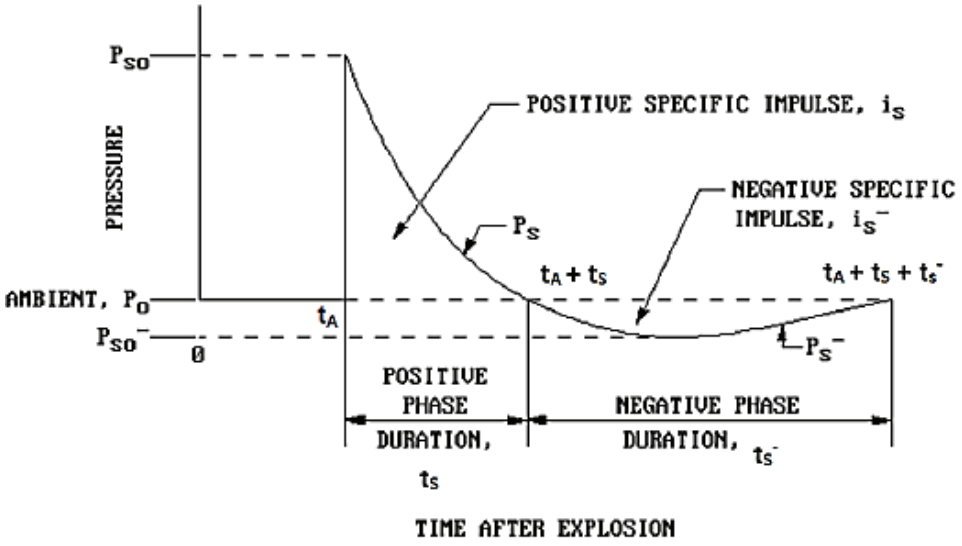

Figure 4.3. Friedlander waveform (Source: U.S. Army Corps of Engineers, 2008).

Incident pressure as a function of time can be mathematically described by making use of Friedlander equation such as:

$$p(t) = \begin{cases} P_0, & t < t_A \\ P_0 + P_{S0}\left(1 - \dfrac{t}{t_s}\right)e^{-\frac{bt}{t_s}}, & t_A \le t \le t_A + t_s \\ P_0 - P_{S0^-}\left(\dfrac{t}{t_{s^-}}\right)\left(1 - \dfrac{t}{t_{s^-}}\right)e^{-4\frac{t}{t_{s^-}}}, & t_A + t_s \le t \le t_A + t_s + t_{s^-} \\ P_0, & t_A + t_s + t_{s^-} \le t \end{cases} \tag{4.1}$$

where P_0 is the ambient pressure, P_{S0} and P_{S0^-} are the positive and negative peak overpressures respectively, b is the empirically determined fit parameter, t_s and t_{s^-} are the positive and negative phase durations respectively. While positive phase is effective in the time domain $t_A \le t \le t_A + t_s$, negative phase is effective in the time domain $t_A + t_s \le t \le t_A + t_s + t_{s^-}$.

Duration has significant influence as much as overpressure considered damage of them on the structure as mentioned before. To take into account these two parameters; therefore, the energy imparted on structure is determined by area under the pressure time

profile which is known as impulse either positive or negative phase. Even if duration of the negative phase is longer than positive one, negative phase can be ignored relatively low amount of their peak overpressure. Therefore positive specific impulse is:

$$i_s = \int_{t_A}^{t_A+t_s} [p(t) - P_0]\, dt \tag{4.2}$$

When incident pressure impinges to the structure on its travelling direction, it is promoted by subsequent blast wind and air particles which are in interaction with structure is reinforced depending on angle of incidence of blast wave. This reinforced pressure is termed as reflected pressure, P_r. Reflected pressure is almost greater than incident pressure due to reinforcement as shown in practical example in Figure 4.4. Reflected pressure was found twice stronger than incident pressure for the applied condition (150 g TNT, 2 m stand-off distance).

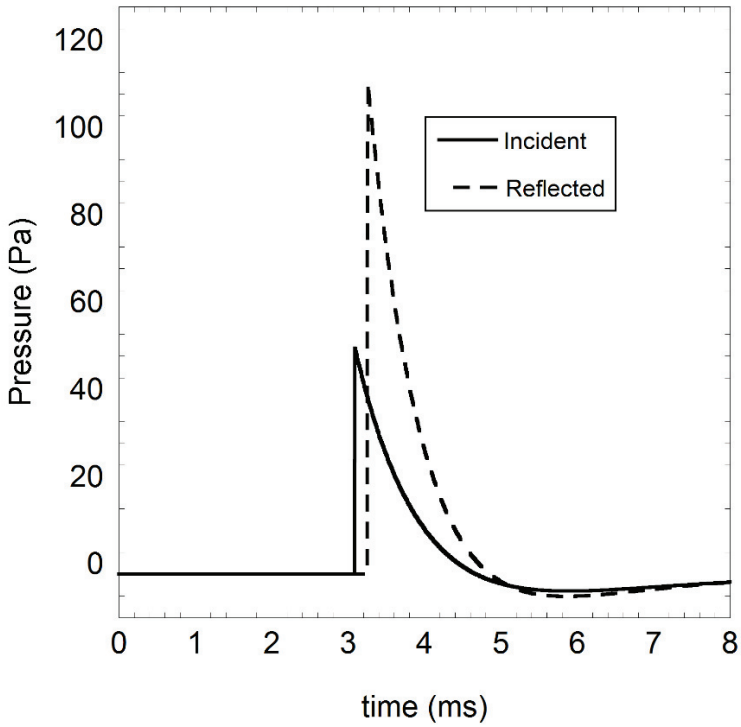

Figure 4.4. Comparison of incident and reflected pressures in practice.

4.1.1. Blast Scaling

In the blast phenomena, blast wave is basically characterized with two important parameters which are weight of charge and stand-off distance. To combine influence of these parameters into a relation, scaled distance relation is used. It also gives a general foresight about the quantity of explosion. Scaled distance is defined as follows:

$$Z = \frac{R}{W^{\frac{1}{3}}} \tag{4.3}$$

where R is the stand-off distance which is a distance between center of explosive and target, W is the equivalent weight of TNT. According to Hopkinson-Cranz scaling law or also called as cube-root scaling (Baker et al., 1985), when two different explosion condition having different weight of TNT, same explosive geometry and type in different stand-off distances and same environmental condition are implemented, equivalent blast waves that include same overpressure and scaled arrival time, positive phase duration and impulse can be obtained at same scaled distances as shown in Figure 4.5.

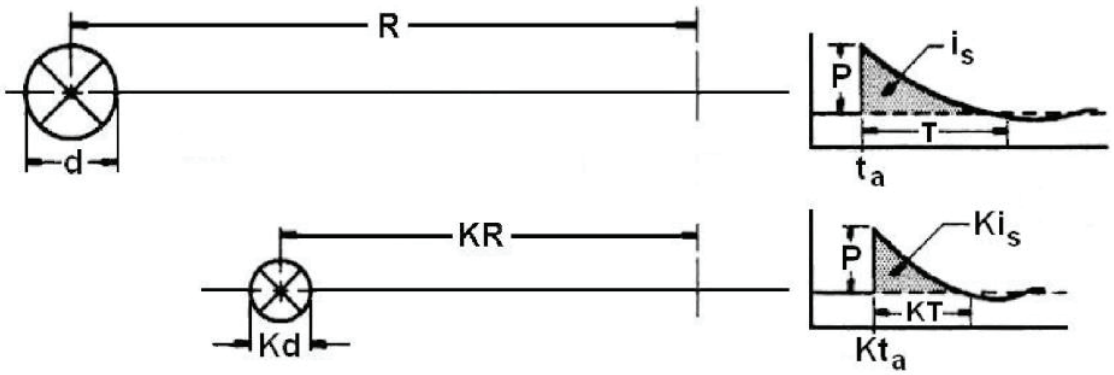

Figure 4.5. Representation of blast scaling (Source: Baker et al., 1985).

As a practical example of the scaled distance, two blast condition having same scaled distance (Z=3.764 m/kg$^{1/3}$) was used. Blast condition having 0.15 g equivalent weight of TNT and 0.2 m stand-off distance creates same influence in terms of peak overpressure with blast condition 150 g equivalent weight of TNT and 2 m stand-off distance (Figure 4.6). Scaled distance relation is useful to express some issues which both weight of charge and stand-off distance are particular importance. For instance, as scaled

distance increases, pressure of shock front decreases and positive phase duration increases due to the expansion of blast wave into air.

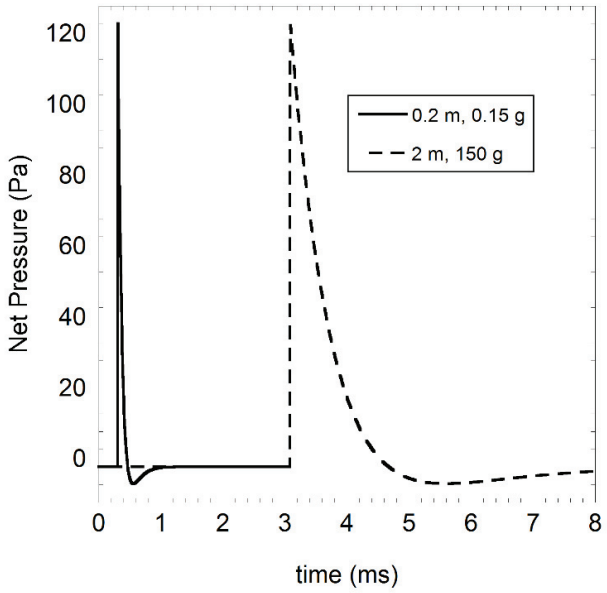

Figure 4.6. Representation of blast scaling in practice.

4.1.2. TNT Equivalency

TNT (Trinitrotoluen) is powerful chemical explosive compound which frequently used as main substance of IEDs and mines. TNT is used as a reference explosive among the whole explosives in blast phenomenon as well. Any explosive is explained in terms of amount of TNT equivalent so that there is a standard to express and measure of explosives. TNT equivalent of any charge of mass can be determined using conversion factors that calculated from ratio between Chapman-Jouguet detonation velocity of charge and TNT as in Eqn. 4.4 (LSTC, 2015). In the current thesis, explosive amount will be denoted TNT equivalent.

$$M_{TNT} = M \frac{DCJ^2}{DCJ_{TNT}^2} \tag{4.4}$$

where M_{TNT} and M are equivalent mass of TNT and concerned explosive mass. DCJ and DCJ_{TNT} are Chapman-Jouguet detonation velocity of concerned explosive and TNT. TNT equivalent and specific energy values of some explosives are tabulated in Table 4.1.

Table 4.1. TNT equivalent and specific energy values of some explosives (Source: Draganić & Sigmund, 2012).

Explosive Type	Specific Energy (kJ/kg)	TNT Equivalent
RDX (Cyclonite)	5360	1.185
HMX	5680	1.256
Nitro-glycerin (liquid)	6700	1.481
TNT	4520	1.000
60 % Nitro-glycerin Dynamite	2710	0.600
C4	6057	1.340

4.1.3. STANAG

STANAG (Standardization Agreement) is an agreement having standardization practiced by North Atlantic Treaty Organization (NATO) allies in the realm of military. STANAG involves standards which are knowledge sharing, process and testing of systems, conditions, etc. Protection level of armored vehicles according to certain conditions can be stated with NATO AEP-55, Volume 2 STANAG 4569 in terms of location of detonation, explosive mass and testing methodology due to requirements for evaluation of system itself and comparison systems among themselves (NATO, 2011). Therefore, armored vehicles can be denoted with their STANAG level.

Table 4.2. Protection levels corresponding to explosive mass (Source: NATO, 2011).

Level	Grenade and Blast Mine Threat		
4	4b	Mine Explosion under belly	10 kg (explosive mass) Blast AT Mine
	4a	Mine Explosion pressure activated under any wheel or track location	
3	3b	Mine Explosion under belly	8 kg (explosive mass) Blast AT Mine
	3a	Mine Explosion pressure activated under any wheel or track location	
2	2b	Mine Explosion under belly	6 kg (explosive mass) Blast AT Mine
	2a	Mine Explosion pressure activated under any wheel or track location	
1	Hand grenades, unexploded artillery fragmenting sub-munitions, and other small anti personnel explosive devices detonated anywhere under the vehicle.		

4.2. Finite Element Modelling

LS-DYNA, explicit finite element software package, was used through the numerical investigations. Since it is quite capable of non-linear dynamic and multi-physics problems that require explicit analysis as solving node by node. A computation loop based on stress-strain relation for each node at the time, n, as follows:

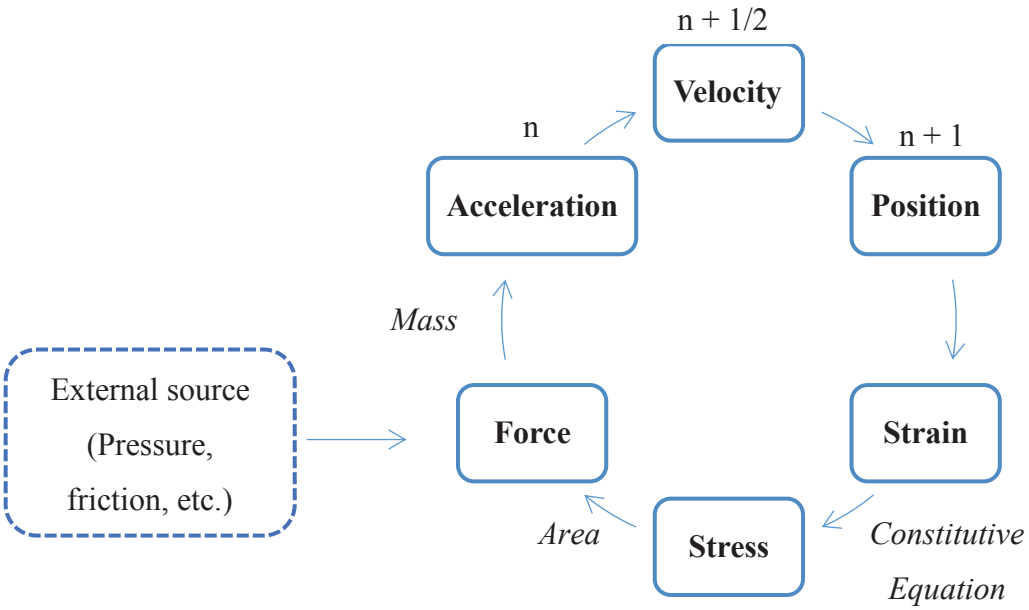

Figure 4.7. Computation steps for explicit analysis

In any Finite Element Analysis (*FEA*), two approaches are followed, which are implicit and explicit. Proper analysis method might be selected considering non-linearity stemming from contact, material and geometry of system and/or static/dynamic situations. While effect of inertia are not counted in static analysis, nodal forces related to inertia and damping effect must be considered in dynamic analysis. In implicit FEA, it is applied incremental route as updating stiffness matrix at the end of each incremental step (which can be based on increment of load or displacement). After each incremental step, a series of trial solutions such as Newton-Raphson iteration are applied to be able to equalize internal structure forces and external applied forces within a certain user defined tolerance. This method is not applicable when many step are required. Since the stiffness matrix is updated and reconstructed following iteration which causes costly analysis. In explicit FEA, it is again applied incremental route as updating stiffness matrix based on geometrical and material changes. Next increment load or displacement is implemented

to updated system. If increments are selected small enough, the result will be accurate but this is time consuming. Therefore, explicit analysis is more suitable as mentioned before when considered non-linear dynamic problem depending upon time resulted from non-linearity of force, contact and material and very short transient situation (blast loading) requiring very small time step.

It must be guaranteed that the time step is lower than the Courrant time step to prevent inaccurate solutions in the explicit analysis. Critical time step (Δt) for solid shell element is (Hallquist, 2006):

$$\Delta t = \frac{V}{cA_{max}} \tag{4.5}$$

where V is the characteristic element volume, c is wave speed in plane stress condition, and A_{max} is area of the largest side.

$$c = \sqrt{\frac{E}{\rho(1-v^2)}} \tag{4.6}$$

where E, ρ, and v are elastic modulus, density, and Poisson's ratio of element material, respectively.

The energy concept has particular significance because blast loading is mainly mitigated through the plastic deformation resulted with increasing internal energy and heat dissipation of absorbing structure. Energy relation based on energy conservation in the LS-DYNA is (Hallquist, 2006):

$$E_{kin} + E_{int} + E_{si} + E_{rw} + E_{damp} + E_{hg} = E^0_{kin} + E^0_{int} + W_{ext} \tag{4.7}$$

where E_{kin}= current kinetic energy, E_{int}= current internal energy, E_{si}= current sliding interface energy (including friction), E_{rw}= current rigid wall energy, E_{damp}= current damping energy, E_{hg}= current hourglass energy, E^0_{kin}= initial kinetic energy, E^0_{int}= initial internal energy, W_{ext}= external work.

In the above equation, left hand side gives the total energy, E_{total}. Work done in permanent deformation and elastic strain energy are given in internal energy. The

individual energy terms in the energy relation can be acquired with activation of GLSTAT in DATABASE_OPTION including ASCII files. Energy relation should be always provided during the calculation. Inspection of calculation can be done via energy ratio presented in LS-PrePost which enables pre and post analyses of the model. Energy ratio (Hallquist, 2006) is expressed by

$$eratio = \frac{E_{total}}{E^0_{total} + W_{ext}} \tag{4.8}$$

4.2.1. Specimen Preparation and Structural Material Model

Shell and core geometries, that is constituent of balanus structure, were created utilizing their numerical model of manufacturing process which is deep drawing process. The purpose of this step is to catch thickness variation and initial stress/strain of the structures such that of real one in order to properly simulate structural behavior of geometries. Blank having constant thickness of 0.5 mm is created using Belytschko-Tasy shell element with five integration points through the thickness. Manufacturing steps were then applied using proper die and punch. Therefore, numerically created specimens that includes residual stress, plastic strain and thickness variation were used as component of sandwich structures through the study. Detailed information about the numerical modelling of manufacturing method can be found in related project by Tasdemirci et al. (2016).

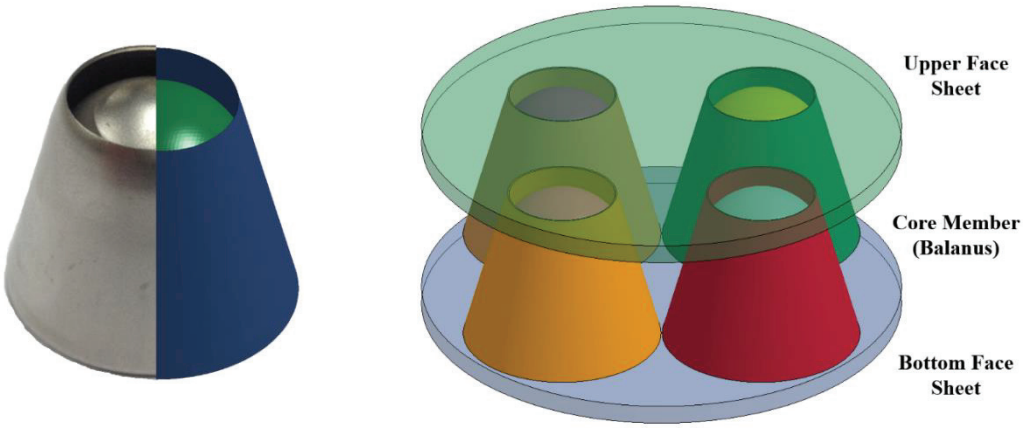

(a) (b)

Figure 4.8. (a) Combined view of numerical model and balanus, and (b) A sample of numerically created balanus sandwich.

Johnson Cook (JC) material model, which is appropriate for most metallic material that subjected to high rate deformation, is used as structural material model to model the flow stress of AISI 304L stainless steel material as emphasized before. In the LS-DYNA, MAT_SIMPLIFIED_JOHNSON_COOK material model was used for sandwich plates because of having relatively higher thickness so that damage could be neglected, while MAT_JOHNSON_COOK material model was used for modelling of balanus structure through the investigation. Simplified JC material model is applicable when the thermal effects and damage are negligible. It is also more efficient in terms of calculation time than JC material model. A fully viscoplastic formulation was implemented for both material models. JC parameters which empirically determined through the material characterization were previously presented in Table 3.2.

4.2.2. Direct Pressure Pulse Experiment Modelling

Direct pressure pulse (DPP) experiment set-up and conducted experiments were also modeled. This modelling aims two stuffs: (i) Validation of material model at higher strain rates and (ii) Acquisition of data that cannot be obtained from experimental results. To do this, validation can be performed with deformation amount and mode of structures, and/or comparison of force-time histories. The numerical model of the DPP testing configurations are presented in Figure 4.9. The components of the experiment apparatus were modelled with MAT_ELASTIC material model. MAT_SIMPLIFIED_RUBBER_WITH_DAMAGE material model was used for modelling of polyurethane material. All sliding parts were constrained in all directions except transitional motion in the z-direction. Initial velocity of the striker bar was chosen according to measured data in the experiment and defined by VELOCITY_GENERATION card. All surfaces in the contact were defined with AUTOMATIC_SURFACE_TO_SURFACE contact algorithm, while ERODING_SINGLE_SURFACE contact algorithm for specimens was used for observing erosion in experimental result. Static friction coefficient was assigned as 0.3, while dynamic friction coefficient was assumed 0.2 in predefined contacts. Striker and transmitter bar, holders and piston were modelled with constant stress solid hexahedra elements in which element formulation is very efficient and accurate.

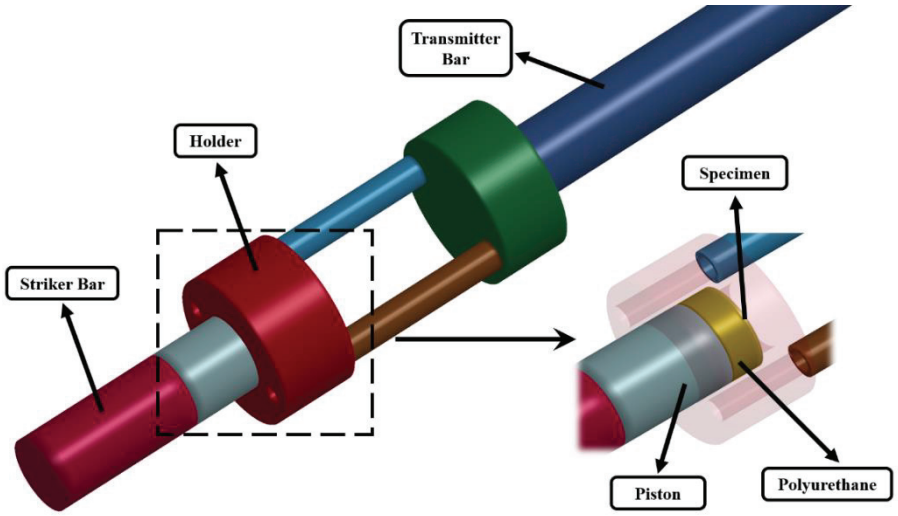

(a)

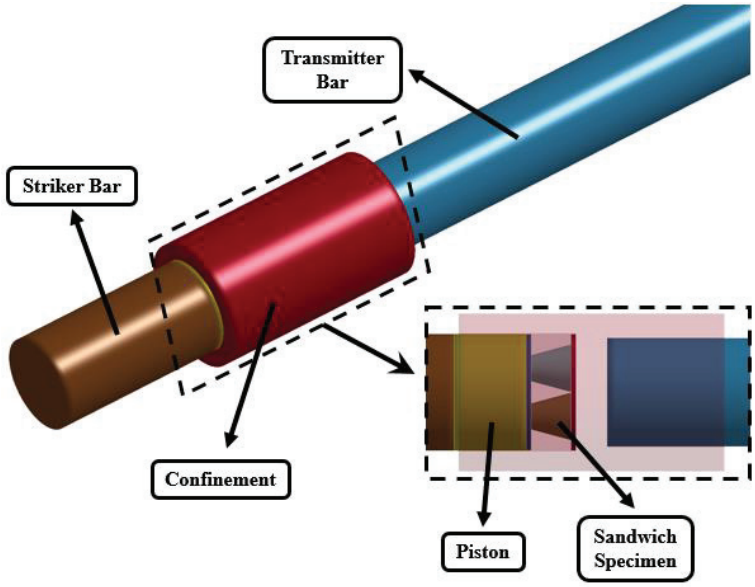

(b)

Figure 4.9. Numerical model of DPP experiment set-up with (a) unconfined holder, and (b) confined holder.

4.2.3. Blast Modelling

In the blast modelling, three different approaches can be employed. Two of them, which are the main approaches, are termed according to their mesh definitions, which are pure Lagrangian and Arbitrary Lagrangian Eulerian (ALE) approaches. Other one is the hybrid method in which pure Lagrangian and ALE methods are coupled.

4.2.3.1. Pure Lagrangian Approach

This approach included just modelling of structures without modelling any explosive or fluid domain is an engineering approach required a few inputs so as to investigate blast response of structure. Imaginary material points and nodes are overlapped and deform simultaneously in the Lagrangian mesh definition; therefore, the position of imaginary material points compared with node does not changed. Also, material passing between elements does not allowed. If the convenient element size is selected, Lagrangian formulation is applicable for structural deformation having relatively lower strains because of mass conservation of each element. Severe mesh distortion may occur in the presence of large strains because of overlapping nodes and material points. Blast loading is applied on the structure via a blast prediction function such as CONWEP function. Blast wave parameters, i.e. incident and reflected pressures, which are used in CONWEP algorithm are found with an analytical fit developed by Kingery and Bulmash (1984) through many empirical blast data of TNT for spherical burst and hemispherical surface burst.

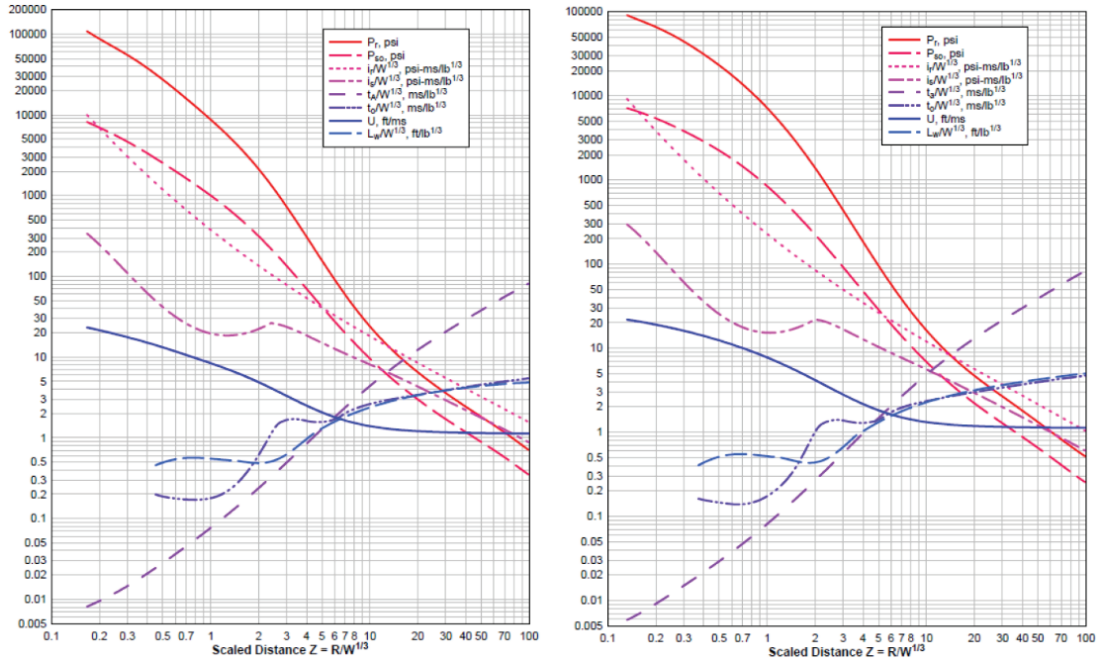

(a) (b)

Figure 4.10. Positive phase parameters for free air burst explosion at sea level using (a) Hemispherical, and (b) Spherical charge (Source: U.S. Army Corps of Engineers, 2008).

Revised version of the graphical representation of these empirical blast data published, Army TM 5-1300 handbook, by US Army Crop Engineers (2008) is presented in Figure 4.10. It provides overpressure, reflected pressure, duration for positive phase corresponding to a certain scaled distance.

CONWEP algorithm was imbedded in LS-DYNA by Randers-Pehrson and Bannister (Randers-Pehrson & Bannister, 1997) as considering angle between imaginary line from center of the explosive to integration point and the normal of the affected surface; therefore, net pressure acting on the each section of predefined segment in CONWEP algorithm is:

$$P(t) = \begin{cases} P_r(cos^2\theta) + P_i(1 + cos^2\theta - 2\,cos\theta), & cos\theta \geq 0 \\ P_i, & cos\theta < 0 \end{cases} \quad (4.9)$$

where θ is incidence angle of blast loading, P_i is incident pressure and P_r is reflected pressure (Randers-Pehrson & Bannister, 1997). *LOAD_BLAST_ENHANCED card in LS-DYNA is used to generate this blast pressure caused by detonation of conventional explosives in the air in cooperation with *LOAD_BLAST_SEGMENT_SET defines segment that is interacted with blast loading. Input parameters in the card are equivalent mass of TNT, charge locations, blast source type and selection of negative phase insertion.

Even though this approach is the most efficient way in terms of total CPU time and the simplest method for implementation, some limitations are available:

- It is inappropriate for complicated geometries which include objects caused shadowing and confinement effects (Randers-Pehrson & Bannister, 1997).
- Particular range of scaled distance is accepted due to the limitation of empirical data. The available scaled distance ranges are 0.178 m/kg$^{1/3}$ < Z < 40 m/kg$^{1/3}$ for the hemispherical surface burst and 0.147 m/kg$^{1/3}$ < Z < 40 m/kg$^{1/3}$ for the spherical air burst (LSTC, 2015).
- TNT equivalence is sometimes inadequate to capture explosive outcomes, i.e. incident pressure varies with scaled radius from charge. For instance, it varies from 0.7 to 1.8 for PETN explosive (Hargather & Settles, 2007).

- It is recommended that stand-off distance is bigger than three times of radius of explosive to acquire reliable results (Schwer, Teng, & Souli, 2015).

Pure Lagrangian approach accompanied by CONWEP algorithm in LS-DYNA gives reasonable results in the conditions apart from limitations. Many researchers found out that experimental results were in good agreement with numerical result implemented CONWEP algorithm as stated in Chapter 2.

4.2.3.2. Arbitrary Lagrangian Eulerian (ALE) Approach

ALE approach provides realistic scenario and includes fluid-structure interaction by modelling explosive, surrounding fluid and structure. Lagrangian formulation based on control mass is inappropriate when large strain (e.g. blast wave propagation into air) is existed because mesh distortion which causes exceedingly reduction of time step arises. Eulerian formulation based on control volume is more proper in these type applications where fluid flow and containment of multi-materials into control volume is permissible. Coordinates of material points vary with time in Eulerian formulation. Also, material motion between elements are allowed. Mesh distortion does not occur because of fixing mesh. However, container domain should be selected as large as possible to meet required condition. In addition, application of boundary condition is hard because imaginary material points and boundary nodes may not be coincided.

In the ALE formulation, Eulerian and Lagrangian formulations are combined taking advantages both of them. Unlike Eulerian formulation, control volume moves in space arbitrarily, hence advection amount of material in the control volume differs because of movement of the control volume (Figure 4.11). Modelled structure with ALE formulation in the LS-DYNA is firstly deformed as Lagrangian, then state variables of elements are advected by following mesh rezoning.

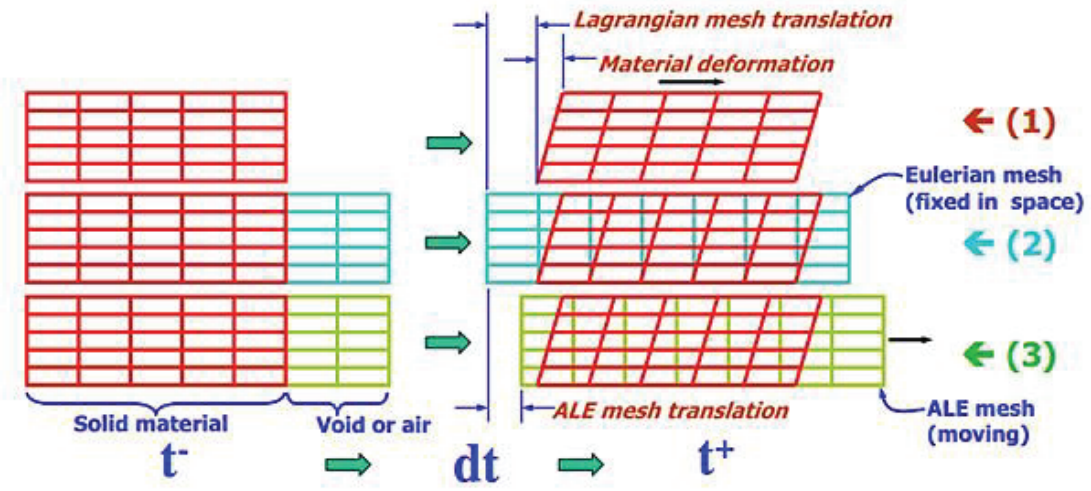

Figure 4.11. Three different mesh definitions: (1) Lagrangian (2) Eulerian, and (3) ALE (Source: Do & Day, 2005).

The drawbacks of this approach when compared to the pure Lagrangian approach: (i) ALE requires a lot more input as modelling component of blast loading process such as constitutive relations, equation of state and coupling parameters. Selection and tuning of these parameters are substantially time consuming process. (ii) ALE is very expensive in terms of total CPU time, and is not suitable for higher stand-off distances because as increasing standoff distance, required air domain also increased so that computational time increases significantly. On the other hand, the fairly distinctive features of this approach can be listed as: (i) Explosive is separately modelled without any restrictions relevant to shape and type of explosive. (ii) Coupling between fluid and structure can be modeled. (iii) There is no limitation on the scaled distance theoretically. (iv) Constitutive behavior of the explosive and fluid can be modeled thanks to usage of equation of state.

In this study, structural elements were modeled as Lagrangian element, while air and explosive elements were modeled as Eulerian element. Explosive and air were defined with Multi Material ALE (MMALE) in which air domain is able to comprise both air and explosive material. Advection of the explosive material was controlled with Van Leer and half index shift having second order accurate advection scheme. Explosion medium and container geometry type were defined by INITIAL_VOLUME_FRACTION_GEOMETRY card. To capture shock front behavior precisely, mesh smoothing for shock waves was implemented. Coupling between explosive and structure were defined by CONSTRAINED_LAGRANGE_IN_SOLID card where coupling type and direction are defined and leakage control is ensured. Penalty based coupling between master (ALE structures) and slave (Lagrangian structure) parts

was used to converse energy. Air domain was selected as a spherical domain because the explosive in the current study is spherical as well. The domain is then meshed to make certain advection of the material properly using HyperMesh meshing software. As depicted Greer, this is because advection is realized only in the surface normal direction of the element (Greer, 2006). Air domain size is selected based on the study by Trajkovski which is minimum mesh design criteria as stand-off distance plus four times explosive radius ($R+4R_{TNT}$) (Trajkovski, Kunc, Perenda, & Prebil, 2014). Numerical model was reduced to 1/8 model because of symmetry. Proper boundary conditions for symmetry planes and non-reflecting boundary condition for free surface were applied as shown Figure 4.12.

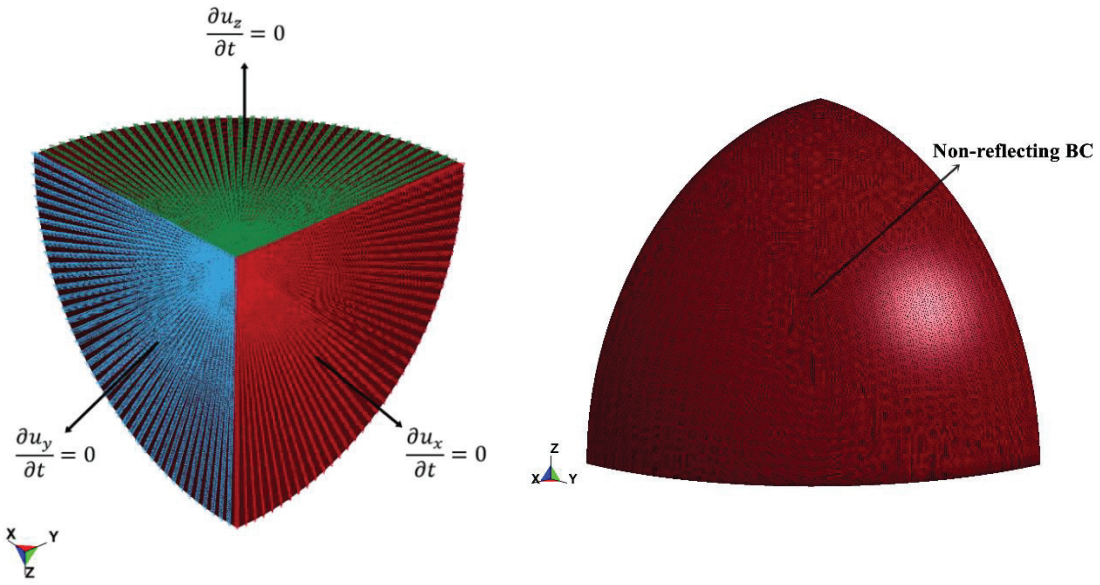

(a) (b)

Figure 4.12. (a) Interior surfaces assigned symmetry boundary conditions, and (b) Exterior surface assigned non-reflecting boundary condition.

Cubic region was placed in the center of spherical domain to prevent element distortion resulted from reducing interior angle. Cubic region size was selected considering radius of explosive. Cubic region can be seen in Figure 4.13. Eulerian mesh movement was controlled via ALE_REFERENCE_SYSTEM_GROUP so as to be adapted the mesh to propagation of shock wave.

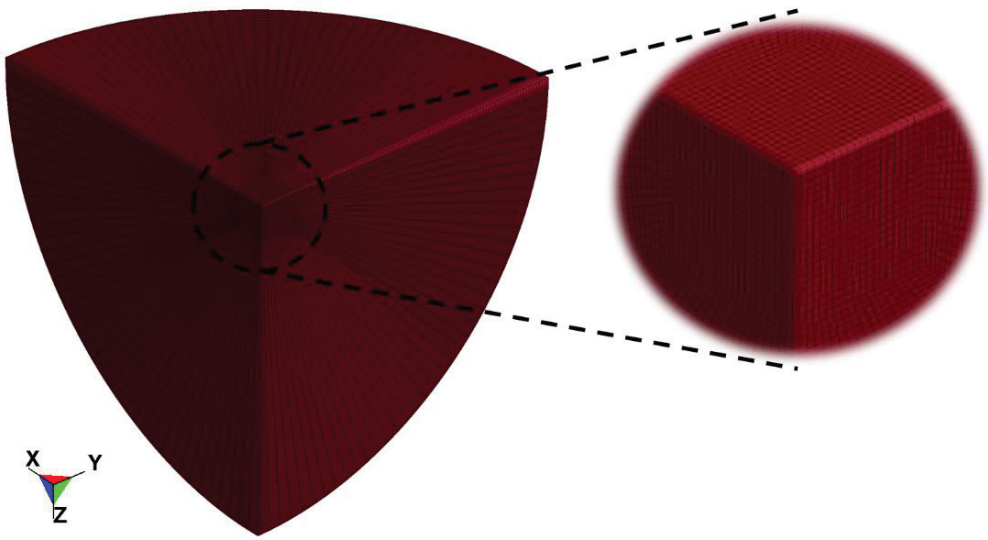

Figure 4.13. Cubic region in the air domain

Material models and Equation of State (EOS)

In order to simulate typical behavior of explosive and air used in this study, equation of state that describes mathematically relationship between state variables (pressure, specific volume, etc.) was used. Two different EOS were employed in the blast modelling. Air is modelled using MAT_NULL material model coupled with linear polynomial EOS and assumed as an ideal gas. The pressure, P, is described in LS-DYNA as (LSTC, 2015):

$$\mathrm{P} = C_0 + C_1\mu + C_2\mu^2 + C_3\mu^3 + (C_4 + C_5\mu + C_6\mu^2)\,\mathrm{E} \tag{4.10}$$

where $C_0, C_1, C_2, C_3, C_4, C_5$ and C_6 are constants, E is the internal energy per unit volume. $\mu = \rho/\rho_0 - 1$, ρ is the current density and ρ_0 is the initial density stated in the MAT_NULL card. Applying gamma law equation of state, therefore, $C_0 = C_1 = C_2 = C_3 = C_6 = 0$ and $C_4 = C_5 = \gamma - 1$. Gamma,γ, is the ratio between specific heats ($\mathrm{C_P}/\,\mathrm{C_V}$) in here. Then, pressure for an ideal gas is calculated by:

$$\mathrm{P}\,(\rho, \mathrm{E}) = (\gamma - 1)\left\{\frac{\rho}{\rho_0}\mathrm{E}\right\} \tag{4.11}$$

TNT explosive was used through the investigation because it reveals pretty ideal behavior with regard to blast wave formation and propagation (Philips et al., 1994). The

material is modelled as high explosive with MAT_HIGH_EXPLOSIVE_BURN material model in company with Jones, Wilkins and Lee (JWL) equation of state. The pressure, P, is expressed as a function of initial internal energy per volume, E, and relative volume, V, as that:

$$P = A\left(1 - \frac{\omega}{R_1 V}\right)e^{-R_1 V} + B\left(1 - \frac{\omega}{R_2 V}\right)e^{-R_2 V} + \frac{\omega E}{V} \quad (4.12)$$

where A, B, R_1, R_2 and ω are the empirically determined coefficient for a particular explosive.

Table 4.3. TNT properties used in the explosive modelling (Source: Toussaint, Fortier, & Dumas, 2012).

ρ_0 (kg/mm^3)	D (mm/ms)	P_{CJ} (GPa)	A (GPa)	B (GPa)	E_0 (GPa)	R_1	R_2	ω	V_0
1.63 10^{-6}	6930	21	371.213	3.231	7	4.15	0.95	0.3	1

ρ_0, D and P_{CJ} are the input parameters of the material model and initial density, detonation velocity and Chapman-Jouguet detonation pressure, respectively.

4.2.3.3. Hybrid Method

Another method of simulating air blast is the hybrid method in which pure Lagrangian and ALE methods are coupled. In this method, explosive is not modelled explicitly. Instead of this, blast loading is applied onto predefined thin an ambient layer adjoining to air domain and calculated using ConWep in the LOAD_BLAST_ENHANCED card as such in pure Lagrangian approach. Created blast wave on the ambient layer propagates into air surrounding structure and eventually impinges over the structure. Outstanding features of this method are providing computational time saving, especially in circumstances including longer stand-off distances, because of reduction of the air domain and elimination of shadowing effect, which are two drawbacks of ALE and pure Lagrangian approaches as emphasized before. However, rest of the drawbacks of both approaches remains in this method even if strengths of the each approach are retained. In construction of the model, all the

parameters involving material and EOS definitions for air, coupling between Lagrangian and ALE elements, advection scheme, boundary conditions, etc. are identical with ALE approach. Air can be modelled as rectangular shape instead of spherical one because explosive is not modelled. The main drawback of this method is to assign certain distance between ambient layer and structure surface which do not form any reflection from surface. Since calculated pressure by ConWep algorithm already involves reflected pressure influence.

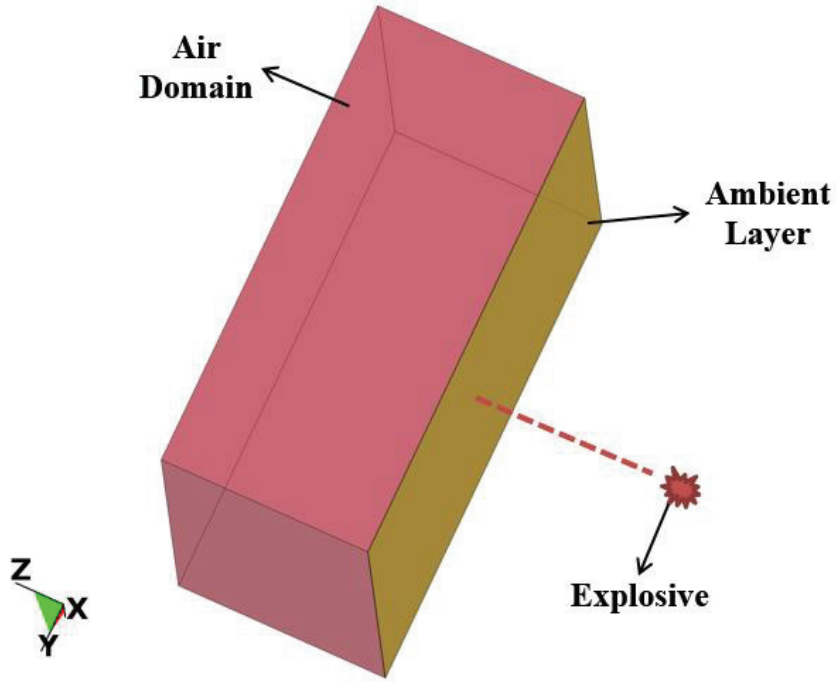

Figure 4.14. Illustration of the hybrid method (Explosive was attached to figure for visualization purpose only).

4.2.4. Calibration Study

In order to find equivalent free air blast condition corresponding to the experiments conducted by DPP testing, calibration study was done considering deformation of plates which is main component of sandwich structures. It is possible to find out the TNT mass and stand-off distance which create similar deformation with that of experiment. AISI 304L stainless steel circular facesheets of sandwich structures having thickness of 3 mm and diameter of 74.3 mm were used to calibrate blast models and DPP test model having unconfined mold. As can be seen in Figure 4.6, a specimen holder was created in all blast models to fulfil the boundary conditions similar to those of unconfined

mold in DPP testing and it was constrained in the whole directions as presuming rigid. Therefore, TNT mass and stand-off distance were empirically found as 40 g and 65 mm respectively, which correspond to experiment resulted of 36.75 m/s impact velocity. These blast parameters were determined by considering scaled distance theory due to the relatively small effective area of the specimen and reducing computational cost. Moreover, parameters used in ALE and hybrid approaches were tuned as accepting ConWep solution as a benchmark. Since this case is out of the whole imposed restrictions when considered limitations. Therefore, mesh convergence study was firstly carried out in which plate was meshed as butterfly mesh as increasing element number per side with a mesh refinement ratio (r) of 1.4. Simulation results in terms of center deflection of the plate were tabulated in Table 4.4. Blast loading was simulated for 25 g TNT and 65 mm stand-off distance using pure Lagrangian approach. It was made use of Grid Convergence Index (*GCI*) with constant grid refinement ratio by Roache (1998). GCI based on three finest responses was implemented in convergence analysis such as:

$$p = \frac{\log\left(\frac{F_3 - F_2}{F_2 - F_1}\right)}{\log r} \tag{4.13}$$

$$F_E = F_1 + \frac{F_1 - F_2}{r^p - 1} \tag{4.14}$$

where F_i is interested response corresponding to i^{th} mesh, F_E is the estimated final value and p is the order of convergence.

Table 4.4. Center deflection results of circular plate

i^{th}	Number of element per radius	Max. Center Deflection of Plate, F_i (mm)
1	32	3.9301
2	23	3.9224
3	17	3.9126
4	12	3.8225
5	8	3.6894

As taking into account three finest meshes and maximum center deflection of plate as interested response, it was found that order of convergence, p, is 0.717 and estimated

final value, F_E, is 3.958 mm. Second finest mesh that approximately corresponds to 1.6 mm element size was chosen as considering computational time of ALE method with 0.9 % relative error.

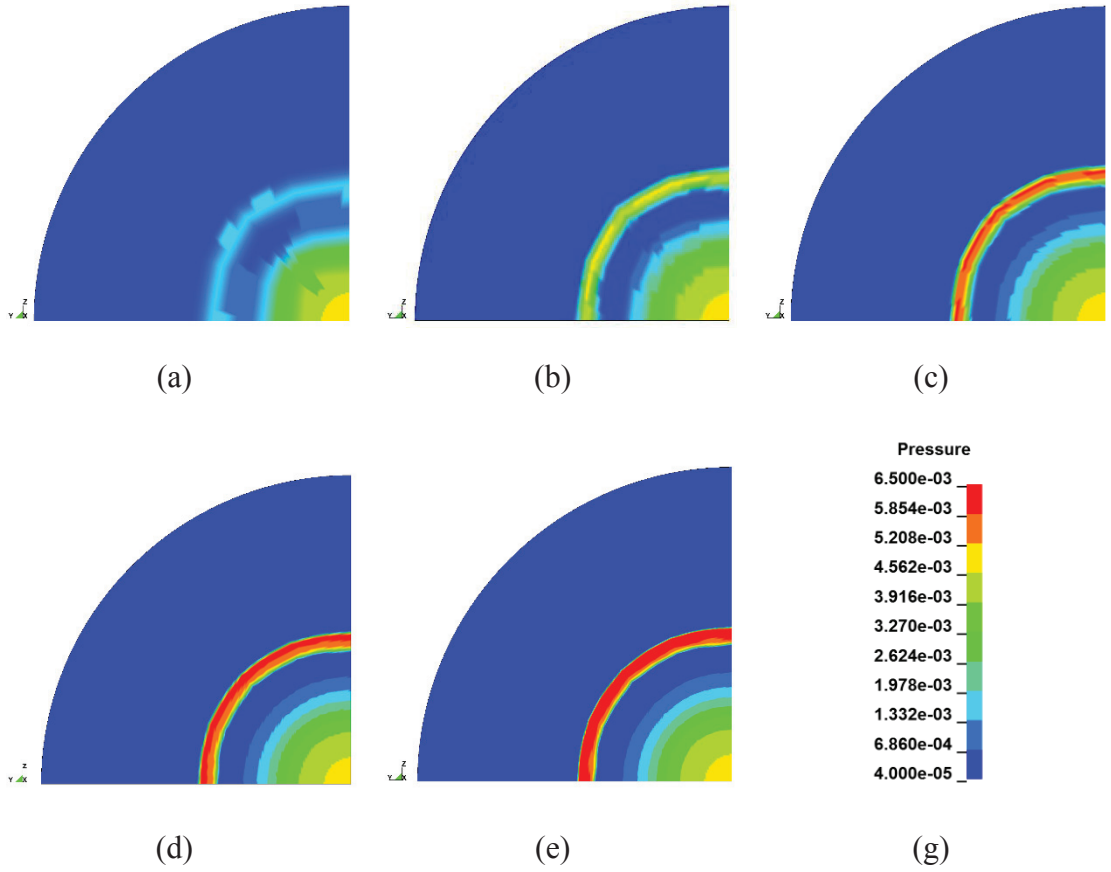

Figure 4.15. Pressure contours of free-field air blast at the same time for different mesh sizes (a) 22 element per side (b) 45 element per side (c) 90 element per side (d) 180 element per side (e) 360 element per side, and (g) Fringe level for all conditions in unit of GPa.

Afterwards, ALE model was constructed as modelling air and TNT corresponding to same condition that of pure Lagrangian approach. Influence of mesh refinement on the propagation of the shock wave was illustrated in Figure 4.15. Fringe range, in that case free field pressure, was fixed a range from 0.00004 to 0.0065 GPa for same simulation time (t = 0.025245 ms) to compare properly. It should be noticed that cubic region element number was kept constant, while element number per side out of the cubic region was gradually increased with a value which is mesh refinement ratio of 2. It can be seen that increase in element number in the air domain affects resolution and amount of the pressure; besides, pressure contours are more visible (Figure 4.15). That is, shock wave

propagation is directly affected mesh density of air domain. GCI was implement again to select proper element size accepting free field overpressure as interested response in that case, and corresponding pressure values at 95 mm were tabulated in Table 4.5.

Table 4.5. Free field overpressure results of air

i^{th}	Number of element per side	Max. Free field pressure, F_i (GPa)
1	360	0.00639
2	180	0.00620
3	90	0.00596
4	45	0.00299
5	22	0.00159

It was found that order of convergence, p, is 0.413 and estimated final value, F_E, is 0.00694 GPa. First finest mesh is selected to capture shock front pressure with 7.9 % relative error from numerically estimated final value.

Finally, hybrid blast model having element size closed to that of ALE approach was created. Both advection and coupling settings were kept same with ALE approach as well. Distance between ambient layer and structure surface was found with a few trials to eliminate any additional pressure reflections. Constructed blast models can be seen in Figure 4.16.

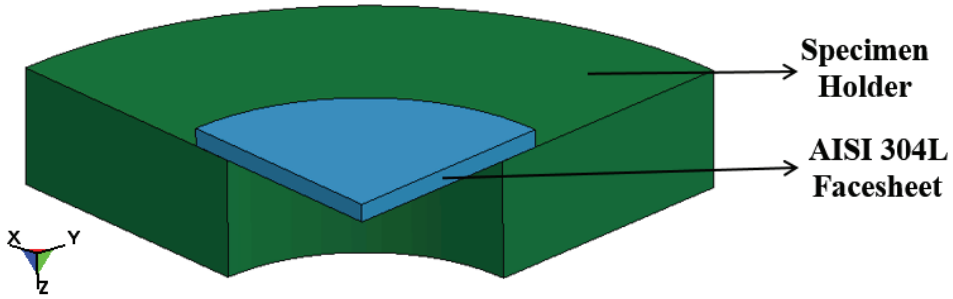

(a)

Figure 4.16. Illustration of blast models (a) Pure Lagrangian (b) ALE, and (c) Hybrid method.

(cont. on next page)

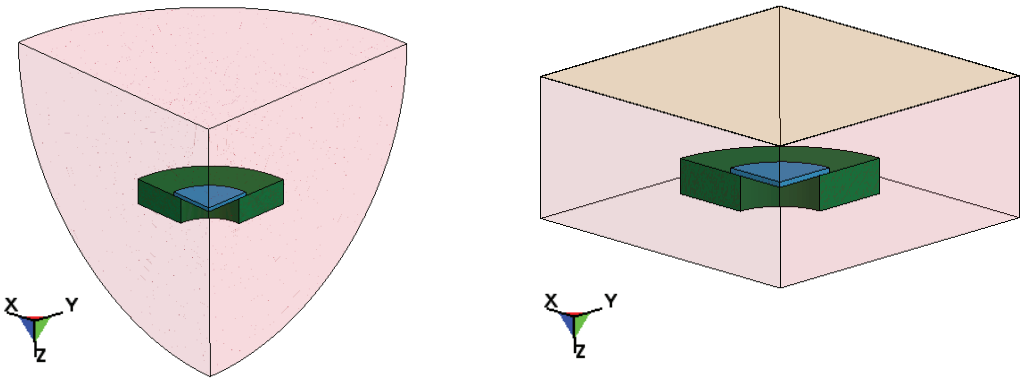

(b) (c)

Figure 4.16. (cont.)

Calibration study results were presented in terms of subjected overpressure and defamation profiles in Figure 4.17 and Figure 4.18, respectively.

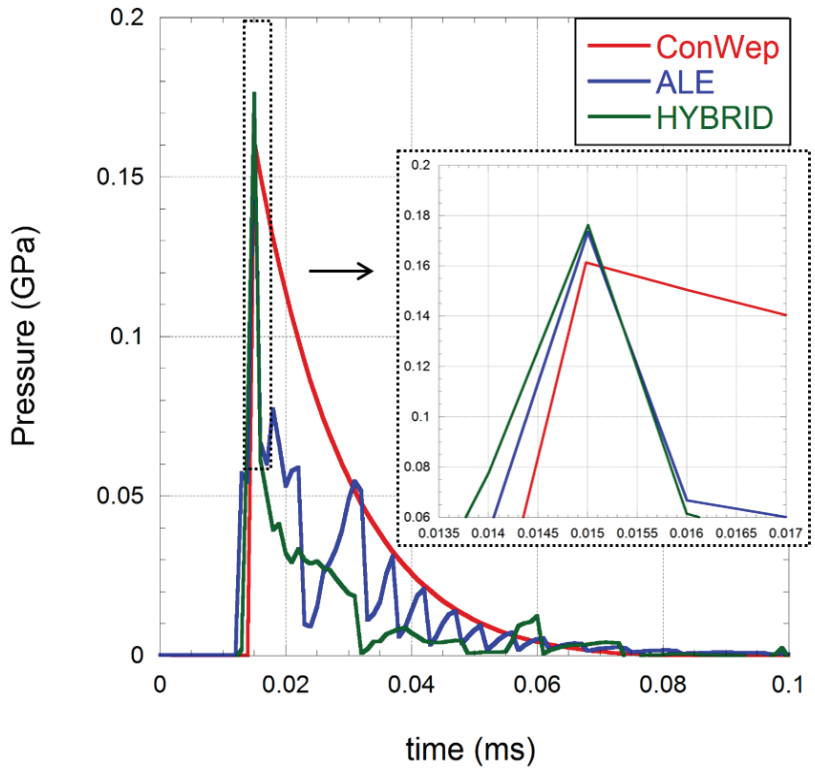

Figure 4.17. Comparison of effective pressures on the front surface of plate.

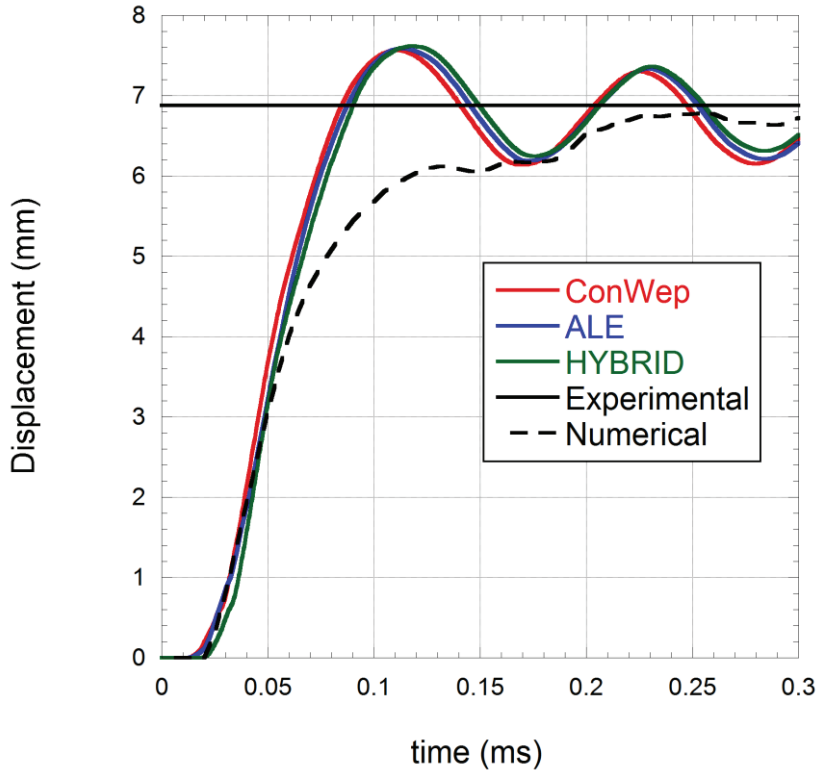

Figure 4.18. Comparison of center displacement of plates.

As depicted Spranghers et al. (2012), structural response which was occurred into two stages was observed. Facesheet firstly begins to move out-of-plane with an initial velocity in the presence shock wave, then facesheet deformation secondly maintains with impinged momentum as vanishing influence of shock front. As can be expected, pure Lagrangian approach, that is ConWep, is conservative method considered the whole blast models. Slight variations between results are arisen from mesh refinement of ALE and hybrid methods as found previously. This approach covers all needed free air explosion characteristics when it is implemented except its limitations. DPP testing as a laboratory scale blast-like experiment can be successfully used to investigate small scale structures as obtaining similar deformation profiles that of free air explosion.

In addition, experimental and numerical results in terms of deformation profiles and force-time history obtained from DPP tests are in good agreement. Differences between results may be originated due to the imperfections such as mesh refinement of numerical model, air squeezing at the beginning of deformation in experiments, or uncertainties in experiment such as heating in specimens, and friction coefficient variations during deformation. Moreover, perfect alignment on contact surfaces were presumed in numerical models.

CHAPTER 5

RESULTS AND DISCUSSIONS

After successfully validation of numerical model of individual and sandwich structures at quasi-static and low strain rates, and verification of material model were performed, structures were investigated various dynamic loading conditions. The first stage of this study can be found in related project carried out by Tasdemirci et al. (2016). Dynamic tests are able to reach up to 10^4 s^{-1} strain rates were conducted via Direct Pressure Pulse (DPP) Experiment set-up, while free air spherical blast condition was provided numerically in the light of verified numerical and material models. Therefore, structural performance of geometries were thoroughly evaluated from quasi-static levels to impulsive loading conditions.

5.1. Experimental Results and Equivalent Blast Conditions

5.1.1. Equivalent Blast Conditions Corresponding to Plate Deformation

The dynamic response of the plates which are the main constituent of sandwich structures were investigated at various impact velocities to understand deformation behavior prior to evaluate performance of sandwich structures. Experiments were conducted with three different impact velocities, which are 32.75, 36.37, and 39.78 m/s, employing DPP experiment set-up having unconfined mold and experienced force by plates corresponding to impact velocity was recorded. Deformation profiles and force-time histories are presented in Figure 5.1 and Figure 5.2, respectively.

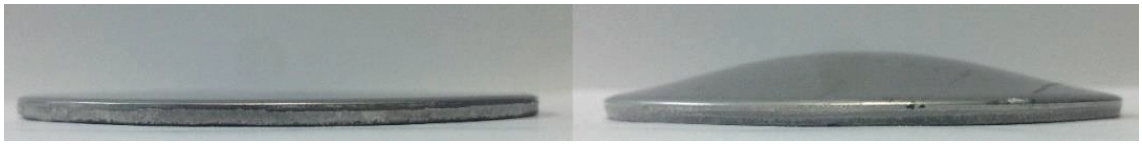

(a) (b)

Figure 5.1. (a) Undeformed plate and deformed plates with impact velocities of (b) 32.75 m/s (c) 36.37 m/s, and (d) 39.78 m/s.

(cont. on next page)

(c) (d)

Figure 5.1. (cont.)

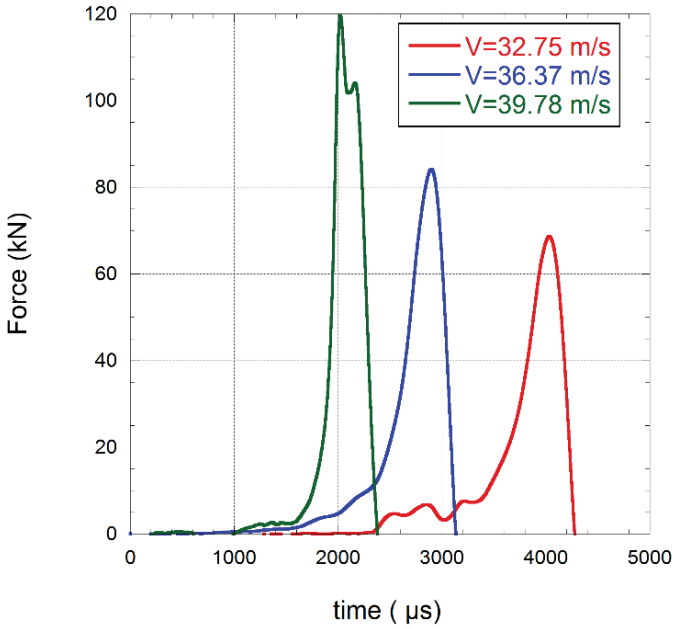

Figure 5.2. Experimental force-time history of plates.

Results from experiments show that as the impact velocity increases, exerted energy on the plate also increases. Therefore, plastic deformation and experienced impact loads obviously increases.

The main advantages of using this mold is to monitor any deformation formation thereby deformation initiation and locations can be identified. All test employed unconfined mold deformation were recorded. It was observed whether there was any structural defect and fracture. No structural deterioration was detected in any unconfined test.

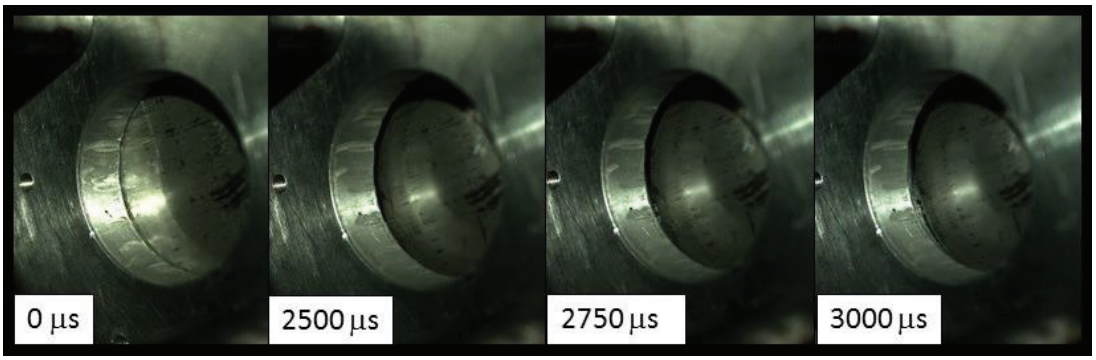

Figure 5.3. Deformation scheme of plate hit by striker having velocity of 36.37 m/s.

As mentioned in calibration study, the equivalent free air blast condition can be found out corresponding to typical DPP experiment using proper specimen holder in explosion modelling. Therefore, relation between impact velocities and mass of TNT at constant stand-off distance of 65 mm was put forward in Figure 5.4. Second order polynomial relation between mass of TNT and impact velocity can be pronounced.

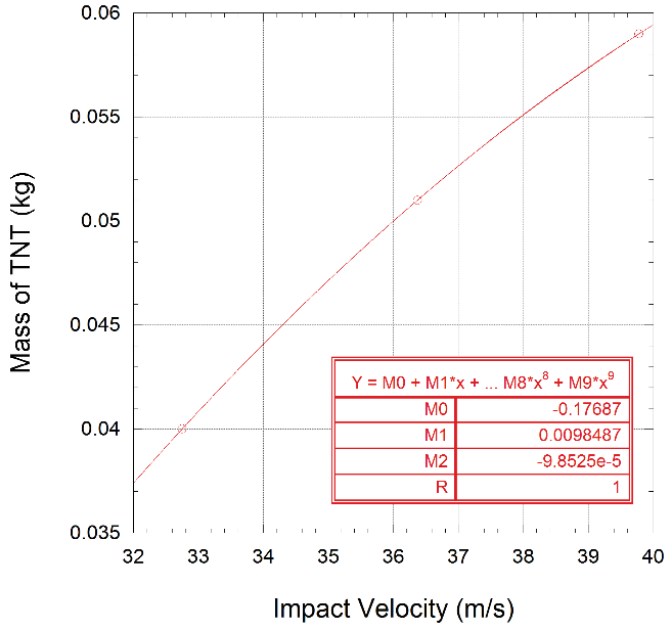

Figure 5.4. Equivalent mass of TNT values at 65 mm stand-off distance corresponding to impact velocities.

TNT mass and stand-off distance were selected again based on Hopkinson-Cranz scaling law considering small size of plates. For instance, scaled effect of 0.04 kg mass of TNT and 65 mm stand-off distance gives same positive peak overpressure with the condition of 9.32 kg mass of TNT and 400 mm stand-off distance.

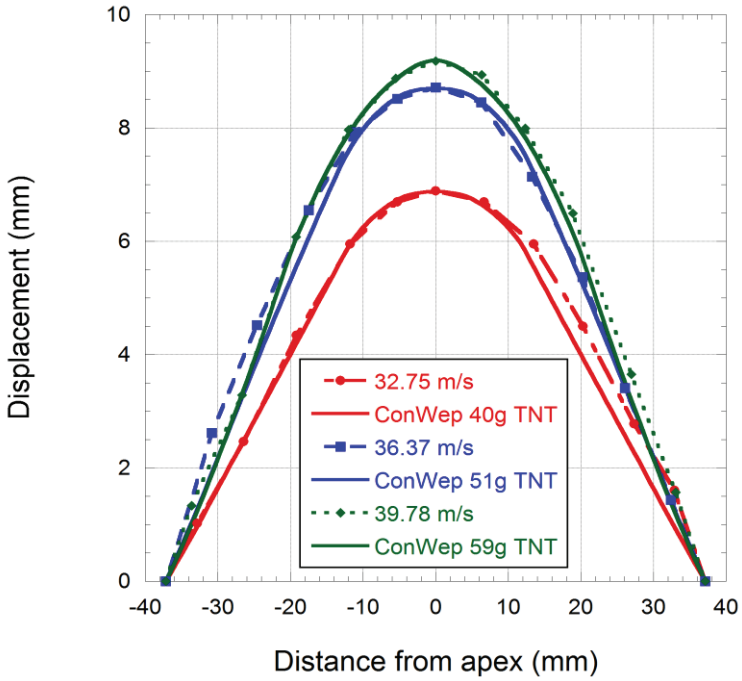

Figure 5.5. Comparison of deformed plates subjected to DPP and blast loading.

Deformed plates in terms of not only center deflection but also rest of the plate are in good agreement. Slight displacement differences between right and left hand side can be interpreted that calculated pressure by ConWep algorithm is symmetrically distributed and implemented. Therefore, the free air spherical explosion effect on the structures in the laboratory conditions can be applied in a controlled and repetitive manner thanks to direct pressure pulse experiment and effective pressure in blast event could be turned into impact loading.

5.1.2. Equivalent Blast Conditions Corresponding to Sandwich Structure Deformation

After being ascertained of equivalent blast conditions of plate, equivalent blast conditions for sandwich structures were determined. To do this, DPP experiment set-up with confined mold having constrained back side was used. All tests were conducted with an average impact velocity of 40 m/s. Blast event was modelled with pure Lagrangian approach. A rigid part was placed at the bottom side of sandwich structures in blast simulation to provide boundary condition same as that of DPP experiment. Equivalent blast conditions to acquire same amount of deformation those of DPP experiment at selected stand-off distance, in that case 75 mm was selected, were found as 0.1 kg mass

of TNT for both balanus and shell sandwich structures, and 0.135 kg mass of TNT for core sandwich structure. As can be seen in figures, reduced numerical model was not implemented for sandwich structures because deformation did not result in symmetrical manner.

It should be noticed that numerical force-time history of sandwich structures was filtered to involve high frequency variability due to selected small calculation step. Negative movement of upper plate after reaching maximum displacement value in blast simulations was ignored and maintained as dashed line. Displacement-time curves of numerical DPP were shifted to origin point of result of ConWep simulation in time domain for comparison purpose. In addition, force-time curves of numerical DPP were intentionally shifted in time domain to equalize termination time.

In Figure 5.6 and 5.7, experimental and numerical DPP experiment accompanying equivalent blast condition of 0.135 kg mass of TNT and 75 mm stand-off distance results of core sandwich specimen is given in terms of their force-time histories, displacement-time histories of upper facesheet, and final deformed top and side views.

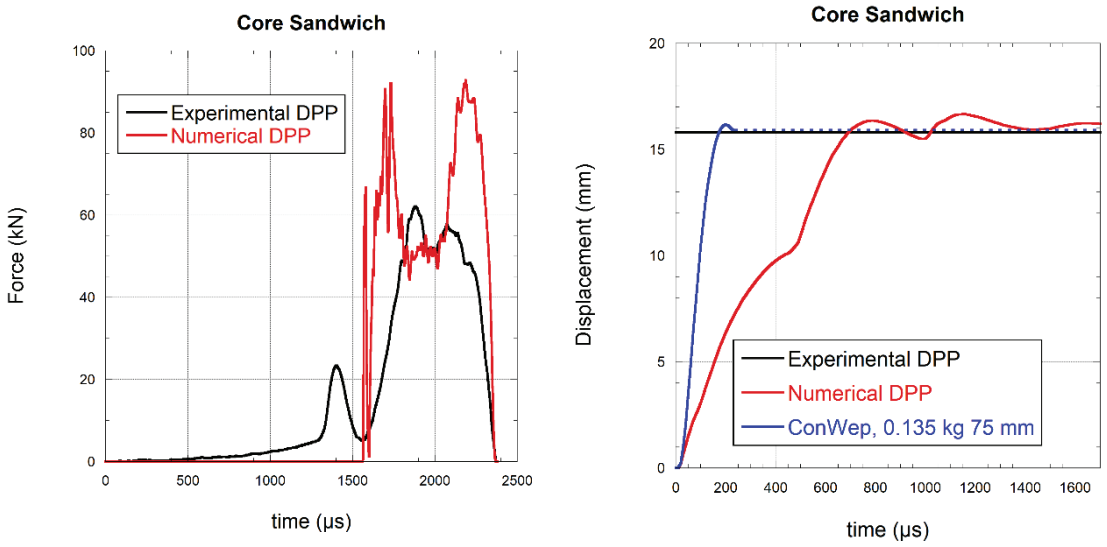

(a) (b)

Figure 5.6. Core sandwich results (a) Force-time, and (b) Displacement-time histories.

(a)

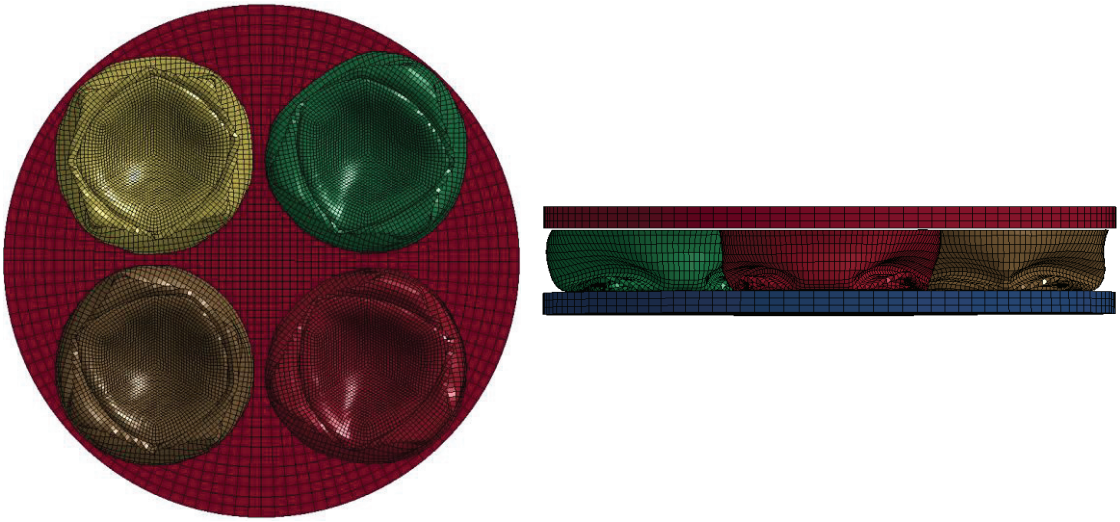

(b)

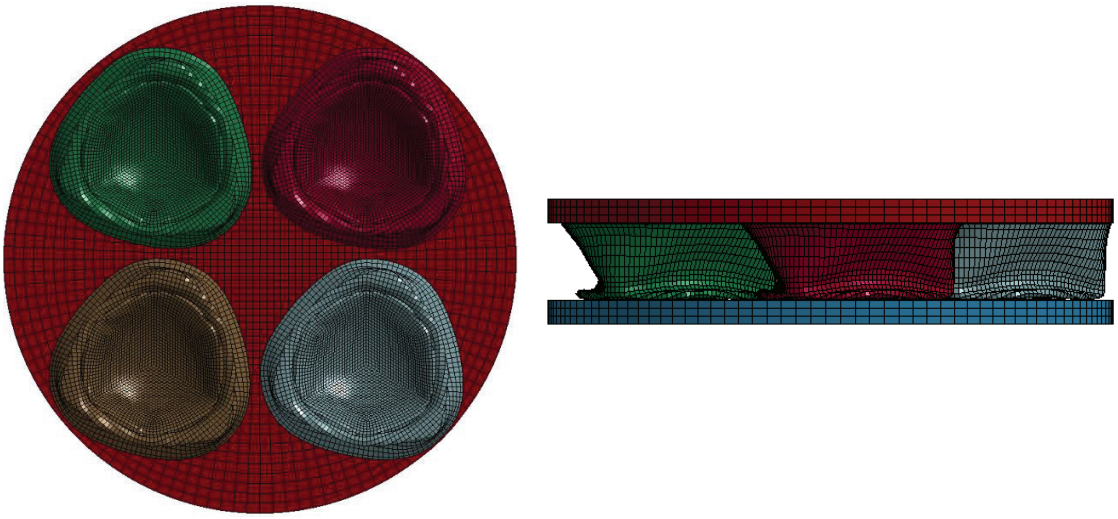

(c)

Figure 5.7. Deformed views of core sandwiches of (a) DPP Experiment (b) Numerical DPP, and (c) Equivalent blast condition.

In Figure 5.8 and 5.9, experimental and numerical DPP experiment accompanying equivalent blast condition of 0.1 kg mass of TNT and 75 mm stand-off distance results of shell sandwich specimen is given in terms of their force-time histories, displacement-time histories of upper facesheet, and final deformed top and side views.

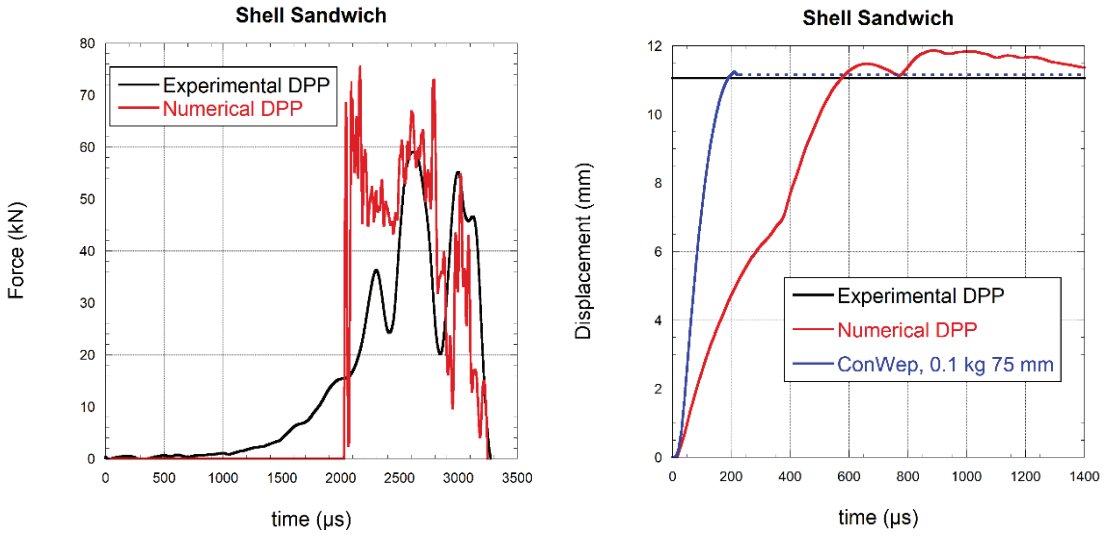

(a) (b)

Figure 5.8. Shell sandwich results (a) Force-time, and (b) Displacement-time histories.

(a)

Figure 5.9. Deformed views of shell sandwiches of (a) DPP Experiment (b) Numerical DPP, and (c) Equivalent blast condition.

(cont. on next page)

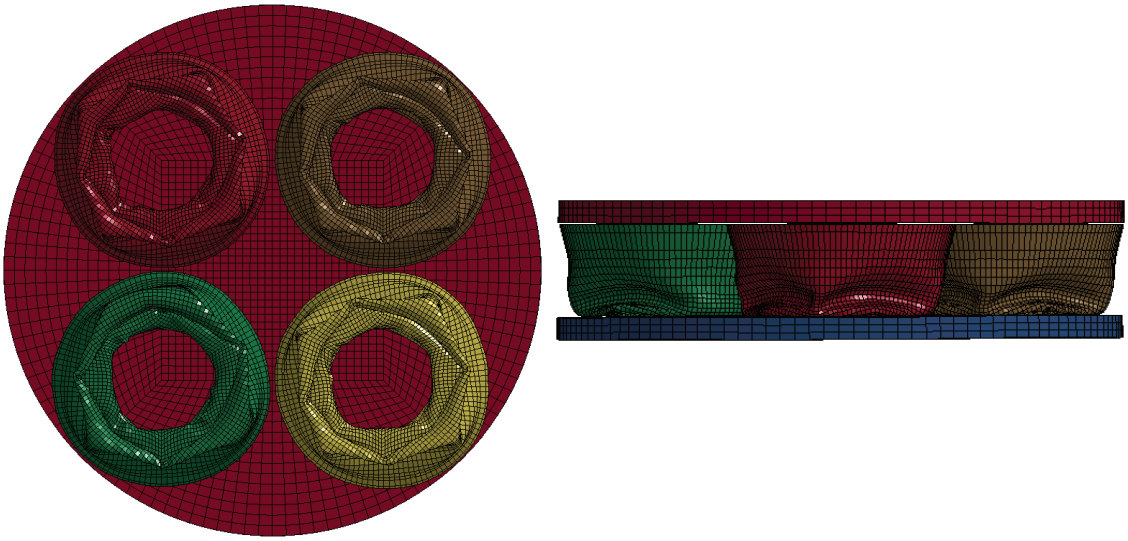

(b)

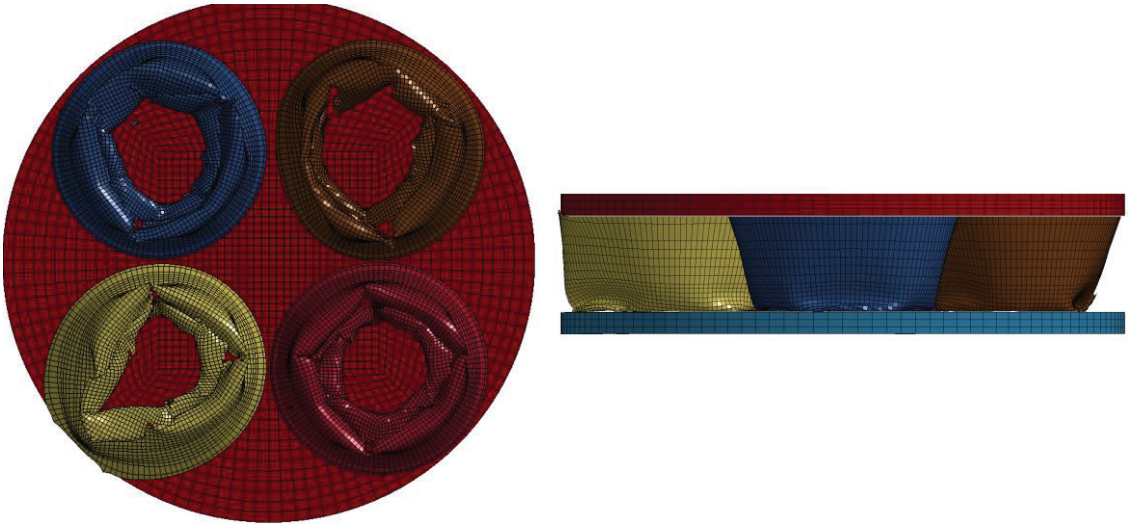

(c)

Figure 5.9. (cont.)

In Figure 5.10 and 5.11, experimental and numerical DPP experiment accompanying equivalent blast condition of 0.1 kg mass of TNT and 75 mm stand-off distance results of balanus sandwich specimen is given in terms of their force-time histories, displacement-time histories of upper facesheet, and final deformed top and side views.

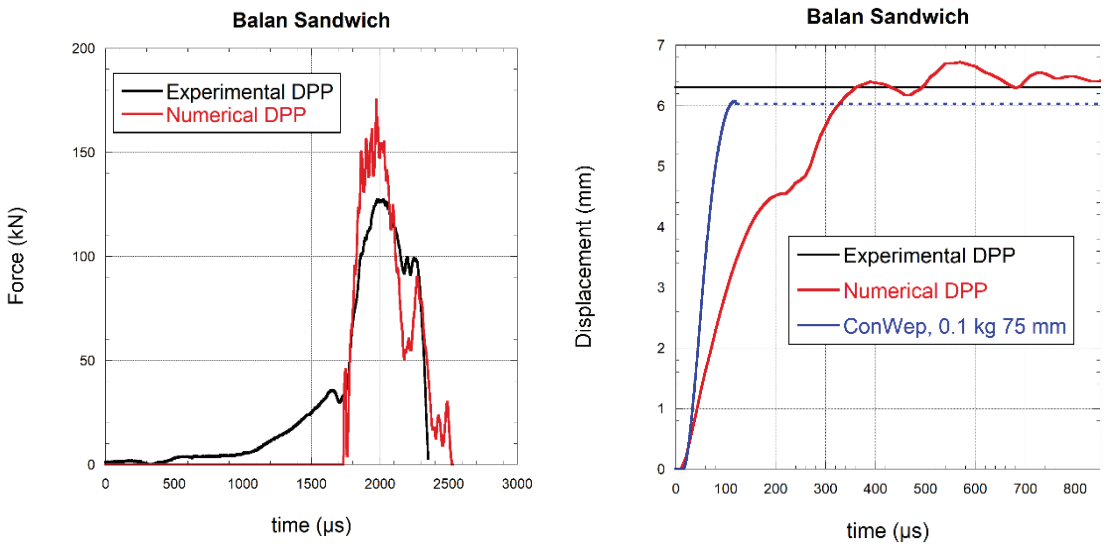

(a) (b)

Figure 5.10. Balanus sandwich results (a) Force-time, and (b) Displacement-time histories.

(a)

Figure 5.11. Deformed views of balanus sandwiches of (a) DPP Experiment (b) Numerical DPP, and (c) Equivalent blast condition.

(cont. on next page)

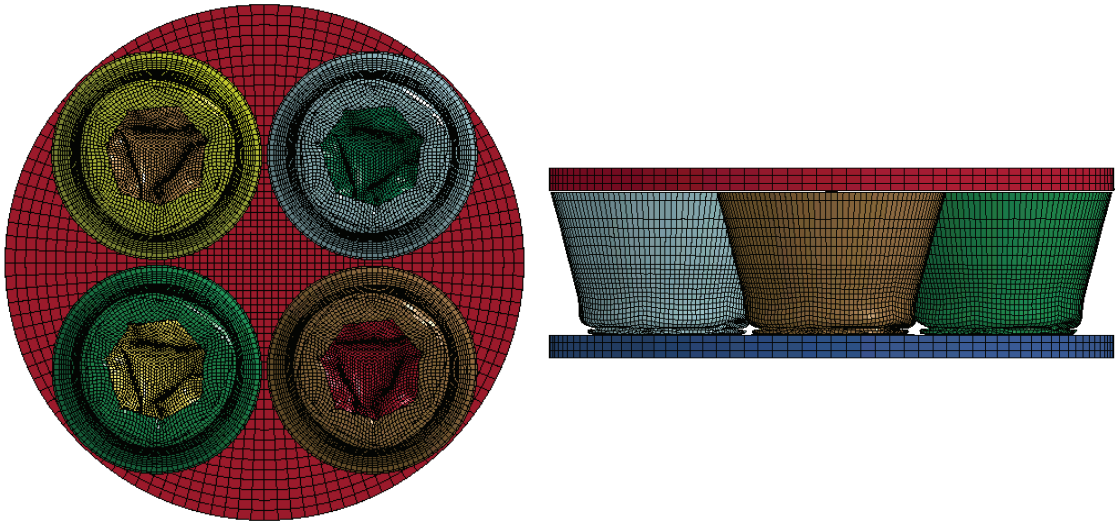

(b)

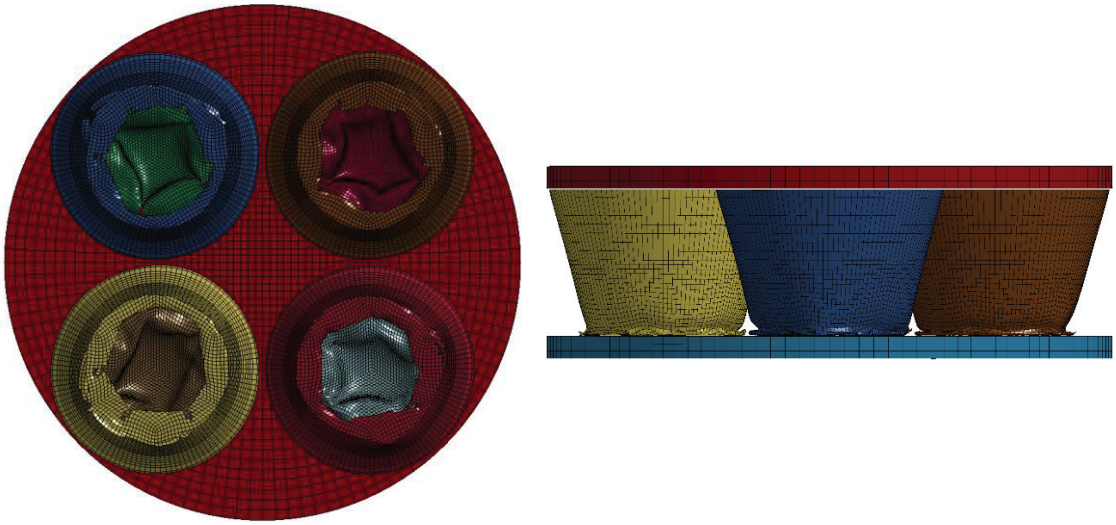

(c)

Figure 5.11. (cont.)

Numerical DPP results are in good agreement with experimental results in catching essential characteristics of deformation behavior, even though the characteristic peak points on the numerical DPP force-time histories were overestimated. Tilting as an imperfection may also be affected in the formation of slight variations as experienced by Fan et al. (2005) for honeycomb structures and Tasdemirci et al. (2015) for combined shell cores. The pre-loading which observed in all tests used confined mold might be ensued from compaction of air in front of the specimen, which creates a loading onto specimen initially. This loading which can be developed out of drag force affected on the striker may be reduced the striker velocity. On the other hand, deformed views of sandwich specimen acquired from experiments and numerical models can be also used to demonstrate achievement of the numerical models. Even if experimental and numerical

DPP results are very similar with respect deformation mode included formation of folding in similar manner, slight differences in deformation modes for DPP experiment and equivalent blast condition, especially for shell, were observed because strain rate in blast event is higher than DPP experiment, which can be understood from force-displacement curves of front facesheet of sandwich structures. However, observed small tearing around the folding, dimpling mode in the core structures, and collapsing mechanism in experimental DPP results are pretty close to obtained results in both numerical DPP and explosion condition. This indicates material and damage models work well even at high strain rates like blast loading.

ALE and hybrid blast models of small scale balanus sandwich structures were also prepared to verify result of pure Lagrangian approach. To do this, air models which mesh convergence analysis was previously done in calibration study were employed. Explosive parameters, likewise, were kept same with those of calibration study. Full numerical model was implemented for hybrid model, whereas half-symmetrical model of air was used in ALE model imposing necessary symmetry boundary condition. The reason is that proposed sandwich structures do not deform symmetrically. Constructed numerical models can be seen in Figure 5.12.

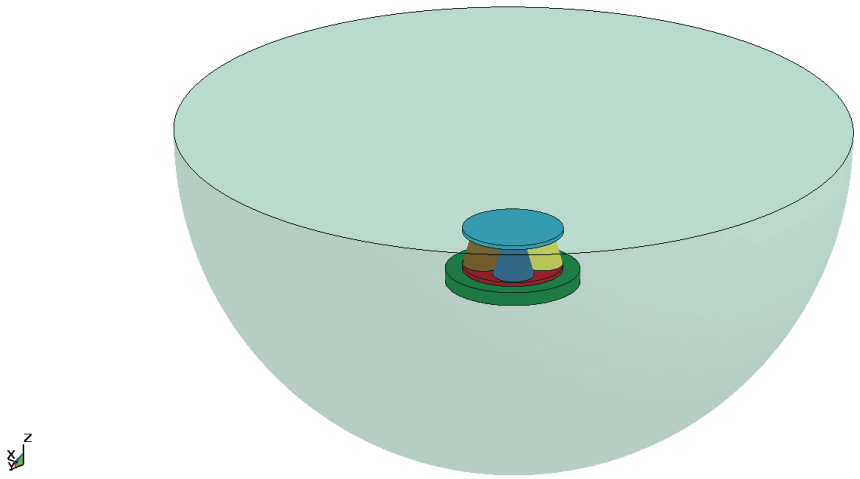

(a)

Figure 5.12. Numerical models of balanus sandwich (a) ALE model, and (b) Hybrid model.

(cont. on next page)

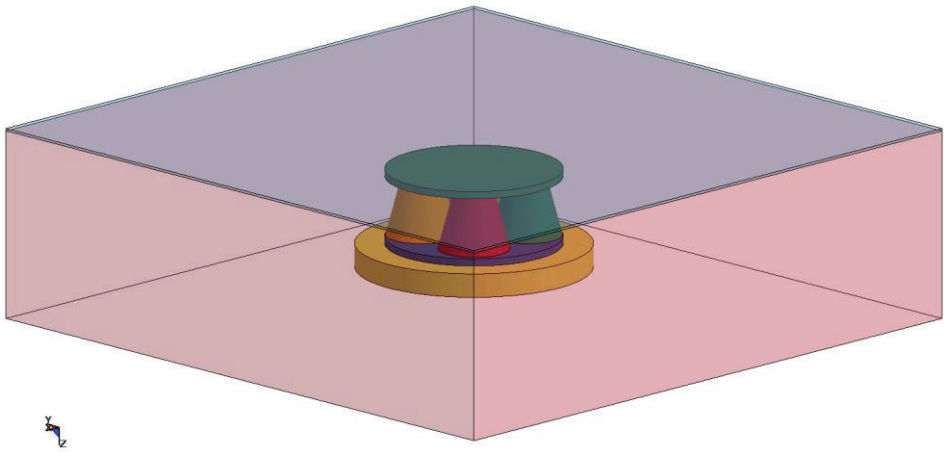

(b)

Figure 5.12. (cont.)

Results of blast models were compared in terms of their upper plate displacement-time histories (Figure 5.13). Well proximity between results were achieved. Pure Lagrangian approach accompanying ConWep algorithm could be employed. Besides, there are some studies that this approach is inadequate to model the whole blast conditions. For instance, Zakrisson et al. (2011) reported large variations between ConWep and ALE formulation results, which caused explosive shape used in their study which was cylindrical shape.

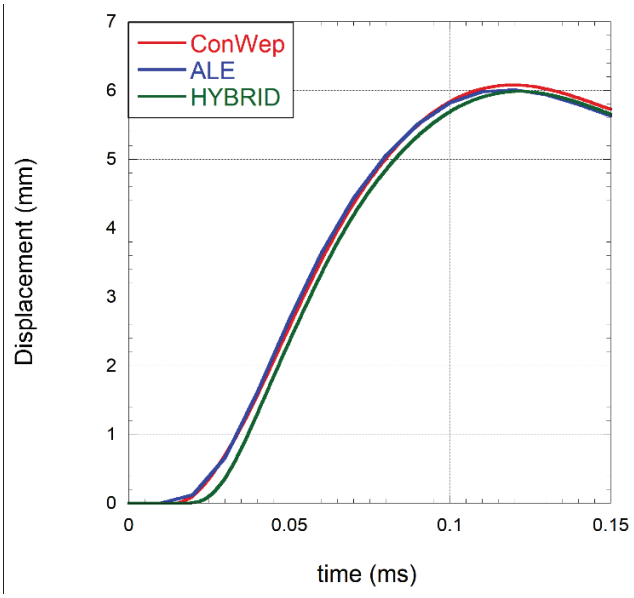

Figure 5.13. Displacement histories of upper facesheet of sandwich structure in blast simulations.

5.1.3. Crushing Behavior of Sandwich Structures at Dynamic Loads

In this section, dynamic behavior of sandwich structures are investigated in detail by making use of finite element analysis of DPP experiment. In addition, strain rate and inertial effects are revealed as comparing dynamic and quasi-static force responses of sandwich structures. Three characteristic peaks on force-time history, which were also observed in experimental results, for three type sandwich structure were probed and interpreted.

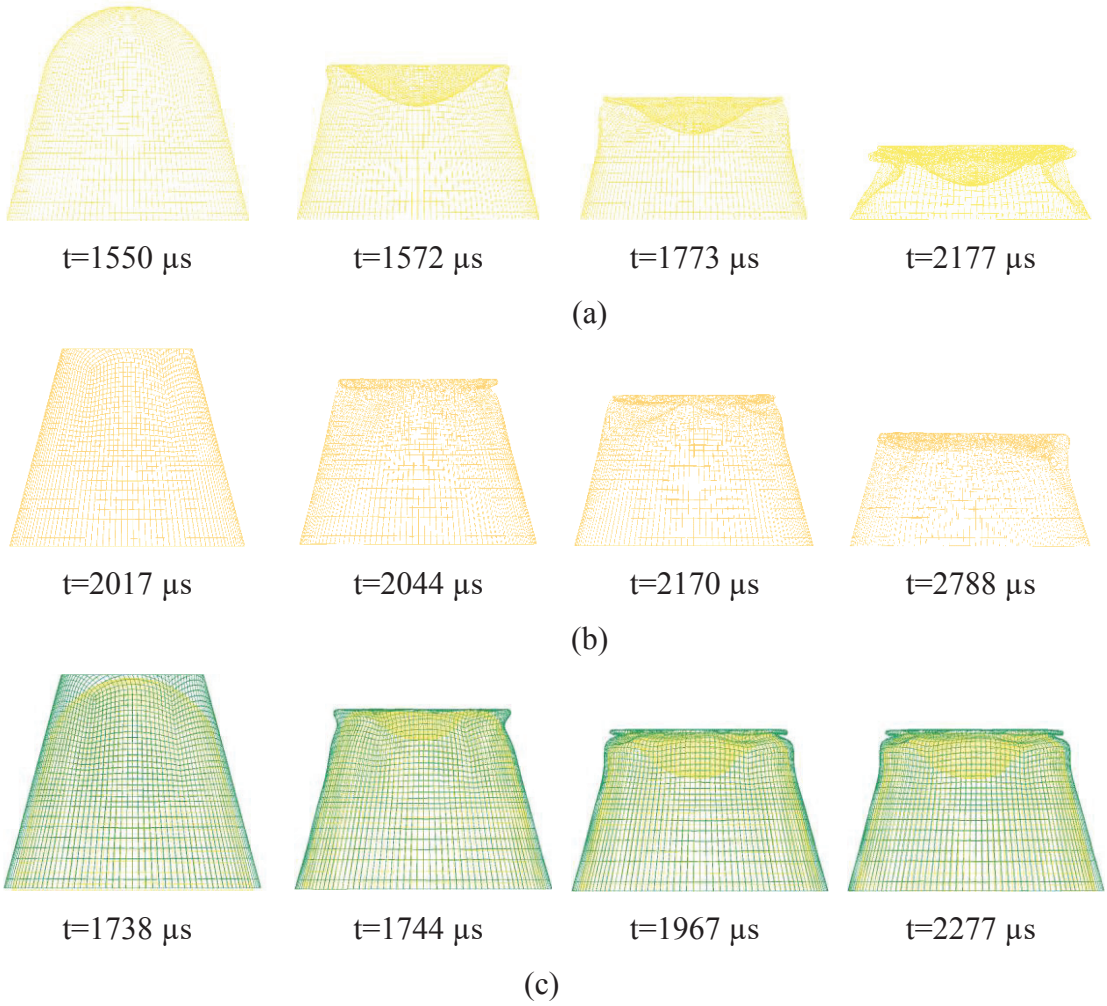

Figure 5.14. Sequential deformed view at different times for unit member of (a) Core (b) Shell, and (c) Balanus sandwich specimen.

In Figure 5.14, deformed views of the selected core units from sandwich structures corresponding to characteristic peak points on their force-time histories were presented comparatively. First and subsequent local maximum points represents a point where

buckling load is overcame and immediately after force drops as completing formation of folding, then carried force progressively increased due to increase in contact area between facesheet and core member until beginning again newly buckling formation resulted as another local maximum point. This collapsing mechanism proceeds by forming new folding as loading maintains; therefore, the energy is absorbed by being suitable for the purpose of utilization of sandwich structures. It is obvious that despite structures are subjected same amount of loading, balanus structure was deformed lesser than others. Whereas the second local maximum point (which is also global maximum point for all configurations) originated in 83 and 73 kN for core and shell sandwich structures respectively, the second peak originated in 173 kN for balanus structure, which is even higher than arithmetical sum of others. As depicted by Tasdemirci et al. (2015) for thin walled metallic core, this is because local flattening formation at the top of balanus structure increase in contact area and prevention of lateral movement of both components of balanus. Therefore, it can be made a deduction that balanus structure could carry a lot of load as a result of lateral support of core member to shell member and interaction between surfaces, which also makes this structure unique. Last deformed views account for unloading stage for the whole configurations in which incident pressure is absorbed completely and spring back effect is observed.

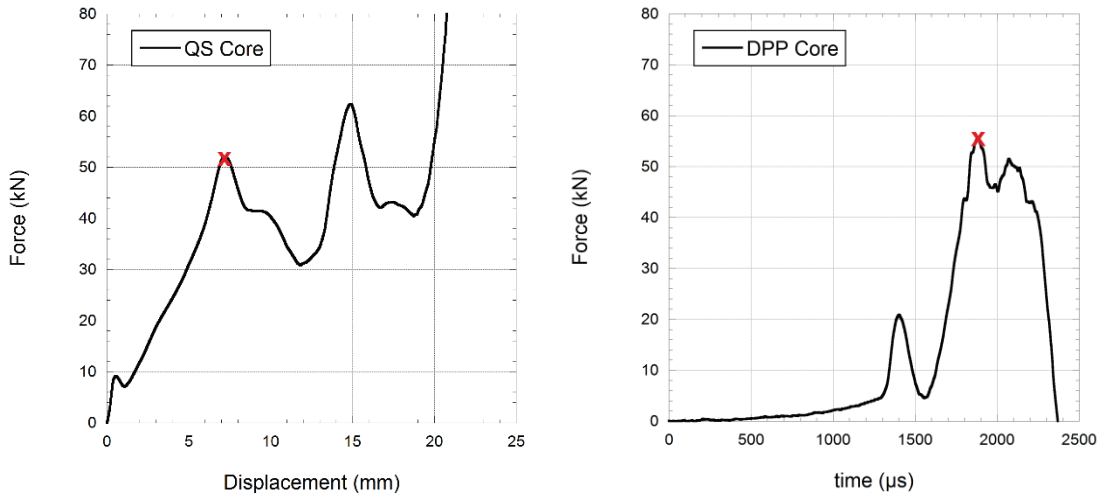

(a) (b)

Figure 5.15. (a) Quasi-static result, and (b) DPP result of core sandwich.

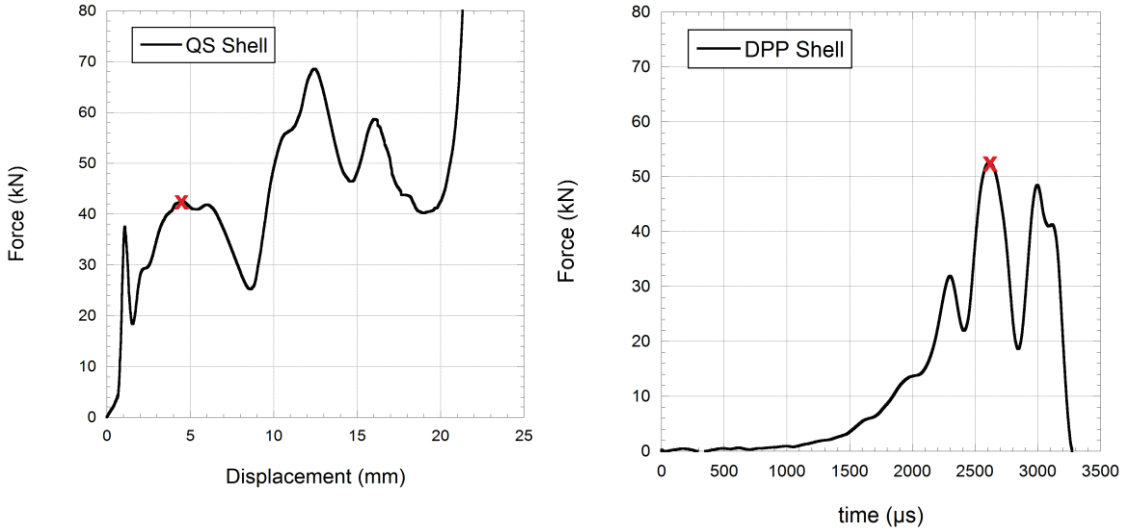

(a) (b)

Figure 5.16. (a) Quasi-static result, and (b) DPP result of shell sandwich.

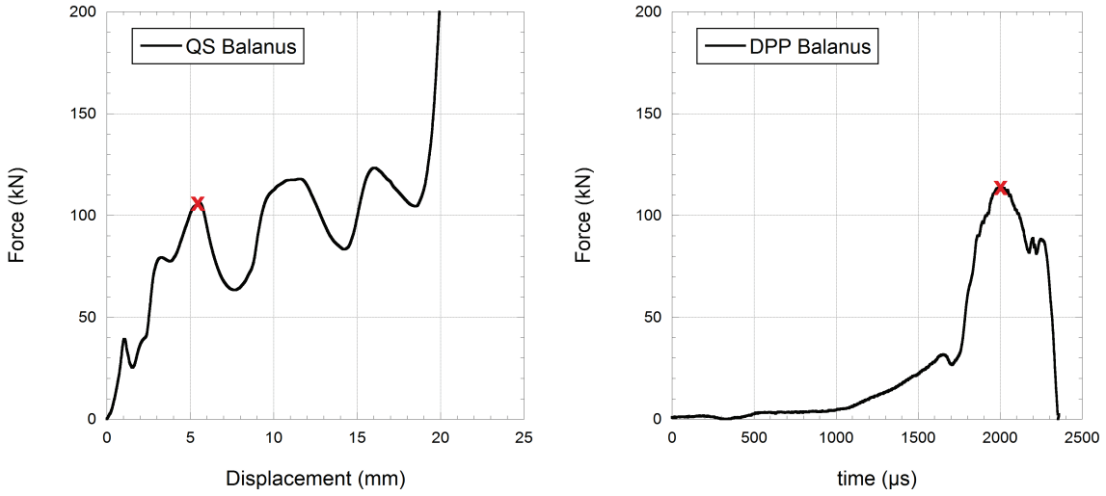

(a) (b)

Figure 5.17. (a) Quasi-static result, and (b) DPP result of balanus sandwich.

The force values corresponding to compression levels during the Direct Pressure Pulse experiment were identified using a symbol on both dynamic and static curves which were comparatively given throughout Figure 5.15 and 5.17. Force-displacement curves of sandwich structures at strain rate of 10^{-3} s^{-1} were taken from related project performed by Tasdemirci et al. (2016). As can be seen from the figures, the static and dynamic force values of sandwich structure at similar deformation levels are 51 and 56 kN for core sandwich structure respectively, 42 and 52 kN for shell sandwich structure respectively and 106 and 125 kN for balanus sandwich structure respectively. The force values carried

by the structure also increased as increasing deformation rate. This increase in force values is partly due to the micro-inertia effect, partly due to the strain rate sensitivity of the AISI 304L stainless steel material which is ingredient of sandwich structures.

After rate and inertia effect were examined, a study was conducted in order to find out effectiveness of balanus sandwich structure in terms of its thickness variation and containing residual stress/strain. To do this, small scale balanus sandwich structure including individual balanus geometries having constant thickness of 0.5 mm (which is initial blank thickness of sheet material) and not containing residual stress/strain were prepared numerically. This individual balanus geometry having constant thickness is in weight of 14.4 g, whereas balanus geometry having thickness variation due to its manufacturing process is in weight of 12.1 g. Balanus sandwich structure included balanus geometries having thickness variation was numerically subjected to pressure pulse created by hitting 40 m/s of striker same as that of other sandwich structure. Comparison of results with regard to compression strains and average carried loads are presented in Figure 5.18.

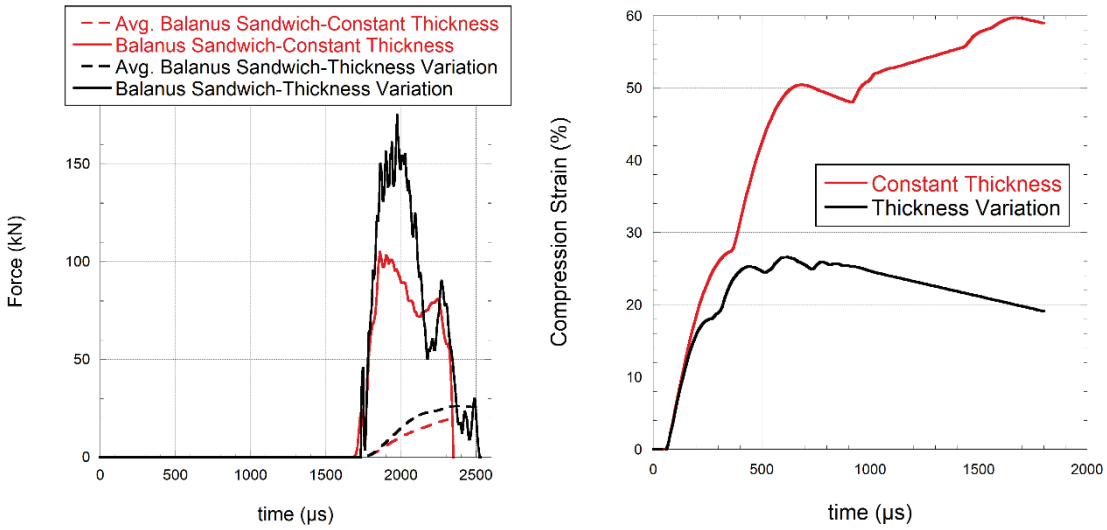

(a) (b)

Figure 5.18. The numerical results of structures (a) Force-time and (b) Compression strain-time histories.

As can be seen results, balanus sandwich structure having thickness variation and residual stress/strain exhibits good performance. For the same incident pressure, it was found that while balanus structure having thickness variation was able to carry up to 37% more load than the other developed structure according to their average experienced

loads, it was less deformed approximately the ratio of 45% at the same time. This may be interpreted with changing in deformation mode shown in Figure 5.19. Deformed views corresponding to same compression level of structures are presented for comparison purpose.

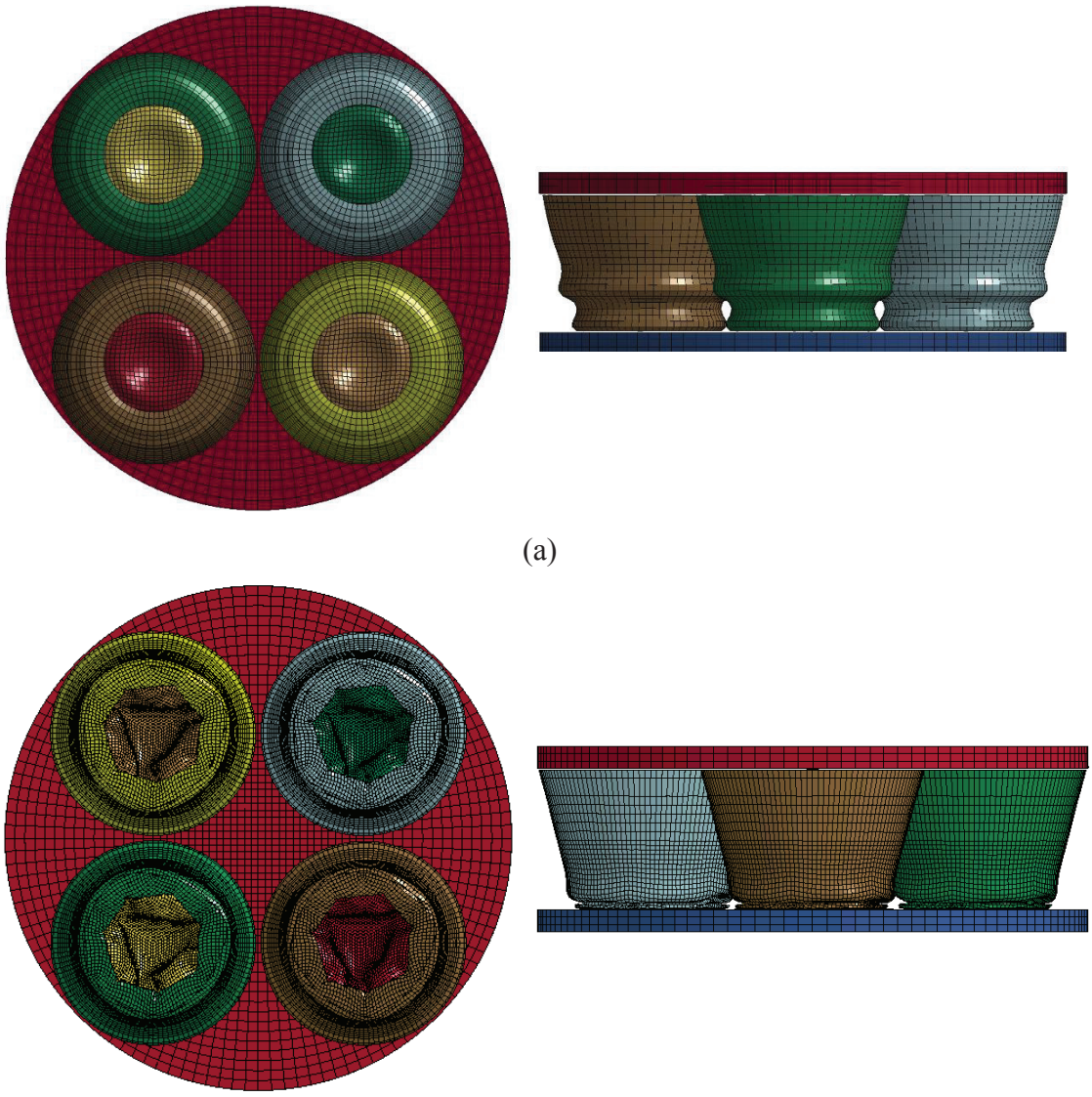

(a)

(b)

Figure 5.19. Top and side deformed view of sandwich structures with (a) constant thickness, and (b) thickness variation.

5.2. Blast Responses of Large Scaled Sandwich Structures

After finishing evaluation of small scaled sandwich structures in terms of force-time history and deformation mode, large scaled sandwich structures were subjected

various blast load to determine their energy absorption capabilities. Simulations were prepared employing pure Lagrangian approach which gives consistent results with other methods as revealed previous sections as much as saving calculation time. For this purpose, balanus sandwich composed of 3 mm thick AISI 304L stainless steel facesheets and 81 individual balanus geometry with 280x280 mm dimension was prepared and back surface of sandwich structure was constrained with a steel plate of 20 mm thick. Prepared sandwich structure can be seen in Figure 5.20.

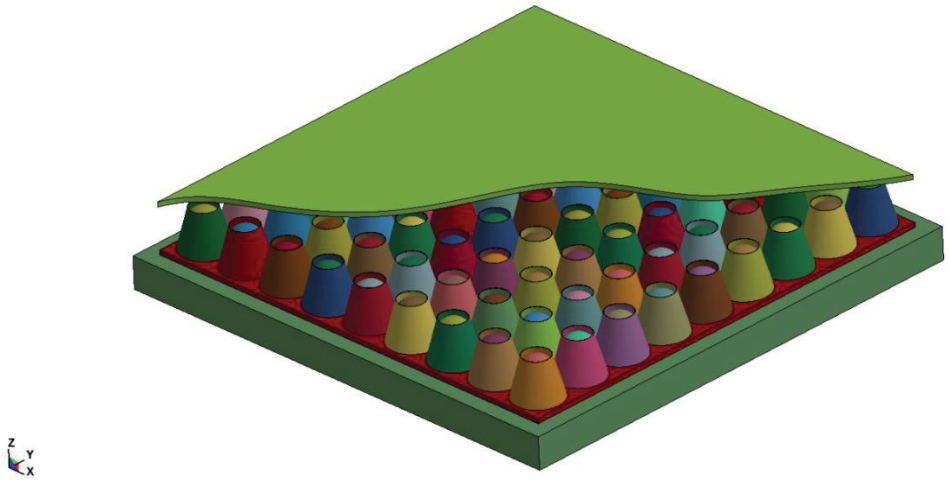

Figure 5.20. Sample of numerically created large scaled balanus sandwich structure.

Firstly, as-received balanus sandwich performance was evaluated at various balanus placement. These configurations are all front, all back, one-front / one-back and front-row / back-row. All sandwich configurations were subjected to same blast loading of 5 kg mass of TNT and 350 mm stand-off distance. Transmitted force to the protected zone and impulse are given in Figure 5.21.

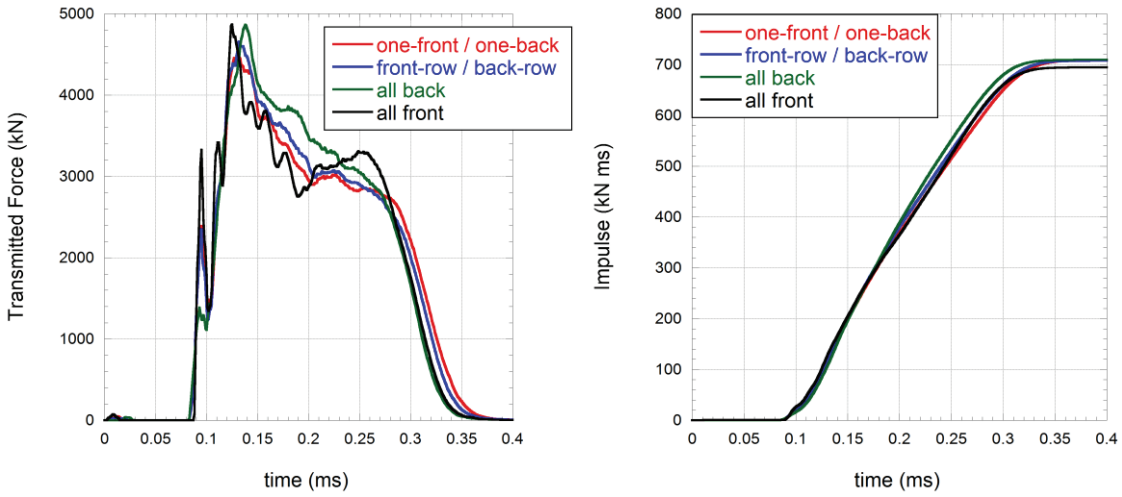

(a) (b)

Figure 5.21. The result of configurations of balanus sandwich structures (a) Transmitted force, and (b) Impulse.

Even though transmitted forces corresponding to arrangement configurations are similar, the impulse which is as important as the transmitted force as emphasized previously has the lowest value of 694 kN ms in the configuration that was positioned all front. Moreover, when the specific absorbed energy (*SAE*) capacities are taken into consideration, it is seen that the best energy absorbing sandwich is the sandwich where the core members are all front in the explosion direction, and the lowest one is the sandwich where all core members are positioned reverse direction against the explosion direction (Figure 5.22).

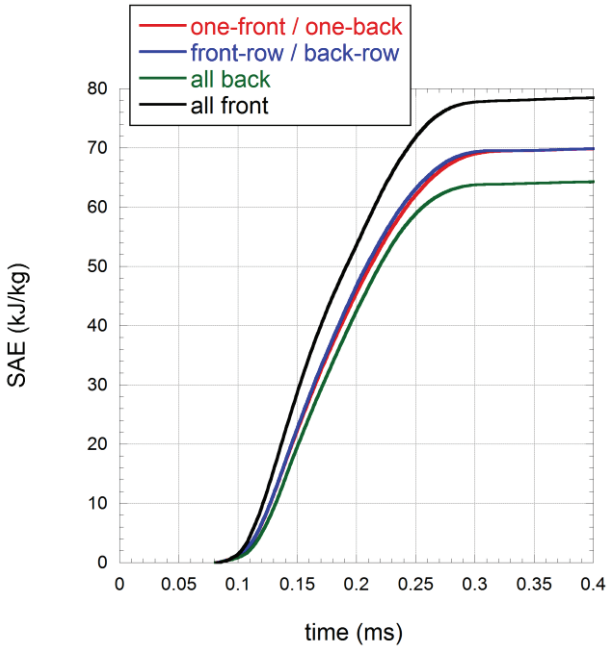

Figure 5.22. Specific absorbed energy (SAE) values corresponding sandwich configurations.

In Figure 5.23, undeformed views of a part of sandwich structures located in center having different arrangement are presented.

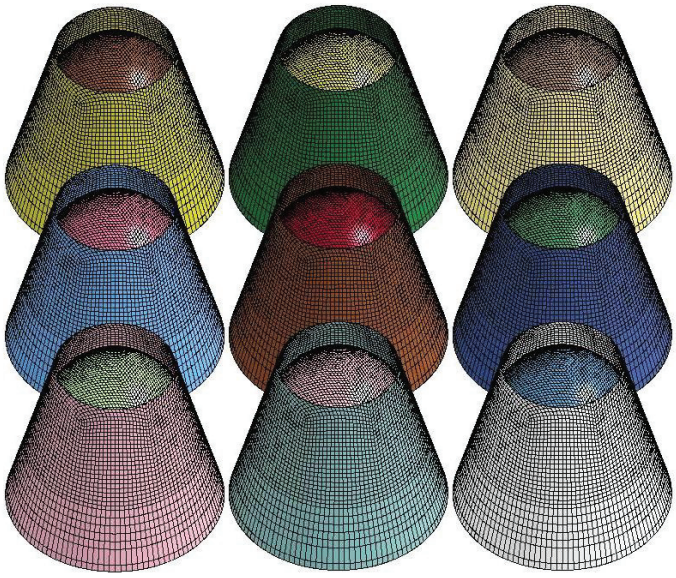

(a)

Figure 5.23. Undeformed view of sandwich structures of (a) all front (b) all back (c) one-front / one-back, and (d) front-row / back-row.

(cont. on next page)

(b)

(c)

Figure 5.23. (cont.)

(cont. on next page)

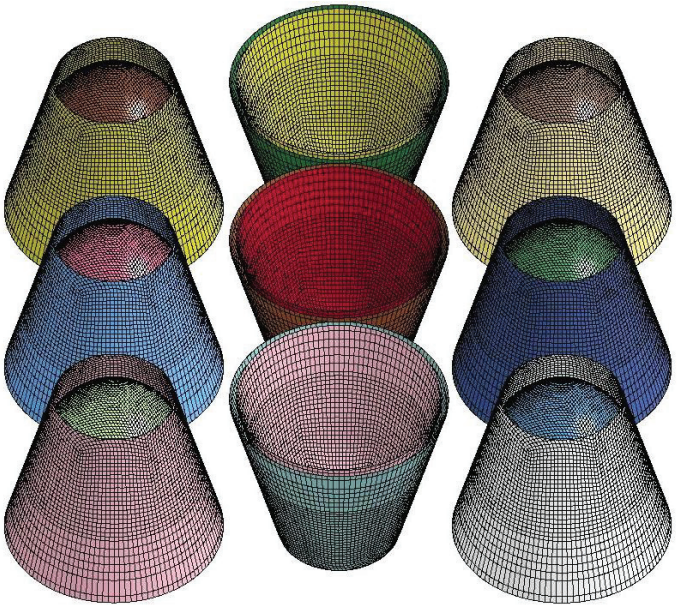

(d)

Figure 5.23. (cont.)

In Figure 5.24, deformed views of a part of sandwich located in center configurations presented above are given.

(a)

Figure 5.24. Deformed view of sandwich structures of (a) all front (b) all back (c) one-front / one-back, and (d) front-row / back-row.

(cont. on next page)

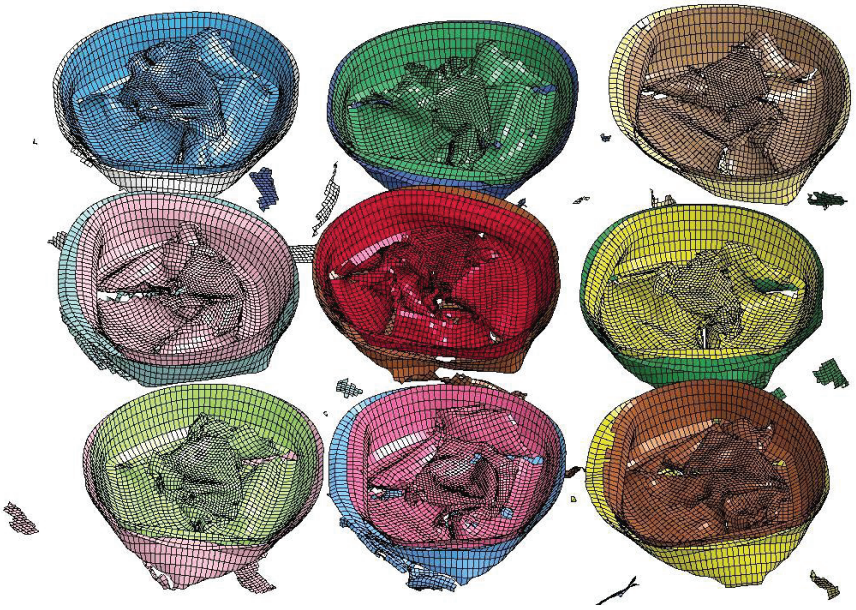

(b)

(c)

Figure 5.24. (cont.)

(cont. on next page)

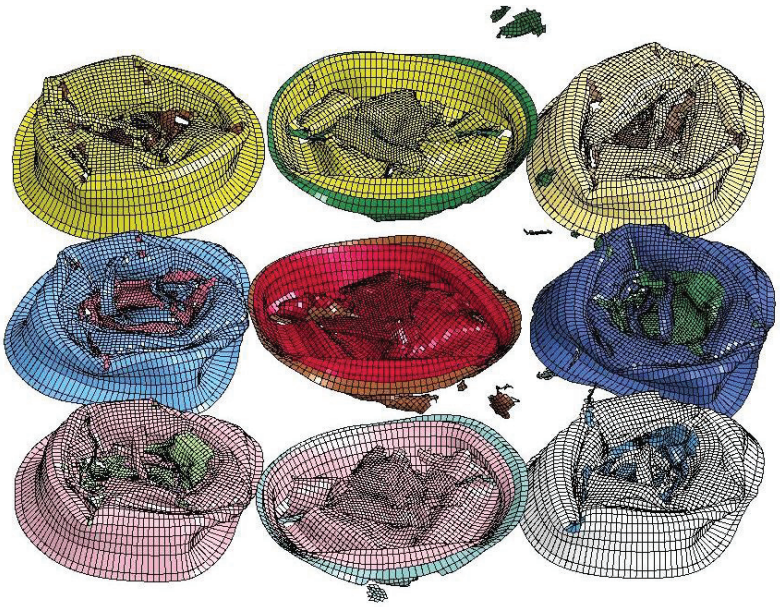

(d)

Figure 5.24. (cont.)

After finding the best placement, effect of heat-treatment on the blast mitigation performance of balanus sandwich structures was investigated. In heat-treatment process, residual stress/strain caused by manufacturing process of geometries might be eliminated. In numerical model, heat-treated specimens were prepared as removing residual stress/strain values from geometries that be contained initially. In this part of the study, the different heat-treatment configurations in all front direction were examined, which are heat-treated shell and as-received core, heat-treated core and as-received shell, and heat-treated both core and shell. These were compared with as-received both core and shell subjected to blast condition of 5 kg mass of TNT and 350 mm stand-off distance. Mass of TNT corresponding to each configuration at constant stand-off distance of 350 mm were found, which gave approximately similar compression strain. Obtained results were tabulated in Table 5.1.

Table 5.1. Mass of TNT corresponding to each configuration at constant stand-off distance of 350 mm.

Configuration	**Mass of TNT (kg)**	**Average Compression Strain (%)**
Heat-treated both of core and shell	2.7	71
Heat-treated shell and as-received core	3.9	74
Heat-treated core and as-received shell	4	73
As-received both of core and shell	5	71

In Figure 5.25, deformed views of unit balanus configurations at certain displacements which correspond initiation of folding formation are given.

In heat-treated configurations given in Figure 5.25, collapsing behavior was completely changed from non-symmetrical one to axi-symmetrical one because material of balanus became more ductile and pliant. Whereas deformation mode of balanus geometries was diamond type in full as-received configuration, it was concertina type in other configurations in which buckling forces can be easily overcame. Peripheral deformation underside of geometry also differs in heat-treated configurations due to deformation mode. Structural tearing was observed the whole as-received specimens.

The result given in Table 5.1 indicates that while as received both of core and shell configuration can withstand blast loading condition of 5 kg mass of TNT and 350 mm stand-off distance, other configurations are going to most probably fail. When compression strain reaches to densification strain, energy absorption capacity of sandwich structure is exhausted thereby transmitted force to the protected zone might be dramatically increased. As a result of this part of study, as-received both of core and shell, and all front configuration outperforms other analyzed configuration in higher scaled distances and might be employed as a blast resistant structure.

Figure 5.25. The deformation histories balanus placed in the center of sandwich structure (a) Heat-treated shell and as-received core (b) Heat-treated core and as-received shell (c) Heat-treated both of core and shell, and (d) As-received both of core and shell.

CHAPTER 6

CONCLUSIONS

In this thesis, blast response of sandwich structures with bio-inspired cores were investigated in detail. The proposed geometry consists of an outer shell and inner core made of AISI 304L stainless steel. Experiments at high strain rates are able to reach up to 10^4 s^{-1} stain rates were conducted using Direct Pressure Pulse experiment set-up, whereas blast loading was applied numerically. Pure Lagrangian, Arbitrary Lagrangian Eulerian (ALE), and hybrid (coupled other two approaches) approaches were used separately in modelling of blast. Sandwich structures and their plates were evaluated at different blast conditions after validation of numerical model was done comparing dynamic experimental and numerical results. Experimental and numerical results were in good agreement in terms of deformation mechanism and experienced average force-time histories. Finally, blast mitigation performance of large scaled sandwich structures including bio-inspired cores were assessed in various configurations. As deducing from detailed experimental and numerical investigations, the specific conclusions related to performed study can be drawn:

- The geometry was inspired from marine crustaceans called as “Balanus” having robust structure was adopted successfully as a core member of sandwich structure. Manufacturing method of this geometries, which is deep-drawing process, causes work hardening in the specimens, which is one of the features that make it unique. The components of balanus geometry were made of AISI 304L stainless steel material that enables deformation plastically because of being very ductile and strain rate sensitive. Therefore, sandwich structures revealed better performance at high strain rates in spite of having thin walled geometries.
- It was shown that pure Lagrangian approach including ConWep algorithm is conservative method among the studied blast models based on their pressure-time histories. This approach covers all needed characteristics of free air explosion when it is implemented except its limitations. Very similar mid-point deflections could be obtained with three types of blast model.

- DPP testing with different kind of molds as a laboratory scale blast-like experiment can be successfully used to investigate blast loading response of small scale structures as obtaining similar deformation profiles and loading schemes with those of equivalent free air explosion. It may substitute for other explosive used blast testing methods as a controllable, easily repeatable, safety and cheaper manner. Moreover, it is possible to monitor deformation progression and failure formation of specimen using high speed camera in DPP experiments used unconfined mold.
- Numerical result of DPP tests are in good agreement with experimental DPP results in terms of trend of effective forces and displacement of upper plate of sandwich structures. Similar deformation schemes are obtained with those of equivalent blast condition. Some differences between numerical and experimental results arises from some imperfections in numerical models and some uncertainties in experiments.
- Balanus geometry outperforms its components based on unit member of sandwich structures corresponding peak points on force-time histories in result of DPP model. Balanus geometry carries more load under same loading condition as a result of lateral support of core member to shell member and interaction between their surfaces, which is another feature that make balanus structure unique.
- The force values obtained from the DPP sandwich tests are higher than their quasi-static values due to increased inertia effects with the deformation rate and the high strain rate sensitivity of the AISI 304L stainless steel material which is ingredient material of sandwich structures.
- The effect of thickness variation and containing residual stress/strain were also investigated. Balanus sandwich with thickness variation and residual stress/strain carried more load up to 37% and was less deformed approximately 45% than balanus sandwich with constant thickness of 0.5 mm and no containing residual stress/strain.
- After material and damage model were successfully verified at static and high strain rates with regards to experienced effective force and deformation modes, blast mitigation performance of large scaled sandwiches was evaluated numerically. Four different types core placement were proposed to find out optimum core configuration. Deformation differences among the proposed

configurations can be interpreted the difference in acoustic impedance value which is the one of the most important parameters in transmission of stress wave. This is due to differences between mating surfaces at which deformation begins and contacting surface transiently.

- Among the proposed core configurations, all front configuration was found as efficient configuration in terms of *SAE* and impulse. It was shown heat-treated specimen cannot be unadaptable at higher scaled distances. Because deformation mode of specimen was completely altered from non-symmetrical one (diamond) to axi-symmetrical one (concertina), which turn specimens into ductile and pliant.

Finally, following suggestions can be offered for future study:

- Full field blast test of proposed sandwich structure can be conducted to obtain further information in deformation mechanism and to check used explosive parameters.
- The effect of foam filling which caused acoustic impedance difference in transmission stress wave in blast loading can be examined. Foam filling strategies can be developed.
- Blast mitigation performance of sandwich structure can be evaluated at different blast threats and boundary conditions.
- Composite facesheets might be employed instead of AISI 304L stainless steel in sandwich structure. Also, dynamic response of multilayer sandwich structures can be investigated.

REFERENCES

Alberdi, R., Przywara, J., & Khandelwal, K. (2013). Performance evaluation of sandwich panel systems for blast mitigation. *Engineering Structures*, *56*, 2119–2130. https://doi.org/10.1016/j.engstruct.2013.08.021

Amini, M. R., Simon, J., & Nemat-Nasser, S. (2010). Numerical modeling of effect of polyurea on response of steel plates to impulsive loads in direct pressure-pulse experiments. *Mechanics of Materials*, *42*(6), 615–627. https://doi.org/10.1016/j.mechmat.2009.09.009

AskNature Team. (2015). Beak provides streamlining : Kingfisher. Retrieved June 5, 2017, from https://asknature.org/strategy/beak-provides-streamlining/#.WTU622iLRhF

Baker, W. E., Cox, P. A., Westine, P. S., Kulesz, J. J., & Strehlow, R. A. (1985). *Explosion hazards and evaluation* (Vol. 5). Elsevier Science B.V. https://doi.org/10.1016/0010-2180(85)90099-9

Bar-Cohen, Y. (2006). Biomimetics--using nature to inspire human innovation. *Bioinspiration & Biomimetics*, *1*(1), P1–P12. https://doi.org/10.1088/1748-3182/1/1/P01

Bellamy, R. F., & Mil. (1988). War Surgery.

Boschstrasse, E. G. (2015). Product catalogue. Retrieved from www.eurenco.com

Chan, B. K. K., & Southward, A. (2011). Balanus improvisus Darwin, 1854. Retrieved April 9, 2017, from http://www.marinespecies.org/aphia.php?p=taxdetails&id=106218

Chen, J., Tuo, W., Zhang, X., He, C., Xie, J., & Liu, C. (2016). Compressive failure modes and parameter optimization of the trabecular structure of biomimetic fully integrated honeycomb plates. *Materials Science and Engineering C*, *69*, 255–261. https://doi.org/10.1016/j.msec.2016.06.087

Chen, W., & Hao, H. (2014). Experimental investigations and numerical simulations of multi-arch double-layered panels under uniform impulsive loadings. *International Journal of Impact Engineering*, *63*, 140–157. https://doi.org/10.1016/j.ijimpeng.2013.08.012

Combes, C. (2001). *Parasitism: The Ecology and Evolution of Intimate Interactions*. Chicago: University of Chicago.

Committee on Gulf War and Health: Long-Term Effects of Blast Exposures. (2005). *Gulf War and Health*. *Media* (Vol. 9). Washington, D.C.: The National Academies Press.

Crupi, V., Epasto, G., & Guglielmino, E. (2012). Collapse modes in aluminium honeycomb sandwich panels under bending and impact loading. *International Journal of Impact Engineering*, *43*, 6–15. https://doi.org/10.1016/j.ijimpeng.2011.12.002

Cullis, I. G. (2001). Blast Waves and How They Interact With. *Shock Waves*, *147*(1), 16–26. https://doi.org/10.1136/JRAMC-147-01-02

Dharmasena, K. P., Wadley, H. N. G., Williams, K., Xue, Z., & Hutchinson, J. W. (2011). International Journal of Impact Engineering Response of metallic pyramidal lattice core sandwich panels to high intensity impulsive loading in air. *International Journal of Impact Engineering*, *38*(5), 275–289. https://doi.org/10.1016/j.ijimpeng.2010.10.002

Dharmasena, K. P., Wadley, H. N. G., Xue, Z., & Hutchinson, J. W. (2008). Mechanical response of metallic honeycomb sandwich panel structures to high-intensity dynamic loading, *35*, 1063–1074. https://doi.org/10.1016/j.ijimpeng.2007.06.008

Do, I., & Day, J. (2005). Overview of Ale Method in Ls - Dyna. *Livermore Software Technology Corp*, 1–48.

Draganić, H., & Sigmund, V. (2012). Blast loading on structures. *Tehnički Vjesnik*, *19*(3), 643–652.

Du, Y., Yan, N., & Kortschot, M. T. (2014). Novel lightweight sandwich-structured bio-fiber-reinforced poly(lactic acid) composites. *Journal of Materials Science*, *49*(5), 2018–2026. https://doi.org/10.1007/s10853-013-7889-1

Fan, X., Verpoest, I., & Vandepitte, D. (2005). Finite Element Analysis on Out-of-Plane Compression Properties of Thermoplastic Honeycomb. *Sandwich Structures 7: Advancing with Sandwich Structures and Materials*, 875–884. Retrieved from http://link.springer.com/chapter/10.1007/1-4020-3848-8_88

Fish, F. E., Weber, P. W., Murray, M. M., & Howle, L. E. (2011). The tubercles on humpback whales' flippers: Application of bio-inspired technology. *Integrative and Comparative Biology*, *51*(1), 203–213. https://doi.org/10.1093/icb/icr016

Fleck, N. A., & Deshpande, V. S. (2004). The Resistance of Clamped Sandwich Beams to Shock Loading, *71*(May). https://doi.org/10.1115/1.1629109

Greer, A. D. (2006). *Numerical Modeling for the Prediction of Primary Blast Injury to the Lung*. University of Waterloo.

Guden, M., Yuksel, S., Tasdemirci, A., & Tanoglu, M. (2007). Effect of aluminum closed-cell foam filling on the quasi-static axial crush performance of glass fiber reinforced polyester composite and aluminum/composite hybrid tubes. *Composite Structures*, *81*(4), 480–490. https://doi.org/10.1016/j.compstruct.2006.09.005

Hallquist, J. (2006). *LS-DYNA Theory Manual*. *Livermore Software Technology Corporation*. Retrieved from http://www.dynasupport.com/manuals/additional/ls-dyna-theory-manual-2005-beta/at_download/file

Hargather, M. J., & Settles, G. S. (2007). Optical measurement and scaling of blasts from gram-range explosive charges. *Shock Waves*, *17*(4), 215–223. https://doi.org/10.1007/s00193-007-0108-8

Harris, V. A. (1990). *Sessile Animals of the Sea Shore* (First Edit). Chapman and Hall.

Hicks, R. R., Fertig, S. J., Desrocher, R. E., Koroshetz, W. J., & Pancrazio, J. J. (2010). Neurological effects of blast injury. *The Journal of Trauma*, *68*(5), 1257–63. https://doi.org/10.1097/TA.0b013e3181d8956d

Highfield, R. (2016). Leonardo da Vinci: genius or humble draftsman? Retrieved June 5, 2017, from http://www.telegraph.co.uk/art/what-to-see/leonardo-da-vinci-genius-or-humble-draftsman/

Hu, L. L., & Yu, T. X. (2013). Mechanical behavior of hexagonal honeycombs under low-velocity impact - theory and simulations. *International Journal of Solids and Structures*, *50*(20–21), 3152–3165. https://doi.org/10.1016/j.ijsolstr.2013.05.017

Institute U.S. Naval Annapolis. (1952). *Marine Fouling and Its Prevention*. MASSACHUSETTS.

Jing, L., Wang, Z., & Zhao, L. (2016). The dynamic response of sandwich panels with cellular metal cores to localized impulsive loading. *Composites Part B: Engineering*, *94*, 52–63. https://doi.org/10.1016/j.compositesb.2016.03.035

Johnson, G. R., & Cook, W. H. (1983). A constitutive model and data for metals subjected to large strains, high strain rates and high temperatures. *7th International Symposium on Ballistics*. https://doi.org/10.1038/nrm3209

Karthick, B., & Maheshwari, R. (2008). Lotus-inspired nanotechnology applications. *Resonance*, *13*(12), 1141–1145. https://doi.org/10.1007/s12045-008-0113-y

Keith Davey. (2000). Barnacles - Life on Australian Seashores. Retrieved April 9, 2017, from http://www.mesa.edu.au/friends/seashores/barnacles.html

Khurram, A. A., Rakha, S. A., Ali, N., Asim, M. T., Guorui, Z., & Munir, A. (2015). Microwave Absorbing Properties of Lightweight Nanocomposite/Honeycomb Sandwich Structures. *Journal of Nanotechnology in Engineering and Medicine*, *6*(1), 1–6. https://doi.org/10.1115/1.4031472

Kilic, A. E. S. A., & Bedir, N. K. S. (2016). Numerical simulation of armored vehicles subjected to undercarriage landmine blasts. *Shock Waves*, *26*(4), 449–464. https://doi.org/10.1007/s00193-015-0576-1

Kingery, C. N., & Bulmash, G. (1984). Air Blast Parameters from TNT Spherical Air Burst and Hemispherical Surface Burst. *US Army BRL: Aberdeen Proving Ground*.

Li, X., Wang, Z., Zhu, F., Wu, G., & Zhao, L. (2014). Response of aluminium corrugated sandwich panels under air blast loadings: Experiment and numerical simulation. *International Journal of Impact Engineering*, *65*, 79–88. https://doi.org/10.1016/j.ijimpeng.2013.11.002

LSTC. (2015). *LS-DYNA Keyword User's Manual* (Version R8).

Myers, M. A., Chen, P., Albert, Y. L., & Seki, Y. (2008). Biological materials: Structure and mechanical properties. *Progress in Materials Science*, *53*, 1–206. https://doi.org/10.1016/j.pmatsci.2007.05.002

National Consortium for the Study of Terrorism and Responses to Terrorism. (2016). Global Terrorism Database. Retrieved January 14, 2017, from http://www.start.umd.edu/gtd/search/Results.aspx?chart=attack&search=turkey

NATO. (2011). *Procedures for Evaluating the Protection Level of Armoured Vehicles Mine Threat* (Vol. AEP-55, 2).

Neff, M., & Fiume, E. (1999). A visual model for blast waves and fracture. *Proceedings of Graphics Interface 2009*, 193–202.

Philips, H., Cates, A., Catlin, C. A., Edmondson, N., Goose, M., Merrifield, R., … Thomas, G. O. (1994). Explosions in the process industries. *Major Hazards Monograph*.

Randers-Pehrson, G., & Bannister, A. K. (1997). Airblast Loading Model for DYNA2D and DYNA3D. *Army Research Laboratory*.

Roache, P. J. (1998). Verification of codes and calculations. *AIAA Journal*, *36*(5), 696–702. https://doi.org/10.2514/3.13882

Schmitt, O. (1969). Some interesting and useful biomimetic transforms. In *3rd Int. Biophysics Congress (Boston, MA, 29 Aug. to 3 Sept.)* (p. 297).

Schwer, L., Teng, H., & Souli, M. (2015). LS-DYNA Air Blast Techniques : Comparisons with Experiments for Close-in Charges. *10th European LS-DYNA Conference, Würzburg, Germany*, (2009).

Soutis, C., Mohamed, G., & Hodzic, A. (2011). Modelling the structural response of GLARE panels to blast load. *Composite Structures*, *94*(1), 267–276. https://doi.org/10.1016/j.compstruct.2011.06.014

Spranghers, K., Vasilakos, I., Lecompte, D., Sol, H., & Vantomme, J. (2012). Full-Field Deformation Measurements of Aluminum Plates Under Free Air Blast Loading. *Experimental Mechanics*, *52*(9), 1371–1384. https://doi.org/10.1007/s11340-012-9593-5

Spuskanyuk, A. V, Flores, S. E., Hayhurst, D. R., Hutchinson, J. W., Hall, P., Mcmeeking, R. M., & Evans, A. G. (2007). The Response of Metallic Sandwich Panels to Water Blast, *74*(January). https://doi.org/10.1115/1.2178837

Tasdemirci, A., Kara, A., Turan, K., & Sahin, S. (2015). Dynamic crushing and energy absorption of sandwich structures with combined geometry shell cores. *Thin-Walled Structures*, *91*, 116–128. https://doi.org/10.1016/j.tws.2015.02.015

Tasdemirci, A., Kara, A., Turan, K., Sahin, S., & Guden, M. (2016). Thin-Walled Structures Effect of heat treatment on the blast loading response of combined geometry shell core sandwich structures. *Thin Walled Structures*, *100*, 180–191. https://doi.org/10.1016/j.tws.2015.12.012

Tasdemirci, A., Sahin, S., Kara, A., & Turan, K. (2015). Crushing and energy absorption characteristics of combined geometry shells at quasi-static and dynamic strain rates: Experimental and numerical study. *Thin-Walled Structures*, *86*, 83–93. https://doi.org/10.1016/j.tws.2014.09.020

Taşdemirci, A., Güden, M., Kara, A., Turan, K., & Sahin, S. (2014). *Development and optimization of blast-resistant hemi-spherical core sandwich structures*. Turkey: The Scientific and Technological Research Council of Turkey (TÜBİTAK).

Taşdemirci, A., Güden, M., Tüzgel, F., Akbulut, E. F., & Güzel, E. (2016). *Design and optimization of energy-absorber biomimetic armor systems*. Turkey: The Scientific and Technological Research Council of Turkey (TÜBİTAK).

Toussaint, G., Fortier, C., & Dumas, S. (2012). Internal Blast in a Compartment-type Vessel. *Defense Technical Information Center*, (November).

Trajkovski, J., Kunc, R., Perenda, J., & Prebil, I. (2014). Minimum mesh design criteria for blast wave development and structural response - MMALE method. *Latin American Journal of Solids and Structures*, *11*(11), 1999–2017. https://doi.org/10.1590/S1679-78252014001100006

Tran, P., Ngo, T. D., & Mendis, P. (2014). Bio-inspired composite structures subjected to underwater impulsive loading. *Computational Materials Science*, *82*, 134–139. https://doi.org/10.1016/j.commatsci.2013.09.033

U.S. Army Corps of Engineers. (2008). *Structures to Resist the Effects of Accidental Explosions*. https://doi.org/10.1061/41171(401)127

Ullah, I., Elambasseril, J., Brandt, M., & Feih, S. (2014). Performance of bio-inspired Kagome truss core structures under compression and shear loading. *Composite Structures*, *118*(1), 294–302. https://doi.org/10.1016/j.compstruct.2014.07.036

Vaziri, A., Xue, Z., & Hutchinson, J. W. (2006). Metal sandwich plates with polymer foam-filled cores. *Journal of Mechanics of Materials and Structures*, *1*(1), 97–127. https://doi.org/10.2140/jomms.2006.1.97

Vinson, J. R. (1999). *The Behavior of Sandwich Structures of Isotropic and Composite Materials*. U.S.A: Technomic Publishing Company, Inc.

Wang, E., & Shukla, A. (2012). Blast Performance of Sandwich Composites with In-Plane Compressive Loading. *Experimental Mechanics*, *52*(1), 49–58. https://doi.org/10.1007/s11340-011-9500-5

Whisler, D., & Kim, H. (2014). A non-explosive test method for generating wide area dynamic blast-type pressure pulse loading on armored panels. *International Journal of Impact Engineering*, *68*, 28–40. https://doi.org/10.1016/j.ijimpeng.2014.02.004

Xue, Z., & Hutchinson, J. W. (2004). A comparative study of impulse-resistant metal sandwich plates, *30*, 1283–1305. https://doi.org/10.1016/j.ijimpeng.2003.08.007

Zakrisson, B., Wikman, B., & Häggblad, H. K. (2011). Numerical simulations of blast loads and structural deformation from near-field explosions in air. *International Journal of Impact Engineering*, *38*(7), 597–612. https://doi.org/10.1016/j.ijimpeng.2011.02.005

Zhang, P., Cheng, Y., Liu, J., Li, Y., & Zhang, C. (2016). Experimental study on the dynamic response of foam- fi lled corrugated core sandwich panels subjected to air blast loading. *Composites Part B*, *105*, 67–81. https://doi.org/10.1016/j.compositesb.2016.08.038